Fatigue and High Temperature Behaviour of the La-doped Bismuth-Ferrite Lead-Titanate System

Sayyed Adam Qaisar

Submitted in accordance with the requirements for the degree of Doctor of Philosophy

University of Leeds

Institute for Materials Research

School of Process, Environmental and Materials Engineering

September 2013

The candidate confirms that the work submitted is his/her own, except where work which has formed part of jointly authored publications has been included. The contribution of the candidate and the other authors to this work has been explicitly indicated overleaf. The candidate confirms that appropriate credit has been given within the thesis where reference has been made to the work of others.

The work in Chapter 7 of the thesis has appeared in publication as follows:
T.P. Comyn, T. Stevenson, S. A. Qaisar, A.J. Bell (2012). High performance piezoelectric materials. Actuator 2012

Acknowledgements

Foremost, my sincere thanks and gratitude go to my supervisors Andrew Bell and Tim Comyn for their support, advice and insight throughout this research - even Tim's hate of LaTeXand LabVIEW wasn't enough to put him off! And to Dragan Damjanovic for his valuable contributions while investigating domains and Rayleigh behaviour.

Thanks go to the Institute of Physics (IoP), Institute of Materials, Minerals and Mining (IOM^3), and the Society of Chemical Industry (SCI) for their financial support allowing me to visit some far-flung (Beijing, Vancouver, Prague) and not-so far-flung (Sheffield!) corners of the world under the veil of *"conference attendance"*. As well as Aero Engine Controls and the Engineering and Physical Sciences Research Council (EPSRC) for their funding for this research.

Further thanks go to V, Irene Zaccari and Jay Keeley for offering the greatest moral and comedic support for the past 4 years whilst also battling the wrath of their own PhDs, and Dean Leyland for his sheer brilliance of inappropriateness. Not forgetting those who have inhabited our little corner of the engineering building tucked away on the 3^{rd} floor, and colleagues in the electroceramics group and IMR for their comradeship throughout, as well as far-flung friends with whom many conferences have been shared.

Finally I would like to thank my parents for their unwavering support throughout the entirety of my academic life - the highs, the lows, they all got me to where I am now and I could not have done this without you.

To you all,

Thank you.

Abstract

For the past fifty years, lead zirconate titanate (PZT) has been the material of choice for the piezoelectric industry with piezoelectric materials showing promise in their applicability to smart devices and structures, from adaptive optics to ultrasonics and sonar. The longevity and reliability of PZT is, as with any commercial material, a topic that is well documented with reported operating lifetimes as large as 10^9 cycles. However PZT is severely limited in the type of thermal environment it can sustainably operate in, with maximum operating temperatures conservatively set around 150°C for commercial materials a new material is required for use in thermally hostile environments.

The basic aim of this research was to investigate the performance of 3% La-doped BFPT as a device at high temperatures, fields and stresses in comparison to equivalent PZT materials and further understanding of fatigue in both materials - essential for use of either as a commercially viable device. As no such, readily accessible, apparatus for testing ferroelectric ceramics existed it was essential to first develop the capability before experimentation could begin.

Upon development of a suitable apparatus, BFLPT and PZT fatigue studies were conducted and the fatigue as a function of domain contributions investigated using weak-signal measurements in bulk materials. Furthermore, using weak-signal measurements a study of domain behaviour at temperature was sought to give insight into the fundamental behaviour of ferroelectric materials at elevated temperatures - something previously only investigated using the likes of synchrotron facilities, and highlighted previously unobserved contribution changes occurring during material ageing.

Contents

Abbreviations

ε_r –Relative Permittivity

AFM - Atomic Force Microscope

BFPT - Bismuth Ferrite Lead Titanate

BFLPT - Lanthanum-doped Bismuth Ferrite Lead Titanate

E_a – Activation Energy

E_{br} – Dielectric Strength

E_C – Coercive Field

EBSD - Electron Back-Scattered Diffraction

EDX - Energy Dispersive X-Ray

GPIB – General Purpose Interface Bus

ICL - Indentation Crack Length

ITO - Indium-Tin Oxide

LVDT - Linear Variable Differential Transducer

MPB - Morphotropic Phase Boundary

P_S - Saturation polarisation

P_R - Remnant polarisation

PFM - Piezoresponse Force Microscopy

PZT - Lead Zirconate Titanate

RoHS - Reduction of Hazardous Substances

SEM - Scanning Electron Microscope

T_C - Curie temperature

T_{depole} – Depolarisation temperature

TEM - Transmission Electron Microscopy

XRD - X-Ray Diffraction

Research Motivation

In the past decade, ferroelectric materials have been increasingly applied to environments that can easily be considered thermally hostile. Applying ferroelectrics to high temperature systems has thus far focussed on the use of PZT, however with commercial PZTs restricted to an approximate maximum operating temperature of 300°C, a desire to exploit the advantages of ferroelectrics has led to an increasing amount of research investigating alternatives to PZT.
To overcome the thermal barrier limiting ferroelectric materials to current applications, a material first discovered in the 1960s bismuth-ferrite lead titanate (BFPT), has been further developed at Leeds by doping with lanthanum to create BFLPT. BFLPT shows promise for high temperature applications often expressing a Curie temperature several hundred degrees Celsius above that of PZT - 632°C. Bismuth ferrite lead titante is not without some drawbacks - high E_C and low resistivity, as well as slight processing issues revolving around the high internal strains, but although doped PZT is readily known to express very high Curie temperatures in excess of the aforementioned temperature for pure material, bismuth ferrrite lead titanates higher achievable strain and mechanical properties are not to be ignored when considering viable alternatives.

1 Literature Review

1.1 Dielectrics

A dielectric material is defined by exhibiting the ability to increase capacitance by virtue of molecular or ionic polarisation, resulting in opposite surfaces of the material acquiring opposite surface charge densities proportional to the amount of polarisation present in the material, whilst still remaining an electrical insulator. [1]

Polarisation is induced as a response to an externally applied electric field resulting in a displacement of ions, atoms or dipoles, depending on material (Figure 1).

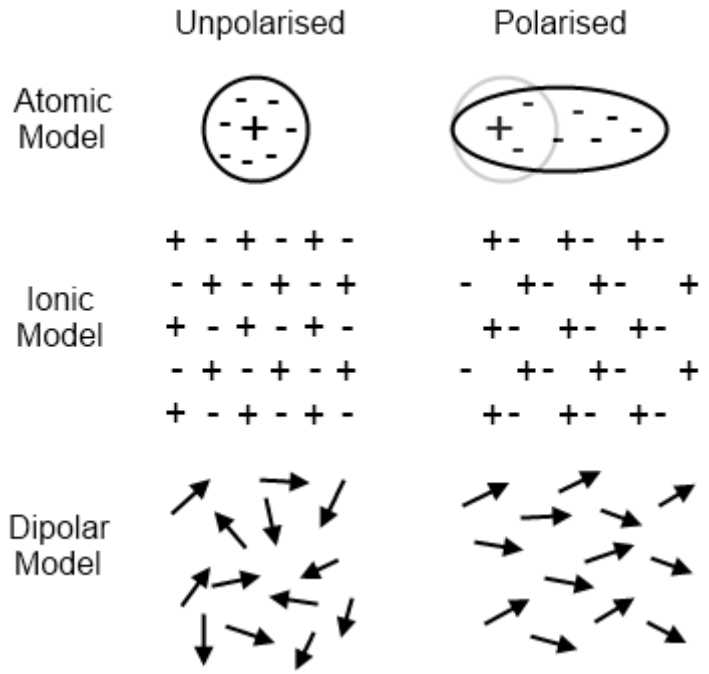

Figure 1: Diagrammatic representations of dielectric polarisation models.

The ionic polarisation, responsible for dielectric behaviour, is caused by the relative displacement of positive and negative ions in ionic non-centrosymmetric crystal structures. The dielectric response of a material can be characterised within a specific frequency range (Figure 2) - where frequencies exceeding the THz range are responsible for distortion of electron orbitals

in the presence of an electric field (atomic polarisation), while ionic polarisation is caused by dipole polarisation at a lower frequency[2].

Understandably the level of polarisation induced in a material, or dielectric dispersion, is highly dependant upon the frequency of the field applied – as the field frequency increases dipolar polarisation is unable to follow the alternating field in the region around 10 GHz (microwave), the ionic polarisation response is lost around 10 THz (far-IR) with atomic polarisation lost at 1,000 THz (Near-UV) high frequency fields only being capable of eliciting an electronic polarisation response from the material (Figure 2).

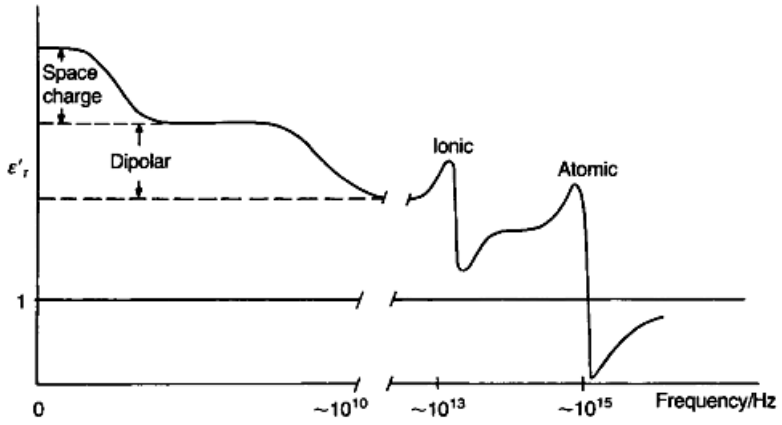

Figure 2: Variation of ε_r with frequency[2].

The efficacy of a dielectric medium is dependant upon several properties:

- Relative permittivity, ε_r – the ratio of the amount of electrical charge that is capable of being stored in the dielectric relative to that of a vacuum[1]
- Dielectric strength, E_{br} –the maximum field a dielectric may be subjected to before dielectric breakdown occurs, often resulting in a permanent conduction pathway through the material[1]
- Dielectric loss, $tan\delta$ – A dimensionless value, representing the dissipation of an applied

electric field through the reorientation of polarisation, manifested as heat [1]

By tuning these properties dielectrics have most commonly been exploited in capacitor technology. With modern electronic devices becoming ever smaller, the need for high capacity yet physically diminutive capacitors has resulted in the use of ferroelectric ceramics as dielectric media. Ceramics cover a wide range of dielectric properties ranging from relative permittivities as low as 6 (comparable to rubber) to ferroelectric compositions in excess of 6,000 (e.g. PZT) [2].

1.1.1 Dielectric Strength

Dielectric materials are widely used as insulators between different conduction pathways to prevent air ionisation and electrical discharge. As the voltage across the dielectric material increases, the applied field also increases. Obviously this field cannot be increased infinitely, eventually a limit is reached whereby a voltage is able to flow from one pathway to the other; in gaseous and liquid dielectrics this is rarely an issue – the discharge typically does not damage the dielectric medium, permitting the re-use of the media upon removal of the breakdown-inducing field. However when a solid dielectric is considered, the breakdown unfailingly leads to physical damage of the medium [1].

There are various mechanisms of dielectric breakdown in solid materials, the likelihood of which depends on the condition of the material and a number of extrinsic parameters (e.g. temperature & humidity).

Table 1: Typical dielectric strength values under STP conditions [1]

Dielectric Medium	Dielectric Strength
Atmosphere (1 atm press.)	31.7 kV cm^{-1} 60 Hz
SF_6 gas	79.3 kV cm^{-1} 60 Hz
Amorphous SiO_2	10 MV cm^{-1} dc field
Borosilicate glass	10 MV cm^{-1} for 10 μs

Internal & External Discharge

By far the most common cause of dielectric breakdown in conventionally prepared materials, internal discharge occurs as a result of microstructural defects (pores, cracks etc.) within the dielectric containing an atmosphere with significantly lower dielectric constant to the host material. A discharge through one of these defects can have many effects on the dielectric –the electrical discharge can erode the dielectric increasing the discharge path length, melt the surrounding dielectric leading to a chemical change in the material or cause a catastrophic failure of the material resulting in large crack formation and material ejection (electrofracture). Furthermore, the possibility of external discharge is also present – for example excessive atmospheric moisture combined with surface contaminants can readily lead to electrical discharge.

Electronic Breakdown

Theorised to be as a result of a free electron in the dielectric's conduction band ionising an atom in the dielectric, an electron avalanche is the most common form of electronic breakdown in electronic materials, however it is very unlikely to occur in common dielectrics as it requires a near defect-less material. A far more common electronic breakdown mechanism in dielectrics is that of electron injection from the metallic electrodes as a result of high fields enabling electron tunnelling into the dielectric[3].

Thermal Breakdown

Whilst subject to high frequency AC field, dielectric losses become increasingly significant – the work done by the applied field rotating dipoles generates molecular collisions, increasing the losses and generating heat within the dielectric. Basic electronic theory shows that for n-type semiconductors, increasing temperature increases the proportion of conduction band carriers, increasing the conductivity. This increase in conductivity further raises the temperature of the dielectric to a point whereby the current increases until a discharge event occurs. Due to the thermal capacity of ceramic materials, this is an ever present issue when considering

using dielectric ceramics as active devices where the thermal change in the material will not be apparent due to the observed external temperature of the ceramic will lag behind that of the ceramic core or any heating points within the material.

Fatigue & Ageing Effects

In certain materials, operating below E_{br} for prolonged periods of time can lead to an increase in conductivity. Several potential causes for this degradation exist, ranging from; atmospheric effects – for example prolonged exposure to high humidity, as well as electromechanical effects elicited by d.c operation resulting in conductive pathways forming from electrode material migration into the dielectric.

1.1.2 Dielectric Loss

As can be expected, dielectric materials have losses whilst in operation dictated by field frequency and material. Electrical energy is lost during ac field cycling - the alternating field eliciting a magnitude and direction change of any dipoles present, the energy loss is typically evident as a thermal change in the material as a result of the opposition to dipolar motion within the dielectric and controls the dielectric constant of the material, represented in equation 1 as a complex value.

$$\varepsilon = \varepsilon\prime - i\varepsilon\prime\prime \tag{1}$$

Where $\varepsilon\prime$ is the permittivity and $\varepsilon\prime\prime$ is the imaginary, both frequency dependent.

1.2 Piezoelectricity

Certain crystalline materials, for example quartz[1] (crystalline SiO_2), are capable of becoming polarised in response to an applied mechanical stress - the *direct* piezoelectric effect. The polarisation response may take place as a separation of charge across the crystal, resulting in a voltage difference between the two surfaces of the crystal. In addition to the formation of charge when subject to mechanical stress, the same crystals exhibit what is known as the *indirect* (or converse) piezoelectric effect; the ability to elicit a mechanical strain, or distortion when subject to an electric field. For example, lead zirconate titanate (PZT) exhibits maximum strain levels in the region of 200-300 microstrain[4]. The type of deformation, extension or compression, is dependant on the direction and polarity of the field applied.

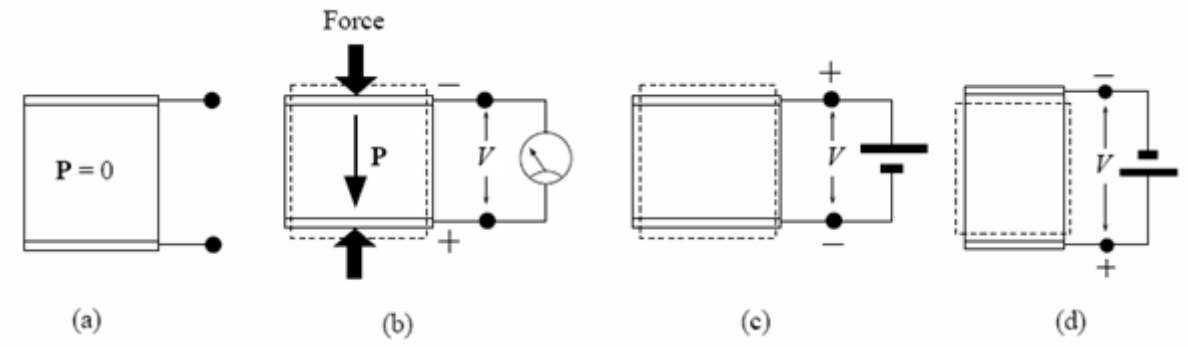

Figure 3: (a) Piezoelectric crystal without an applied stress or field; (b) A crystal strained by and applied force, inducing a crystal polarisation generating surface charges and a potential difference; (c) An applied field induced strain; (d) Change of induced stain as a result of changed polarity of the applied field.[1]

It is this very behaviour which defines the piezoelectric effect.

1.2.1 Crystal Structure

Piezoelectric materials are completely reliant upon crystallography to define their properties - only certain crystals are capable of exhibiting piezoelectric behaviour.

Before being able to identify the crystal structures capable of eliciting a piezoelectric re-

sponse to external influence, we must have a basic grasp of crystallography - specifically the key structures important for piezoelectric activity. Materials consist of a structure repeated throughout its entirety, which can be reduced down from a vast crystal array to a single 3-dimensional crystallographic unit - the *unit cell*, which stands as the blueprint for the structure of the entire material, and by virtue the entirety of the material's properties. The unit cell dimensions are referred to by the *lattice parameters* - **a, b, c**, for example in a cubic material all 3 parameters are equal (Figure 4) thus giving an undesirable centro-symmetric structure.

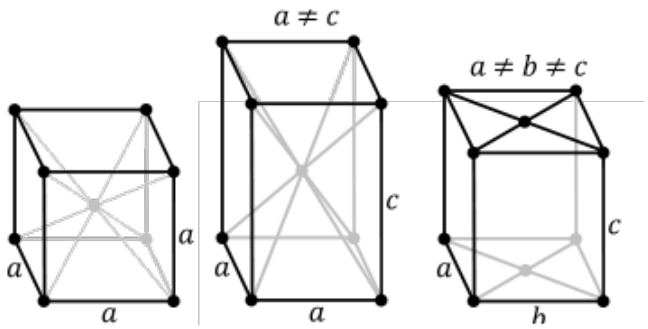

Figure 4: Crystal structures (left to right): cubic body centred, tetragonal body centred and orthorhombic base centred[1].

In centrosymmetric materials (eg. cubic close packed) any point on any constituent ion is a centre of symmetry. When unstressed, this symmetry is obvious as there is no net polarisation in the unit cell due to the coinciding of the centres of mass for positive and negative ions shown by drawing a vector r from the centre of mass (point O) to any charge and then reversing the vector to find a charge of the same type (Figure 5, left). As is expected, under stress the unit cell is distorted, however the centres of mass do not change as the deformation is perfectly symmetrical in all directions, causing a zero net polarisation.

Therefore in order for a material to exhibit piezoelectric behaviour the lattice parameters must be non-centrosymmetric in order to remove one, or several, symmetries.

Piezoelectrics, with their non-centrosymmetric crystalline structure, have ions of opposite charge connected by a vector passing through the centre of mass, O. When unstressed, the

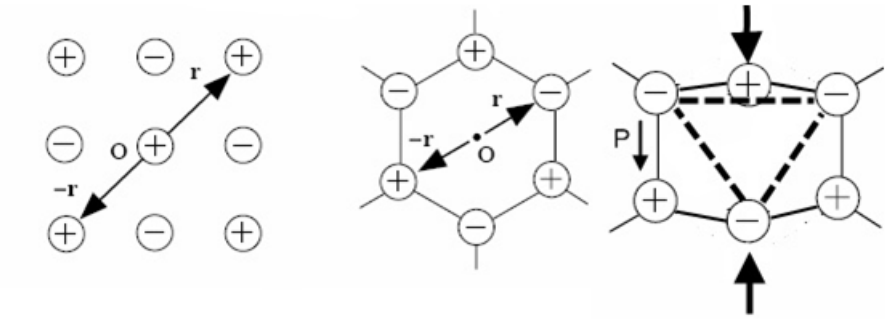

Figure 5: Left - a centrosymmetric unit cell (NaCl) with centre of mass O, Centre - A non-centrosymmetric, unstressed hexagonal unit cell with centre of mass O, Right - Showing the displacement of positive and negative charge, resulting in a shift of mass centre. [1]

centre of mass for both the positive and negative ions coincide, however when stressed, as shown on the right in Figure 5, the two centres of mass are displaced, resulting in a net polarisation P, exhibiting the direct piezoelectric effect. Despite this behaviour, when the stress is along a different direction (Figure 6), there may not be a net dipole formed in the same direction as the stress even if there is a net polarisation in a different direction [1].

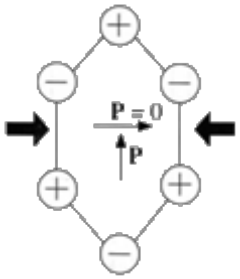

Figure 6: Direct piezoelectric effect on polarisation. [1]

1.2.2 Piezoelectric Notation & Constants

Piezoelectric properties are highly directional, as such there is complexity in describing the corresponding directions of the various properties; polarisation, strain, stress and electric field. These properties produce a 3rd order tensor, giving an expression for piezoelectric behaviour of:

$$P_i = d_{ijk} T_{jk} \tag{2}$$

If T_{jk} is the applied mechanical stress and P_i is the induced polarisation in direction i, then the two are linearly related by d_{ijk} the piezoelectric coefficient. The symmetry of this 3rd order tensor allows the notation to be reduced to a 2nd order in Voigt form[5]:

$$P_i = d_{ij} T_j \tag{3}$$

Voigt notation is the typically addressed form for describing and referring to piezoelectric phenomena and their directionality - with *1, 2 & 3* directions permissible for i (electric field) and shear planes of *4, 5 & 6* available for j (mechanical strain) about the polar axis, where the *3* direction is regarded as the polar axis (Figure 7).

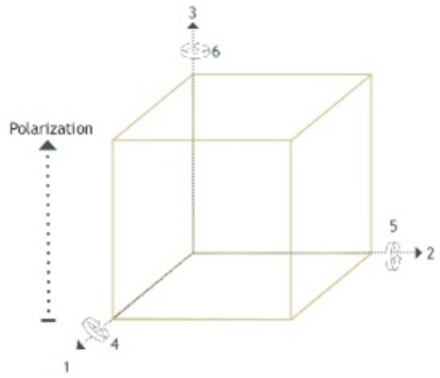

Figure 7: Designation of axes in piezoelectric materials.[6]

The most useful of these coefficients are:

- **d** - piezoelectric charge coefficient (Figure 8). An expression of the ratio of strain developed in the material to the applied field *or* conversely the ratio of charge developed in response to applied stress. Unit pC N^{-1} or pm V^{-1}
- **g** - piezoelectric voltage coefficient. An expression of the ratio of developed strain to the

applied charge density or electric field geneated by applied unit stress. Unit V mN^{-1}

- **k** - piezoelectric coupling coefficient
- **s** - elastic compliance. Strain to stress ratio
- ε - dielectric permittivity

These notations are given along with subscript numbers of directionality outlined previously, the first number giving the direction of electric field whilst the second gives the direction of the mechanical stress or strain present.

Possibly the most important coefficient arising from piezoelectric behaviour, the piezoelectric coupling coefficient. It describes the conversion of mechanical energy to electrical or vice-versa in the material. The square-root of the ratio of electrical energy stored to that applied, or when expressing the converse effect, mechanical energy stored to that applied (Equation 4)[2] gives a value for this parameter.

$$k_{eff}^2 = \frac{\text{electrical energy converted to mechanical energy}}{\text{applied electrical energy}} = \frac{d^2}{s\varepsilon} \tag{4}$$

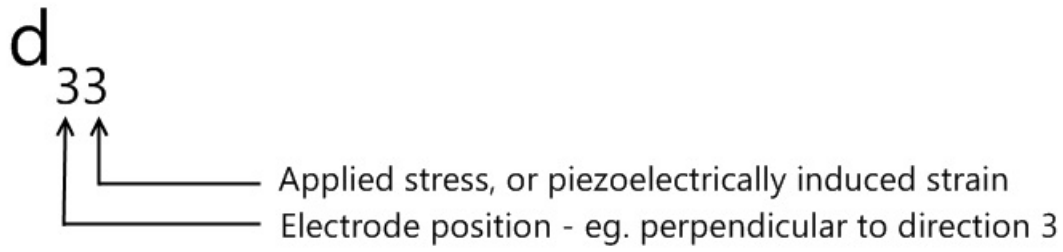

Figure 8: Notation of piezoelectric charge coefficient.

1.3 Ferroelectricity

Ferroelectricity is the expression of a characteristic polarisation behaviour by a material; that of a spontaneous/remnant polarisation below a material-specific temperature which can be reversed by the application of an external electric field (Figure 9)[7].

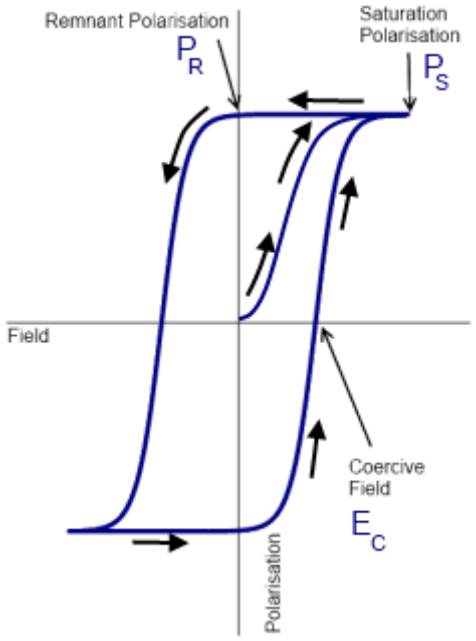

Figure 9: Typical hysteresis behaviour of a ferroelectric exhibiting a characteristic remnant polarisation.

Ferroelectric behaviour was first observed in Rochelle Salt (potassium sodium tartrate) in the early 1920s by Valasek[8], later discovery of ferroelectric behaviour was found in barium titanate (1945) leading to an explosion of viable ferroelectric compositions in the 1950s[9]. Isostructural with perovskite, a naturally occurring mineral, barium titanate is referred to as a *'perovskite material'* and possesses the same simplified ABO_3 structure (Figure 10). This structure is distorted, when a remnant polarisation is present at room temperature, into a body-centred tetragonal structure where a and c crystal dimensions are non-equivalent.

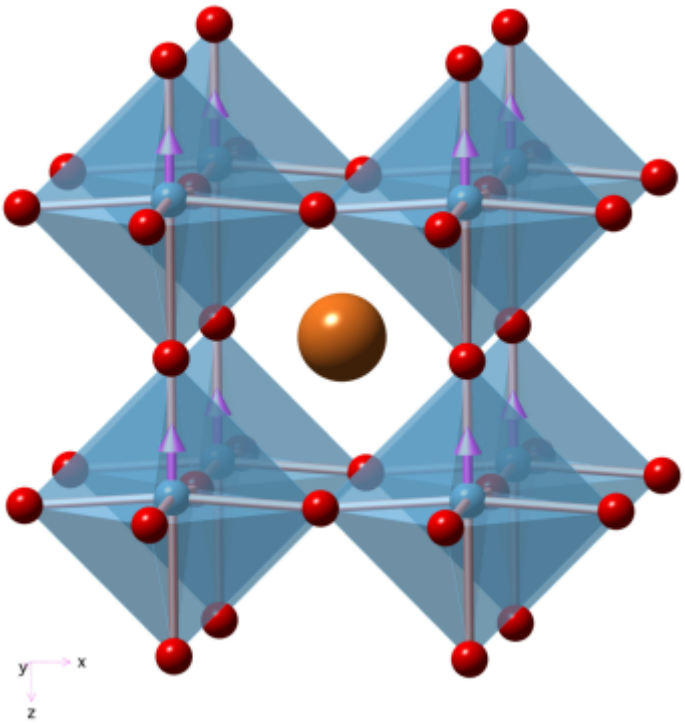

Figure 10: Crystallographic structure of barium titanate, where orange - barium, red - oxygen, blue - titanium.

1.3.1 Domains & Poling

In a fashion analogous with ferromagnetism, ferroelectric materials possess a domain structure, spontaneously formed during a phase change when cooling the paraelectric phase through T_C[2]. The domains are formed by virtue of electric dipoles assuming an energetically favourable order forming distinct regions of polarisation from 7 nm[10] to 15 μm[11] in size - producing the domain structure, surface charge and simultaneously domain walls with their own associated energy. The minimum favourable domain size can be limited by various synthesis techniques (sol-gel, chemical co-precipitation, pulsed laser deposition)[12–16] and bulk or thin-film growth. The polarisation vector of the spontaneously formed domains follows alignment in certain crystallographic and energetically permissible orientations, comprising of 180° (Figure 11), and non-180° domains[7,17–21] (Figure 12) while resulting in a zero net polarisation.

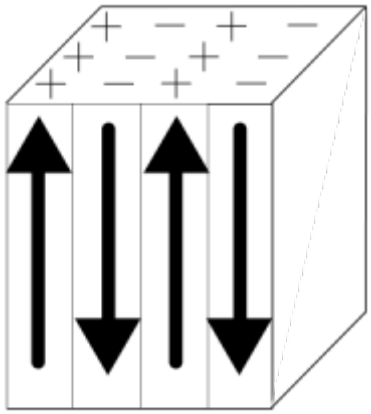

Figure 11: Formation of 180° domains in an antiparallel fashion to reduce energy.

The creation of a remnant polarisation within a polycrystalline ferroelectric ceramic is feasible by the action of applying a sufficiently large external field - termed *'poling'*. Although there are different methodologies for achieving the same effect, the simplest method of poling involves heating the chosen ferroelectric material to a defined temperature, applying an external field for several minutes - domain reorientation parallel to the field takes place producing a net macroscopic polarisation vector, along with an expansion parallel to the direction of the field

and contractions in perpendicular directions producing a spontaneous strain within the material. Once subject to an applied field these domains contribute to the piezoelectric response of a ferroelectric, enhancing the intrinsic crystallographic piezoelectric contribution due to motion of the domain walls[22,23].

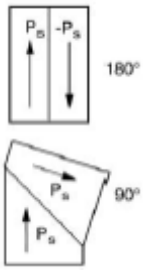

Figure 12: Illustration of adjacent 90° and 180° domains in a tetragonal ferroelectric perovskite.[22]

Of note is that by definition poling is only feasible in ferroelectric materials; a piezoelectric crystalline material (e.g. quartz) with no remnant polarisabilty possible cannot be poled and exhibits macroscopic piezoelectric properties[22].

1.3.2 Hysteresis Behaviour

Of the most important properties a ferroelectric possesses, the capacity for polarisation switching by an applied field is paramount - this behaviour is due to two phenomena occurring. One being the *intrinsic* contribution, originating from lattice changes within domains. The second, *extrinsic* contribution occurs by domain switching, this behaviour is readily observed as the characteristic polarisation-field hysteresis (Figure 9). At low AC fields, the material response follows that of equation 3 with a linear, Rayleigh-like, response[24] as the field is not sufficiently strong to switch domains which are unfavourably oriented. At higher fields, the unfavourable domains begin to switch in a crystallographically permissible direction in parallel with the field until polarisation saturation is achieved (Figure 9 - P_S). As the saturation field is removed, some domains reorientate in non-field-parallel directions reducing the measured polarisation from P_S to a lower, yet still significant value at zero field, a remnant polarisation - P_R. Thus in order to

achieve a zero macroscopic polarisation the application of an oppositely biased field is required (Coercive field - $\pm E_C$). With further increases in the negative field, domain switching in the opposite direction to that of a positive field bias occurs leaving a typically symmetrical hysteresis loop.

1.3.3 Temperature Dependant Properties

As eluded to previously (Section 1.3.1), ferroelectrics have an operational temperature window, above which the material behaves as a paraelectric. This ferroelectric-paraelectric transformation is defined as the temperature at which the spontaneous polarisation of a ferroelectric becomes zero[7] and is one of the key factors defining the useful limits of a ferroelectric and its applicability in applications where the environment is thermally hostile.

For example below T_C pure PZT has a tetragonal structure with a displaced central Zr or Pb cation causing a dipole moment (Figure 13, right). If heated above T_C PZT transforms into a cubic phase (Figure 13, centre and left) removing all spontaneous polarisation.

This behaviour is explained by the Curie-Weiss law:

$$\chi = \frac{A}{T - T_C} \tag{5}$$

As T (material temperature) approaches T_C, the electric susceptibility (χ) of the material approaches infinity (A is a material specific constant).

1.3.4 Pyroelectric Effect

Ferroelectric materials possess a temperature dependant spontaneous/remnant polarisation, whether single-crystal or poled ceramic, this temperature-induced polarisation change is accompanied by a readily detectable change in surface charge[1,2].

$$p = \frac{\delta P_R}{\delta T} \tag{6}$$

The effect is defined by equation 6, whereby δT - temperature change, induces the polarisation change δP thus quantised as the pyroelectric coefficient.

1.4 Transformation Toughening

A phenomenon observed in zirconia, transformation toughening occurs during crack formation. The presence of a concentration of stress at the crack tip is sufficient to produce a crystallographic phase transition from tetragonal to monoclinic, with the associated volume change in the phase change[25]. In the case of partially-stabilised zirconia this volume change is typically in the region of a 4-6% increase[26].

In the case of electroceramics, cracks have been observed preferentially occurring at grain boundaries with a propensity towards crack growth parallel to the *33* direction[27]. Owing to the longer c axis, compressive stresses in the y direction arise, leading to crack tip shielding and a toughening effect. If the ferroelectric ceramic is poled perpendicular to the crack, this effect is much less pronounced because only a few domains are left for ferroelastic switching, compounding the anisotropic behaviour of transformation toughening.

In electroceramics a crack as well as the poling direction are aligned in the *33* direction, and the mechanical load is parallel to the *31* direction. A tetragonal crystal structure with a c axis slightly longer than the a axis (usually 12%) is assumed in figure 14, with the high stresses at the crack tip in the *31* direction lead to 90° ferroelastic domain switching localized around the crack.

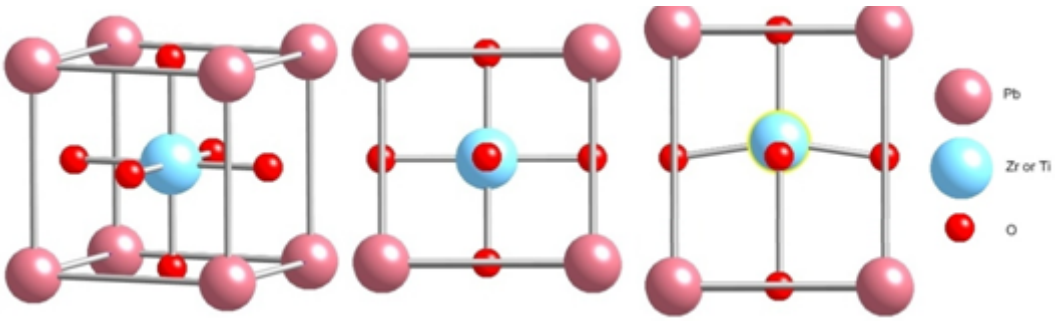

Figure 13: $Pb(Zr, Ti)O_3$ crystal structures above its Curie temperature (230 °C), left and centre; and below T_C exhibiting a tetragonal structure and a spontaneous polarisation, right.

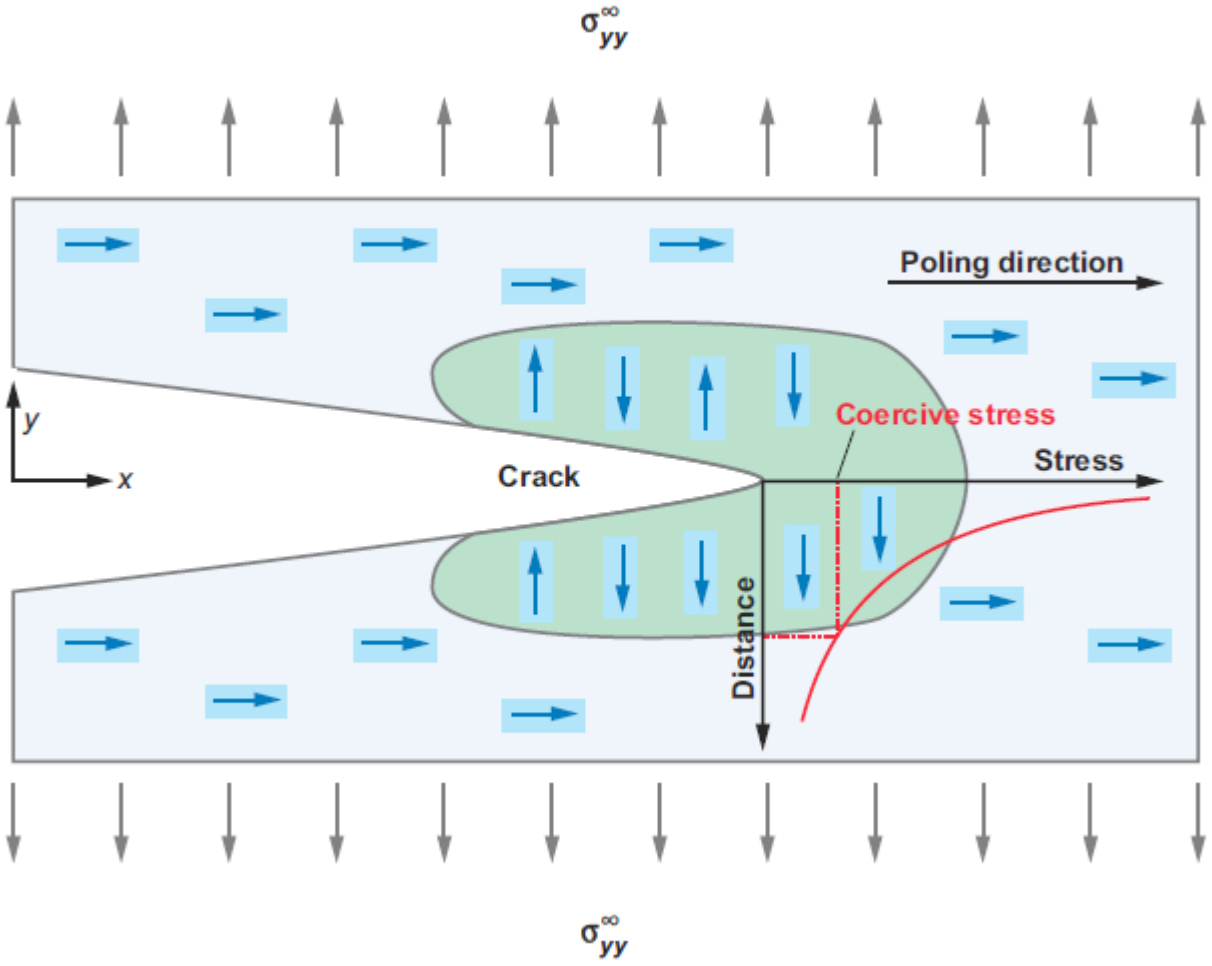

Figure 14: A micromechanical model explaining the fracture toughness anisotropy by domain switching.[28].

1.5 Lead Zirconate Titanate

Since its first development in 1951[29], lead zirconate titanate (PZT) has become the material of choice for the piezoelectric industry, far surpassing the applications of $BaTiO_3$. Being a perovskite, PZT follows the standard compositional arrangement of ABO_3 with lead and titanium/zirconium occupying the A and B sites respectively with a crystal structure similar to that of $BaTiO_3$ and follows a solid solution formulation of $Pb(Zr_{1-x}Ti_x)O_3$. Reasons for PZTs place as the cornerstone of commercial electroceramics are its enhanced piezoelectric properties, capacity for operation at temperature[2] (150 °C, approx. half depolarisation temperature for undoped PZT with d_{33} stability reported as high as 200 °C[30]) and further enhancements possible by inclusion of dopants.

1.5.1 Morphotropic Phase Boundary

The morphotropic phase boundary (MPB) was originally defined as a temperature independent compositional modification resulting in an abrupt structural change in a material, specifically that of a piezoelectric. Previously, the structural change associated with the phase boundary was thought to occur at a specific, well defined composition making the phase boundary region practically non-existent[31]. In 1970[32], the view of the MPB as a narrow compositional area with negligible width was disproved, being replaced with the currently accepted theory that the MPB is a compositional area that is largely temperature independent in which tetragonal and rhombohedral phases co-exist with varying concentrations of each phase present[2] permitted by energetic degeneracy. Solid solution systems are expressed as a chemical equation, balanced by molar percentages, for example the PZT system shown in Figure 15 takes the form; $Pb(Zr_{1-x}Ti_x)O_3$.

The observation that enhanced properties exist within a range of concentrations is verification of current MPB theory in terms of mixed phase co-existence. The enhanced properties being caused by degenerate Gibbs energies associated with the presence of two crystal phases[23] in the binary solid solution, allowing optimum domain reorientation during poling of the material[33].

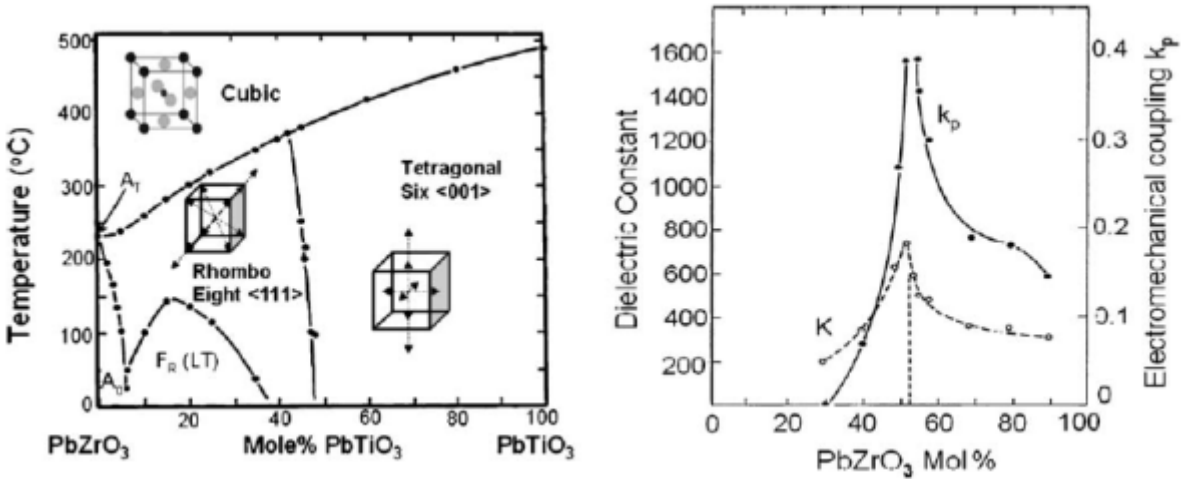

Figure 15: Morphotropic phase boundary (left) and enhanced dielectric and piezoelectric properties (right) in the PZT system.[23]

However, recent studies have since disproved the temperature independence of the MPB[34], thus making the term *morphotropic* phase boundary a misnomer in the discipline.

1.5.2 Temperature

Given the effects temperature has on polarisation and permittivity, it is not unreasonable to expect a change in domain behaviour with temperature in a ferroelectric material. Current research[35] suggests that there is a temperature dependence in PZT-based materials pertaining to the ratio of irreversible to reversible domain contributions to the overall piezoelectric response

1.5.3 Doping – Soft & Hard Ferroelectrics

The perovskite structure adopted by some ferroelectrics is surprisingly accommodating of elemental substitutions in its structure, with notable changes in material properties possible as a result of a substitution level as low as 0.05 at.%. There are three types of dopant available for exploitation in ferroelectrics acceptor, donor and isovalent dopants, with acceptor and donor doping producing hard and soft variants of the material respectively; acceptor dopants have lower charge than that of replaced ions, while donors are the opposite. The *hardness* of the

ferroelectric refers to the mobility of the domains and hence its polarisation behaviour [22,23,36,37].

For comparison typical dopants used in PZT are;

- Hard doped (eg. K^{1+}, Na^{1+}, Fe^{2+}, Al^{3+}) material has comparatively low domain mobility and is capable of being subjected to high electrical and mechanical stresses by virtue of low permittivity, low dielectric losses, high E_C and high mechanical quality factors
- Soft doped (eg. La^{3+}, Nb^{5+}, Sb^{5+}) material is much more domain active, with high domain mobility.

The acceptor doping, to form a hard composition, is electrically balanced by oxygen vacancies. These vacancies are capable of diffusion in the oxygen octahedra of the material - permitting them to orientate with domain directions, stabilising the domain wall structure and limiting overall domain mobility. Meanwhile, the mechanism for donor doping is electronic compensation by virtue of valence electrons or double negative charged lead vacancies [38].

1.5.4 PZT Compositions

With doping comes differing compositions of PZT that have to be referenced and referred to with relative ease. A widely accepted nomenclature is that of:

Table 2: PZT Nomenclature

Soft	Hard
PZT-5	PZT-4
PZT-5A	PZT-8
PZT-5J	
PZT-5H	

1.6 High Temperature Ferroelectric Materials

With engineers heavily reliant upon PZT and its modified counterparts to fulfil the requirements of new ferroelectric applications, a limit is being reached forcing the range of materials available to expand further. In a field where temperatures as low as 200 °C considered as 'high temperature', new research is being focussed on delivering high T_C, high activity materials capable of filling the temperature range where PZT cannot operate. Several materials show promise as high Curie point materials (Table 3), however their drawbacks for example - low activity, high leakage - mean they are of little real–world use, while materials with high T_C and low activity are less than ideal for the likes of actuation, but are more than viable solutions where sensors are required as signal amplification is achievable.

Table 3: Properties of some high temperature piezoelectric materials

Material	T_C (°C)	d_{33} (pC N^{-1})	ρ (Ω m) (T °C)	Ref.
(Bi, La)$BiFeO_3$-$PbTiO_3$	295	264		[39]
$PbZrO_3$-$PbTiO_3$	**350**	**500**		
(K, Na)NbO_3	420	180		[40]
$(K_{1/2}Bi_{1/2})TiO_3$	437	69		[41]
$SrBi_2Nb_2O_9$	438	10		[42]
$BiScO_3$-$PbTiO_3$	450	460	2x10^6 (277)	[43]
	445	390	3x10^8	[44]
$SrBi_4Ti_4O_{15}$	530	20		[45]
$PbNb_2O_6$	570	100		[46]
$BiFeO_3$-$PbTiO_3$	635	160		[47]
$Bi_4Ti_3O_{12}$	675	20	10^{10}(100)	[48]
$CaBi_4Ti_4O_{15}$	790	12		[49]
Bi_3TiNbO_9	914	7		[50]
$GaPO_4$	930	4.5 (d_{11})		[51]

Although a cursory glance gives some promise of solving the high temperature ferroelectric problem, things are not always so simple - several materials have a reported activity an order of magnitude below that of PZT (highlighted, table 3) - far from useful for actuation; some have processing difficulties or still contain high amounts of lead; others possess high resistivity,

activity and T_C, but are prohibitively expensive to produce on anything more than a laboratory scale.

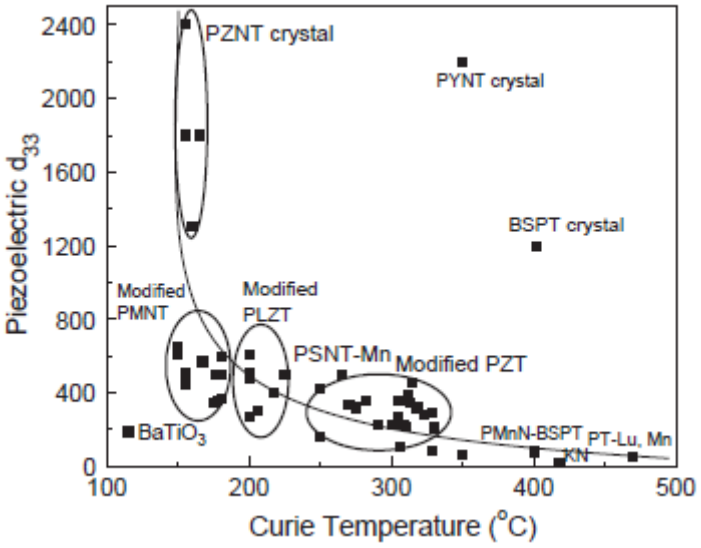

Figure 16: Piezoelectric coefficient in pC N^{-1} as a function of Curie temperature for various materials.[52]

Figure 16 shows a variety of bulk perovskite materials and the relationship of high T_C and d_{33}.

1.6.1 Modified Lead Zirconate Titanate

With pure PZT depoling around 350 °C, modification of the system about the MPB tends towards a reduction in T_C with the advantage of increased activities depending upon dopant[53–55] - a far from ideal situation.

1.6.2 Bismuth-Scandate Lead-Titanate

BSPT appears to be the ideal solution to high temperature applications - with a high T_C around 450 °C, and d_{33} higher than undoped PZT and a high resistivity aiding poling. Further, the ability to process by conventional mixed oxide routes it is, on paper at least, a very attractive

material to put into production for high temperature use. But all is not as it seems, BSPT has an Achilles' heel - Scandium is the key culprit costing $7,200 per kilogram, preventing any possible adoption of BSPT unless in high value applications where the cost is significantly outweighed. However this can be reduced slightly by forming a system with BFPT and titanium & magnesium doped bismuth oxide, while retaining a high T_C (450 °C)and piezoelectric activity (328 pC N^{-1})[56].

1.6.3 Bismuth-Ferrite Lead-Titanate

Bismuth ferrite lead titanate (BFPT) has been a focal point for research where a high Curie material is required[57,58]. With a large spontaneous strain of approximately 18%[59,60] and a Curie temperature exceeding 600 °C BFPT is a potential candidate material for high temperature actuators and sensors, but the system is not without its drawbacks, chief amongst which is an inherent difficulty to pole to saturation.

Replacement of iron in the bismuth ferrite-lead titanate system already produces the aforementioned wildly expensive bismuth scandate-lead titanate ferroelectric. An alternative approach of doping, rather than replacing, a member of the system shows promise, specifically with respect to doping on the A-site with lanthanum[61]. Although a reduction in T_C is observed it is still adequate for high temperature applications and still retains a reasonable enough piezoelectric activity that consideration for use in actuation is viable.

1.6.4 Lead Niobate

Lead niobate ($PbNb_2O_6$) with a Curie temperature in excess of 550 °C[62] seems tempting as a ferroelectric for use in high temperature applications. However, the material exists in two stable forms - rhombohedral at low temperature and tetragonal at elevated temperature, neither of which are capable of piezoelectric behaviour. The only permissible way for lead niobate to possess piezoelectric activity is to quench the tetragonal phase to form a meta-stable orthorhombic structure[62] - adding a further processing step to lead niobate's already lengthy and high tem-

perature processing requirements[63] for a material with a d_{33} in the region of 70 pC N^{-1} possible after doping[64].

1.6.5 Gallium Orthophosphate

Gallium orthophosphate ($GaPO_4$) shows promise from the start by being a lead-free piezoelectric material, combined with a 930 °C transition temperature[51], excellent for high temperature environments, it appears to cover all requirements for a piezoelectric to be used in thermally hostile environments. Existing only as a man-made crystal, processing is invariably by precise single crystal synthesis routes and the material exhibits no ferroelectric behaviour, limiting it to use in transducer applications in d_{11} operation[51].

1.6.6 Potassium Bismuth Titanate

The potassium bismuth titanate system ($K_{0.5}Bi_{0.5}TiO_3$ – KBT), with ferroelectric and piezoelectric properties reported as early as the 1960s[65], is initially promising considering a reported T_C of 380 °C[66] and the absence of lead in its composition. Piezoelectric activity in a pure KBT is adequate, but can be significantly improved by forming a tertiary system with sodium bismuth titanate and bismuth titanate (NBT-KBT-BT) - a nearly 300 °C T_C remains with activity increased to 173 pC N^{-1} for an MPB composition[23], this can be further enhanced by replacing bismuth titante with lithium-bismuth titanate (NBT-KBT-LBT) - d_{33} 216 pC N^{-1} and T_C 350 °C T_C[67].

1.6.7 Summary

The problem of applying ferroelectric materials to high temperature environments is one that is partly solved - as far as exploiting the direct piezoelectric effect is concerned there are already materials capable of fulfilling high temperature operational requirements, however where the converse effect is desired there is little consensus on a specific material of choice, with cost and processability limiting the selection further.

Of the materials presented, the bismuth oxide-lead titanate system produces several materials capable of fitting high temperature requirements as both an actuator and sensor, while also being readily processable. Taking cost into account, the obvious choice being that of lanthanum-doped bismuth ferrite-lead titanate - offering increased activity over undoped BFPT, reduced cost to BSPT while still retaining a high T_C it is at first instance, a viable ferroelectric material for use at high temperatures.

1.7 Bismuth-Ferrite Lead-Titanate

Formed as a solid solution between rhombohedral bismuth ferrite and tetragonal lead titanate, the $x\mathrm{BiFeO_3}$–$(1-x)\mathrm{PbTiO_3}$ system was first reported in 1961 by Fedulov[68,69]. Individually bismuth ferrite and lead titanate are two materials capable of exhibiting ferroelectric behaviour and very high phase transition temperatures; bismuth ferrite possesses a T_C of 850 °C[69], while its systemic partner lead titanate resides at 490 °C[7] - promising a high Curie point ferroelectric ceramic when combined in a solid solution.

1.7.1 Structure

The BFPT system displays strong ferroelectric behaviour around a morphotropic phase boundary (Figure 17), residing at $x = 0.62$-0.7 composition[68] existing in a mixed phase of both tetragonal lead titanate and rhombohedral bismuth ferrite and subsequently further investigated[70,71]. At this composition the expected high Curie temperature of the system is presented - 632 °C[59].

1.7.2 Properties

With the Curie point of the BFPT system being far in excess of that of PZT (386 °C[73]) and the large spontaneous internal strain of approximately 18%[59] implying a large ferroelectric polarisation at a morphotropic composition of 70% bismuth ferrite to 30% lead titanate (70–30 composition), it is a very desirable material for use in high temperature environments. Furthermore piezoelectric measurements have been made on compositions around and beyond the MPB by Comyn *et al* yielding a high-field d_{33} coefficient of 160 pm V^{-1} showing that even with a T_C advantage over PZT, BFPT possesses a high piezoelectric coefficient that is very similar. In addition to a highly sought-after Curie point, piezoelectric and strong ferroelectric behaviour, BPFT has also been found to exhibit an antiferromagnetic nature - possession of antiparallel magnetic domains (Néel ordering)[74,75], classifying the material as a multiferroic. Multiferroic materials possess unusual physical properties, giving them potential practical applications for new magnetoelectric memory devices[74,76–78].

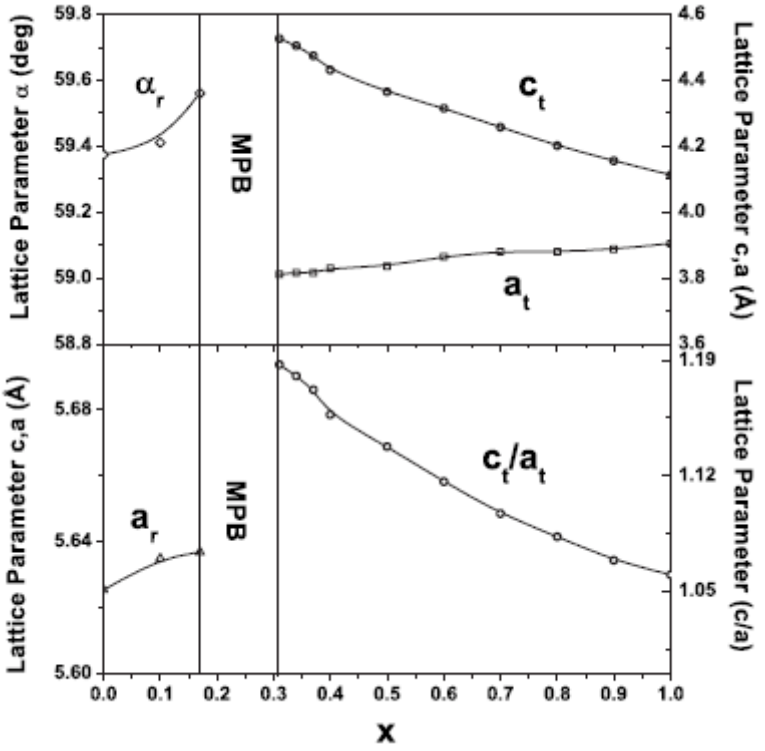

Figure 17: Phase diagram of the $x\mathrm{BiFeO_3}$–$(1-x)\mathrm{PbTiO_3}$ system [72]

Understandably BFPT has great potential in high temperature applications; however a study by Comyn *et al*[47] revealed that the large spontaneous strain can inhibit ferroelastic switching in the material, giving the property of being difficult to pole and requiring a high coercive field to attain reasonable d_{33} values further compounded by electrical measurements of BPFT proving difficult, with the material possessing a high conductivity[58] potentially caused by oxygen vacancies and Fe^{2+}:Fe^{3+} hopping[79], resulting in electrical breakdown during poling before saturation can be achieved.

1.7.3 Doping

As discussed (Section 1.7.2) conductivity is a problem of the BFPT system. Bismuth ferrite domain walls are capable of conduction, contributing to the conductivity of BFPT[80,81] domain wall conductivity variances attributed to differing domain wall alignments whereby 180° domain walls are the most conductive. This is followed by 109° and 71° walls contributing the least to conduction[82] due to variance in polarisation along the domain walls, creating an electrostatic field which can attract charge carriers (oxygen vacancies etc.).

In order to improve the electrical properties of the BFPT system, inspiration has been taken from bismuth ferrite and PZT research[80,83–85] with attempts being made into small amounts of doping ($\leq$5% at.) the solid solution on the A and B sites with La[61,86,87], Ga[88,89], Sb[90] and Sc[57] to increase resistivity and improve ferroelectric characteristics, at the expense of a lower T_C.

Table 4: Effects of Dopants on the xBiFeO$_3$–$(1-x)$PbTiO$_3$ System

Dopant	T_C (°C)	d_{33} (pC N^{-1})	Ref.
Lanthanum$_{(10\%at.,B-site)}$	386	163	[91]
Gallium	540	52	[88]
Scandium$_{x=0.55}$	440	300	[57]

Further, La doping has been observed to improve piezoelectric and dielectric properties[92,93] of PZT, improving the contributions of the lead titanate member in the BFPT system.

1.8 Multilayer Devices

Typical monolithic structures created for testing in laboratories although ideal for the research environment, are of little use to actuation and positioning applications. They are difficult to package, with typical bulk ferroelectric material requiring an electric field in the region of several kV mm^{-1}, making bulk materials rather undesirable as large voltages will be required to drive them. In addition, piezoelectric activity is generally in the region of 250-500 pm V^{-1}, resulting in an effective displacement from the material that is approaching the millimetre scale. However bulk materials are of significant use when used in detector/sensor applications.

Multilayer devices allow operation at lower voltages while also being capable of displacements in microns and millimetres, far exceeding the capabilities of their bulk counterparts. The increased displacement comes about because of the multilayer structure; with bulk the displacement that is possible at any field is equivalent to $E \times d_{33}$. For a multilayer device, the piezoelectric effect is accumulated by the action of all the active layers of the structure making displacement equivalent to $n(E \times d_{33})$ where n is the number of active layers (Figure 18). This is further aided by the exceptional layer thinness (typically 10-80 μm[6]) resulting in a comparatively low applied voltage equating to a large applied field thus leading to a device displacement typically well into the millimetre region as opposed to hundreds of microns, with further mechanical amplification possible.

Fabrication of multilayers is done on industrial scale, outlined is a methodology employed by Noliac A/S.

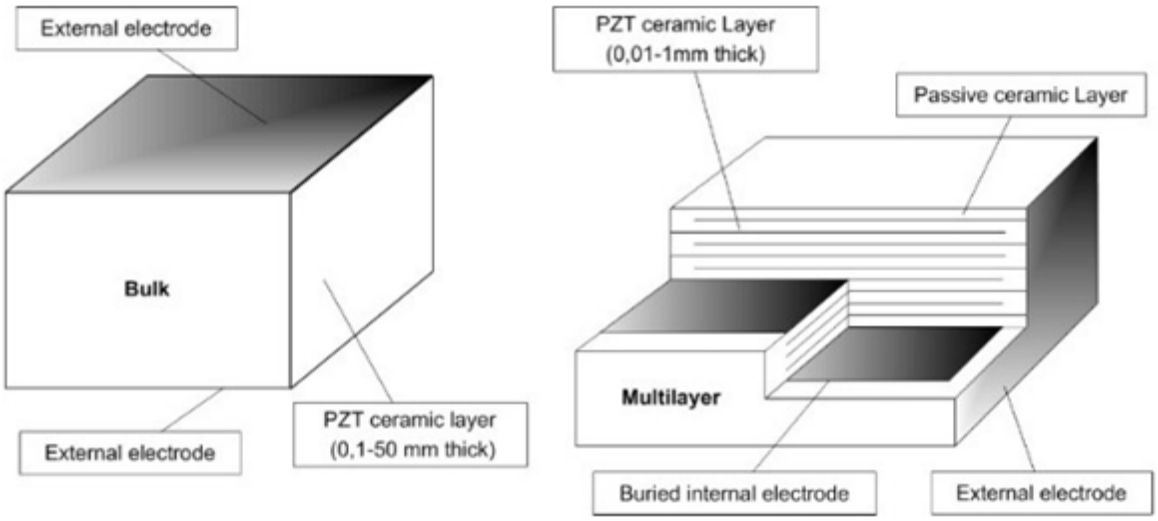

Figure 18: Comparison between bulk/monolayer ceramic and multilayer ceramic devices.[6]

For the following example PZT will be used as the material being synthesised.

Initial fabrication steps are identical to those for producing a bulk ceramic, namely;

- The mixing of raw materials (PbO, ZrO_2, TiO_2 and any additives if needed) by use of dry mixing followed by a wet mixing regime using a ball or attrition mill
- Drying of the slurry, followed by sieving
- Calcination typically 2 hours at 900-1000 °C

Following preparation, the synthesised powder is mixed with various organic additives and solvents to aid stability of the suspension which is consequently milled to ensure homogeneity. Post-milling the viscosity of the organo-powder slurry is evaluated prior to tape casting. The measurement of viscosity is a quality control measure used by manufacturers to ensure that during the tape casting process the slurry is not too viscous resulting in a very slow casting, nor has a low viscosity leading to material run-off and poor thickness control.

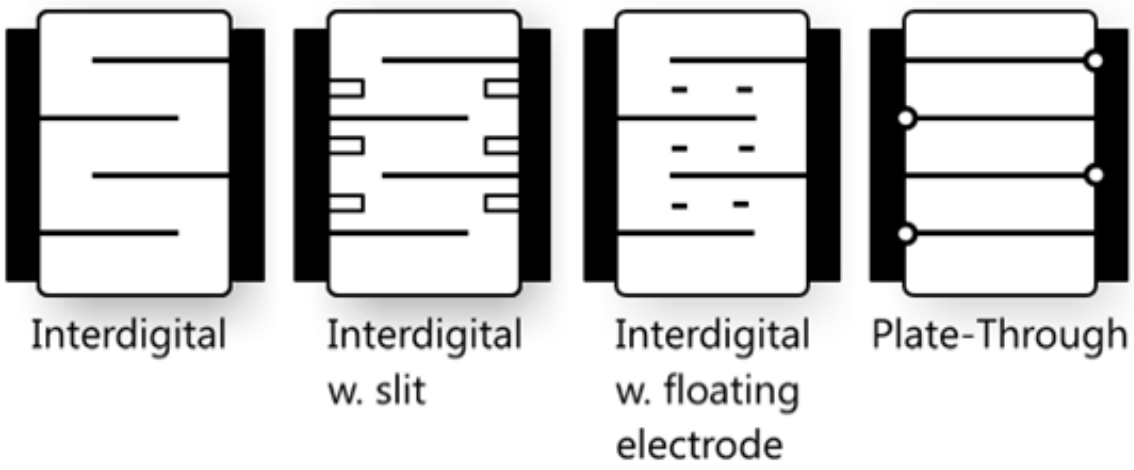

Figure 19: Electrode configurations for multilayer ceramic actuators.

Once the slurry is verified as being correct for production, it is deposited onto a rolling cellulose-acetate sheet, with thickness controlled by a movable doctor blade (Figure 20). The tape is then stripped from the carrier sheet and cut into pieces in anticipation of multilayer build-up to form one of several possible structures (Figure 19).

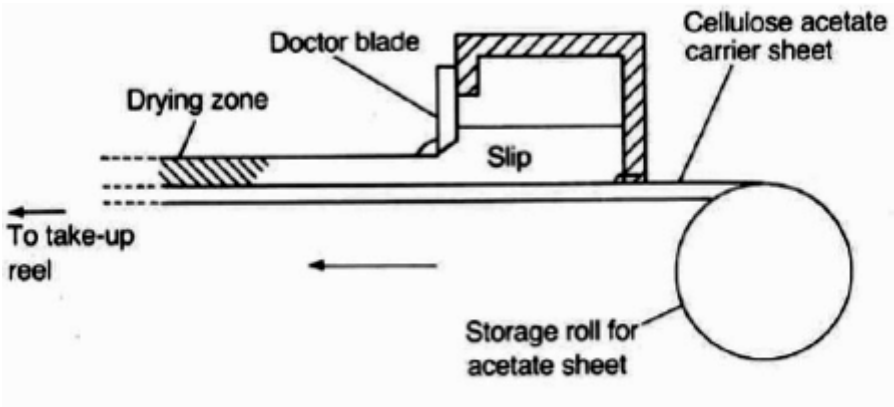

Figure 20: Schematic representation of tape casting apparatus.[6]

Build-up is a cyclic process, following the cycle:

This cycle is repeated until the device is built-up to the desired specification, after which

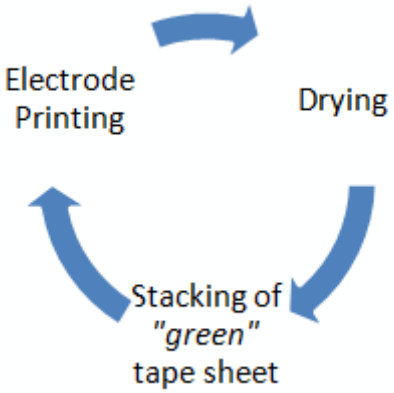

Figure 21: Tape casting multilayer fabrication cycle.

the layers are uniaxially pressed to promote adhesion and heated above the glass transition temperature of the binder. Samples are then cut from this block, binder is burned out by slow heating (up to 500-700 °C), and sintering takes place (1200-1300 °C for Pt electrodes, 1000-1100°C for Ag/Pd) in a protective atmosphere prior to external electroding to make electrical contact possible, lapping and finally poling.

2 Rayleigh Behaviour

As previously discussed (Section 1.3.2), typical behaviour expressed by piezoelectric materials is that of a hysteresis response to applied stresses and electric fields, an effect dominated by non-180° domain wall motion. However, at low stress and field values, the material response can be observed as almost linear - established results show the theoretical behaviour of ferroelectric ceramics at weak-fields to be analogous to that of magnetic susceptibility, where ν is the Rayleigh coefficient, χ_{init} is reversible magnetic susceptibility:

$$\chi(H) = \chi_{init} + \nu H \tag{7}$$

It follows from Eq. (7) that for ferroelectric ceramics, weak-field behaviour follows:

$$d_{33} = d_{init} + \alpha X_{max} \tag{8}$$

where X_{max} is the maximum amplitude of stress applied, d_{33} is the piezoelectric coefficient in the polar direction, parallel to the applied stress, d_{init} is the piezoelectric coefficient at zero stress and α is the Rayleigh co-efficient expressing irreversible domain contributions to the total piezoelectric effect. One key assumption is made when applying this theory to the behaviour of ferroelectric ceramics - that the applied alternating stress is not eliciting a domain volumetric change.

The Rayleigh behaviour of piezoelectric materials is of significant importance as it allows the understanding of how the material will perform in *real world* scenarios where the material may be subject to a variety of static or dynamic mechanical loads and fields.

2.1 Domain Contributions

The domain-wall contributions to the piezoelectric effect have been subject of many studies[21,24,94–99] - initially theorising that these contributions were due to nucleation and growth

of domain walls. Subsequent investigations have exploited Rayleigh behaviour of ferroelectric materials at weak fields/stresses. At subcoercive fields/stresses only small displacements of domain walls takes place, but crucially no switching occurs[a], eliciting a region of linear material response (Figure 22) thus allowing the application of Rayleigh theory to ferroelectric materials – this is particularly important when investigating the causes of fatigue in materials - as it gives an insight to domain behaviour in a non-destructive manner which has little effect on a sample due to the weak-field nature of any applied field or stress. From this it is possible to glean a quantitative description of the two distinct contributions to the observed piezoelectric response – *intrinsic* and *extrinsic* contributions, which are now discussed.

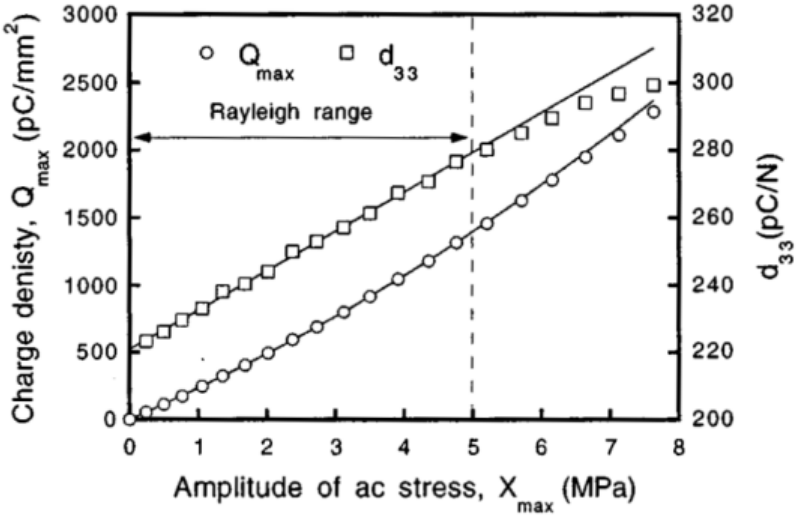

Figure 22: Charge density Q and piezoelectric coefficient d_{33} in PZT-Nb ceramic as a function of AC stress. The Rayleigh region is highlighted by the arrow[100].

2.1.1 Instrinsic Contributions

Instrinsic contributions take the form of polarisation change within the material – this contribution can be observed in piezoelectric materials as all that exists is a lattice polarisation contribution to the measured response, however in ferroelectrics reversible domain motion is

[a] An assumption is made regarding domain volume - there is no volumetric change when subject to these applied weak forces or fields.

coupled with the polarisation change. These coupled contributions are represented by d_{init} in equation 8.

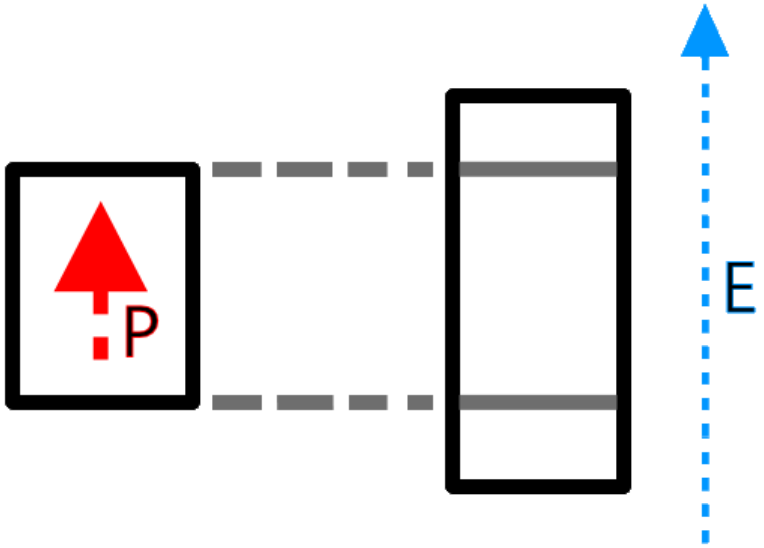

Figure 23: Diagrammatic representation of intrinsic contributions with an applied electric field.

2.1.2 Extrinsic Contributions

Extrinsic contributions are inherent to ferroelectric materials with their domain structure – extrinsic contributions arise from irreversible domain wall motion within the linear *"Rayleigh"* region of response (Figure 22).

However, these two contributors are not independent, Pramanick *et al*[99] further used Rayleigh experimentation alongside time-resolved synchrotron X-ray diffraction to examine the two contributors to the piezoelectric effect: intrinsic – lattice and polarisation contributions, and extrinsic – domain and domain wall contributions) presenting a theory that intrinsic and extrinsic contributions are coupled – i.e. free expression of intrinsic contributions is not possible without domain wall motion or elasticity else the intrinsic contribution is clamped.

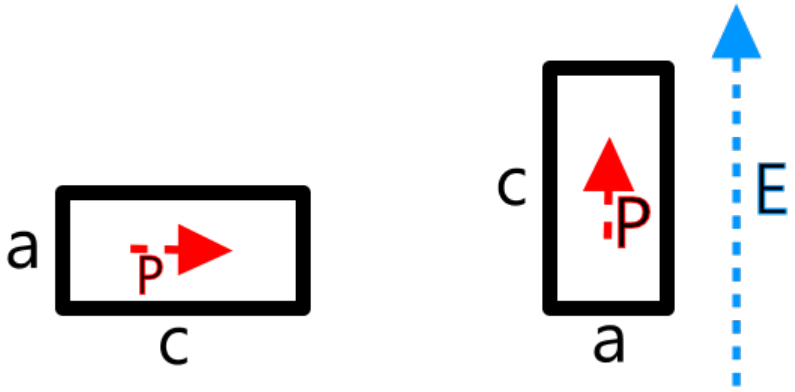

Figure 24: Diagrammatic representation of extrinsic contributions with an applied electric field.

3 Fatigue & Ageing

When working with ferroelectric materials, especially fatigue and longevity studies of the materials, it is imperative to distinguish between the property changes caused by fatigue and ageing. In this chapter, the differences between the two phenomena are discussed with an outlook to minimising the effects of ageing in fatigue studies.

3.1 Fatigue

With new applications emerging for piezoelectric ceramics supplementing the vast range of current applications, and with devices typically operated under cyclic electrical and/or mechanical loading. Typically, fatigue is associated with the resultant effects of these *dynamic* environmental changes a material or device is subject to, resulting in degradation of P_R and P_S, a great deal of interest is being contributed towards characterising the stability and longevity of ferroelectric devices and indeed their failure mechanisms.

3.1.1 Electric Field

Typical lifetimes for thin-film devices were initially in the region of 3-5x10^6 cycles, which when operating at high frequencies is an extremely short usable life, making fatigue a key problem

to understand and overcome for the widespread use of ferroelectric materials in novel applications and environments[101]. Unfortunately, although several models (e.g. electrode-ferroelectric microcracking[102,103] space charge layer formation at electrodes[14,104] and accumulation of point charge defects[105,106]) have been theorised, the exact nature of fatigue remains elusive.

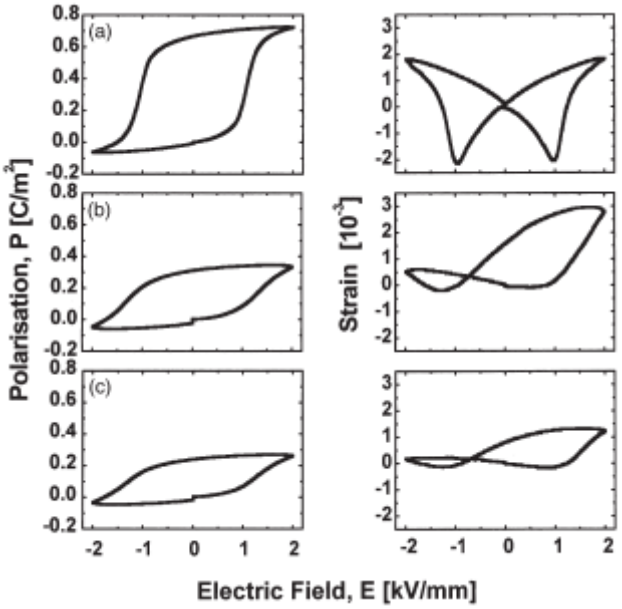

Figure 25: Polarisation-field and strain-field measured for a PZT sample fatigued at 1.96 kV mm^{-1}, 50 Hz. (a) 0 cycles; (b) $3x10^6$ cycles; (c) 10^8 cycles.[107]

By far the most notable indicators of fatigue[107–109] are exhibited in polarisation-field and strain-field measurements, readily observed as a bulk phenomenon expressed as an asymmetrical strain-field hysteresis response and reduced P_R (Figure 25). The primary indicator of this bulk fatigue being the decay of P_R. With different materials and compositions exhibiting, in certain instances[108,110] notably different lifetimes before degradation, material choice is paramount for a reliable device. Understandably the most damage, and macroscopic fatigue, is inflicted upon a material when subject to the most extreme cycling fields; typically those greater than E_C[111,112].

Four stages of polarisation fatigue have been observed thus far for PZT:

1. An incubation stage with a near-constant P_R.

2. Starting at approximately 10^5 cycles, P_R begins to exhibit a logarithmic dependence upon cycle count, with a smaller (circ. 5%) degradation observed for unipolar fatigue[113].

3. A saturation regime.

4. A recovery stage after 10^9 cycles, where the remnant polarisation is rejuvenated[114].

The origins of this decay in performance have been found to arise from one of, or a combination of the following electrochemical and mechanical phenomena:

- Pinning of domains and domain walls by point defects[115], space charges[106,116–118] or oxygen vacancy[119–121], in the bulk[105]
- Formation of conductive corrosion paths from contaminated electrodes[107]

Combined with the capacity for self heating - during high frequency operation monolithic structures in particular generate a significant amount of heat caused by dielectric loss[122–125] capable of a temperature delta of 90 °C in as little as 200 seconds (Figure 26), an accurate appraisal of the fatigue methodologies in effect can become difficult as other effects, in this case thermal depoling, cause reduction in pizeoelectric activity and material response.

3.1.2 Electrode Chemistry

Point defects, given their charged nature, have been commonly found to diffuse through a ferroelectric when subject to electric fields in excess of E_C. However it is highly unlikely that a solitary point defect will be sufficient to prevent domain wall movement, suggesting that agglomerates of the aforementioned defects are required to cause domain pinning.

The entrapment of defects is fuelled by the decrease in potential energy experienced at grain, domain and ferroelectric-electrode boundaries[126,127] where such interfaces form Schottky barriers where metallic electrodes are employed. Thus with a large proportion of defects occurring at metallic electrode surfaces, investigating the effects differing electrode material has on fatigue response has become a focus of research.

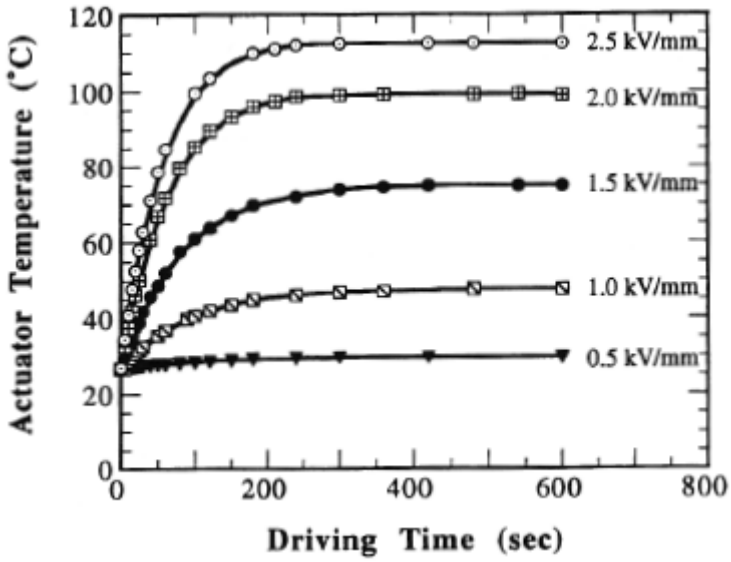

Figure 26: Heat generation of a PZT multilayer actuator while driving under differing electric fields at 400 Hz[125].

Understanding the interfacial characteristics of the ferroelectric and electrode highlight the differing work functions, as well as the mismatch in lattice constants, suggesting that if an electrode material with a lattice constant and work function similar to that of the ferroelectric was used, a reduction in point defect agglomerates would be observed, contributing to an increased device lifetime.

Considering the potential impact of the ferroelectric–electrode interface, various investigations[117,128,129] into the suitability of ceramic electrodes for increased lifetime of piezoelectric devices have been conducted in thin film materials, highlighting p-type oxide electrodes; ruthenium oxide (RuO_2)[130], iridium oxide (IrO_2)[131], strontium ruthenate ($SrRuO_3$)[132,133] and (textured) $LaNiO_3$[134] as plausible replacements to conventional metal (Pt, Au, Ag) electrodes. The results of work by Vijay and Desu[117] highlighted the influence of electrodes on lifetime (Figure 27) with ruthenium oxide-electroded PZT far outliving its platinum counterpart. This increased lifetime was attested to the increased interface stability between electrode and ferroelectric when RuO_2 is used, allowing the migration of oxygen vacancies into the electrodes. Although the use of RuO_2

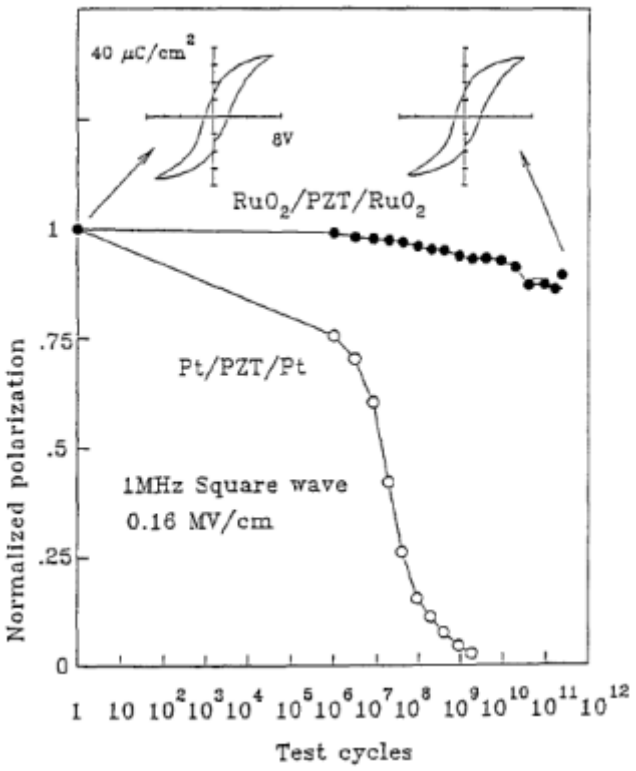

Figure 27: Comparison of fatigue properties of PZT films on Pt and RuO_2 electrodes.[117]

is not without its pitfalls particularly the characteristic of an undesirably high leakage current, these can be overcome by using an alternative synthesis routes to conventional solid-state processing[135].

However, the applicability of differing electrode species when considering bulk and multilayer structures is debatable – the Schottky barrier formed by the workfunction mismatch between PZT and Pt electrodes is less of a problem when the driving field is as large as when driving bulk structures.

3.1.3 Point Defects & Agglomerates

Describing fatigue in ferroelectrics is a difficult task, with many different phenomena contributing to the macro-scale observable fatigue response, we must start looking at point defects in the

unit cell of the ferroelectric.

Point defects do not match the electronic structure of the rest of the material they occupy, and when polarised are capable of altering the polarisation and electronic behaviour (eg. band gap) in their vicinity, and the loss off ferroelectric behaviour of the host unit cell due to an inability for polarisation to reorientate with an applied field. However, point defect effects are not only evident after cycling the material - they are also involved in the poling process, contributing to the overall energetic stability and possessing some control on the energetic minimum occupied post-poling. In the instance of the defects being charges, subject to an applied field, agglomerates occur - due to field-induced migration across a diffusion gradient within the domains of the ferroelectric, interacting heavily with the domains of the host material[136]. This interaction leads to pinning of the domain walls, inhibiting domain switching[137].

Oxygen Vacancies

Oxygen vacancies have an influence on fatigue behaviour, an understandable observation given that oxygen vacancies in PZT are the most mobile defect present at room temperature[138,139].

Initial theory concluded that superoxidation during material processing was occurring leading to degradation of electrode surfaces when subject to an AC field, resulting in Schottky-type defects caused by vacancy pinning - leading to electrode degradation and evolved oxygen[140]. This remarkable observation of evolution of oxygen from the surface has since been dismissed as incorrect[121], but not without substantiating the theory of point charge agglomerates being the dominant source of fatigue[141]. Although there is widespread consensus regarding the influence of oxygen on fatigue[120], its influence with respect to bulk material is ample source for debate.

3.1.4 Microcracking

Chemistry and electronic configurations are not all that can elicit fatigue in ferroelectric materials subject to alternating fields. Obviously, when subject to an applied field a ferroelectric material goes through a dimensional change, imparting a strain. This strain is not only macro-

scopically evident, but evident in the microstructure - with cracks in the same dimensionality as the domains.

As evident from previous discussion, various studies have been conducted on field-induced fatigue in ferroelectric materials. Study by Liu *et al.*[142] utilised liquid indium electrodes on PZT thin films to investigate the inter-domain interface before and after cycling - their findings suggested that the strain mismatch at the interface of 90° domain walls led to the formation of microcracks, later branching along the walls to form microcrack tree structures and leading to an irreversible loss in polarisation. Similar structures were observed by Lupascu and Rabe[143], but were interpreted as point defect agglomerates. Further structures have been observed[144] and their formation attributed to crack formation as a result of dielectric breakdown.

The question arises, what causes microcrack formation and growth? Is the crack formed by dielectric breakdown in sufficiently porous ceramics leading to arcing and the violent formation of the crack from this discharge event, or is the crack formed as a direct result of the strain and only propagates due to discharge across the crack.

In order to answer this question, an examination of the effect of large and small electrostrictive coefficients on field-induced strain needs to be considered.

3.1.5 Mechanical Stimulation

As early as 1955[145], it was understood that static stress can be detrimental to piezoelectric materials causing partial, and in extreme cases complete depolarisation, this subsequently led to numerous studies of PZT behaviour under stress and its effect on piezoelectric activity. One indispensable and accomplished study conducted by Berlincourt *et al.*[146] (1963) showed that a ferroelectric to antiferroelectric phase change was possible in modified PZT (Ti^{4+}, Sn^{4+}) using pressures parallel to the polar axis as low as 4,000 PSI (27 MPa) for compositions with the minimum Ti^{4+} in the B-perovskite position to exhibit ferroelectricity.

The majority of initial research[146,148] focussed on transducer applications, but had limitations due to a lack of understanding with respect to mechanical boundary conditions at the

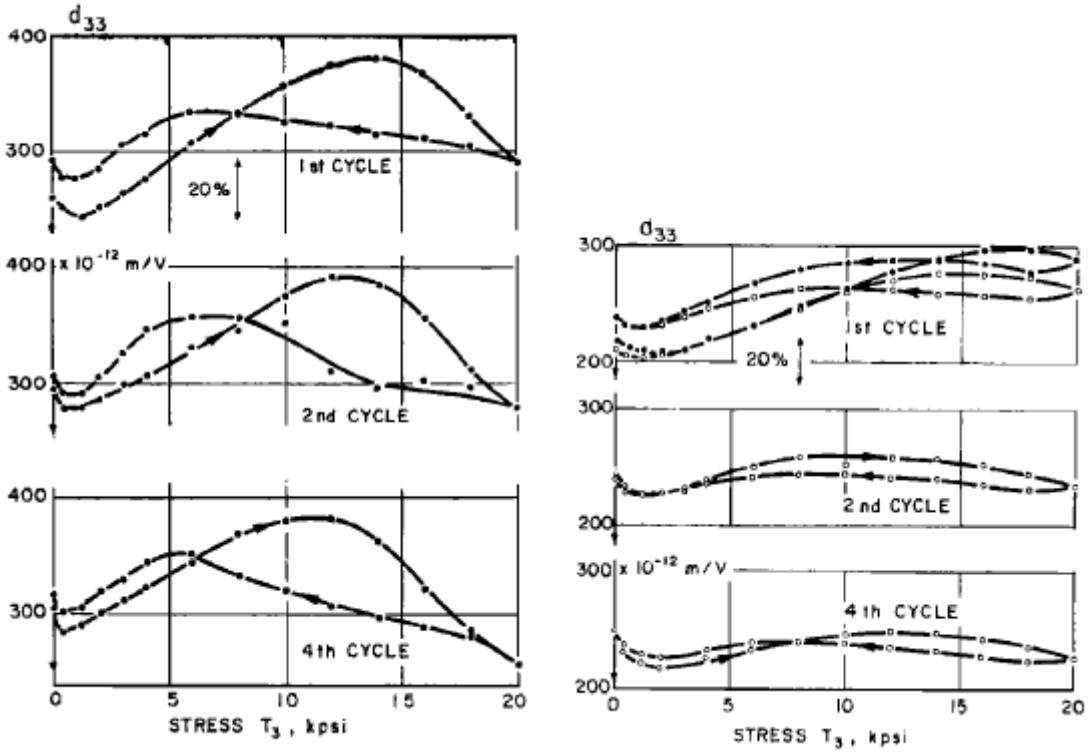

Figure 28: d_{33} as a function of parallel stress for PZT-4 (left) and PZT-8 (right) at first, second and fourth cycles.[147]

time. Current understanding is such that the piezoelectric non-linearity is derived from contributions from both intrinsic contributions (single domain response) and extrinsic contributions (domain wall motion)[7,149]. With extrinsic contributions accounting for up to 50% of the dielectric response[150] in specific circumstances. However, this is not reason enough to dismiss all initial studies; in 1968 Krueger conducted a study of various PZT compositions, hard PZT-4 & PZT-8 and soft PZT-5A & PZT-5H[147,148], and their evolving sensitivity to compressive stresses applied parallel and perpendicular to their polar axis. The two hard compositions and two soft were respectively found to exhibit similar behaviour whilst subject to pole-parallel loading; both PZT-4 and PZT-8 exhibited large d_{33} percentage changes (Figure 28) and adequate recovery, with enhanced piezoelectric activity observed under low cyclic loading (Figure 29).

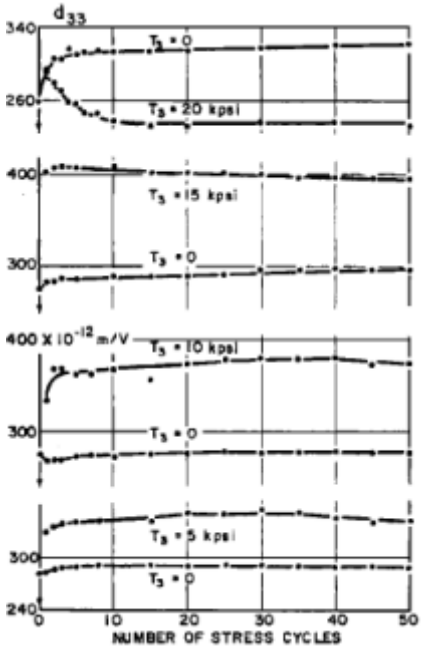

Figure 29: d_{33} as a function of number of cycles for various peak compressive stresses on PZT-4.[147]

While PZT-5A and PZT-5H exhibited initial stages of depolarisation (Figure 30) at loads as low as 55 MPa (5A) and 17 MPa (5H) and no enhanced activity with low-load load cycling. The conclusions derived from the investigation, although very general, still hold valid today with

more recent investigations[151–154] increasing in sophistication - employing the likes of external actuation to better aid load control, yet have yielded similar results to those from almost forty years ago: enhancement in piezoelectric activity observed under uniaxial clamping (Figure 31 & 32)[155].

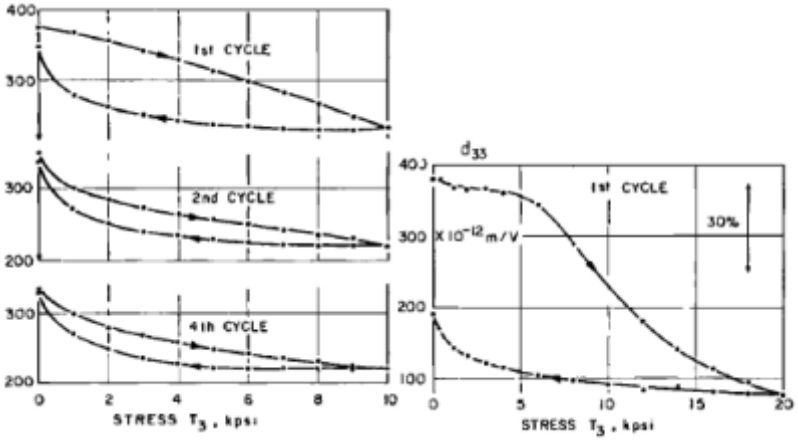

Figure 30: d_{33} as a function of parallel stress for PZT-5A.[147]

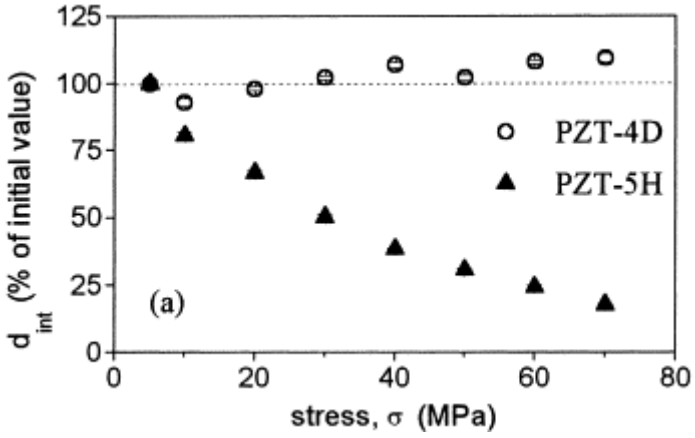

Figure 31: Change in the piezoelectric parameters after static loading as a function of the applied stress.[156]

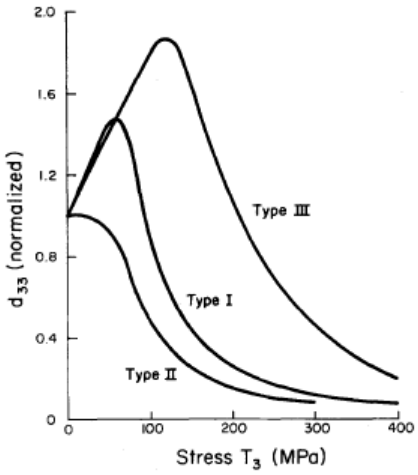

Figure 32: Effect of sustained one dimensional stress on d_{33} of type-I, -II and -III PZT.[155]

3.2 Ageing

In the most restricted sense of the term, ageing in poled ferroelectric ceramics produces changes in material properties which unlike fatigue, take place without the influence of an applied field, stress or temperature change, but rather with the passage of time[2] under *static* environmental conditions. This phenomena, typically associated with the reduction of domain wall mobility, can be investigated quite readily by virtue of changes in observed hysteresis behaviour exhibited as a *"pinched"* strain-field loop (Figure 33) and loops in the absence of a DC bias appearing offset[157].

An interesting observation by Jonker[158] revealed that ageing in 95% $BaTiO_3$–5%$BaZrO_3$ could be *"reset"* by heating the material above T_C into the tetragonal phase for a sufficiently long time - short periods spent above T_C are theorised to be insufficient for the polar direction change from (100) to (110) to take place, further corroborating theory pertaining to restriction in domain wall motion as the culprit of ageing. Further investigation[98] with new techniques exploiting linear material response to applied fields (Section 2) have conclusively shown that domain wall pinning is the contributor to ageing in ferroelectric ceramics (Figure 34).

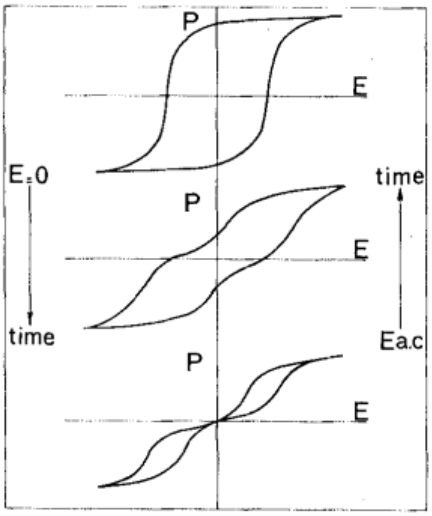

Figure 33: Ferroelectric hysteresis loops showing increased constriction upon ageing in barium titanate[158].

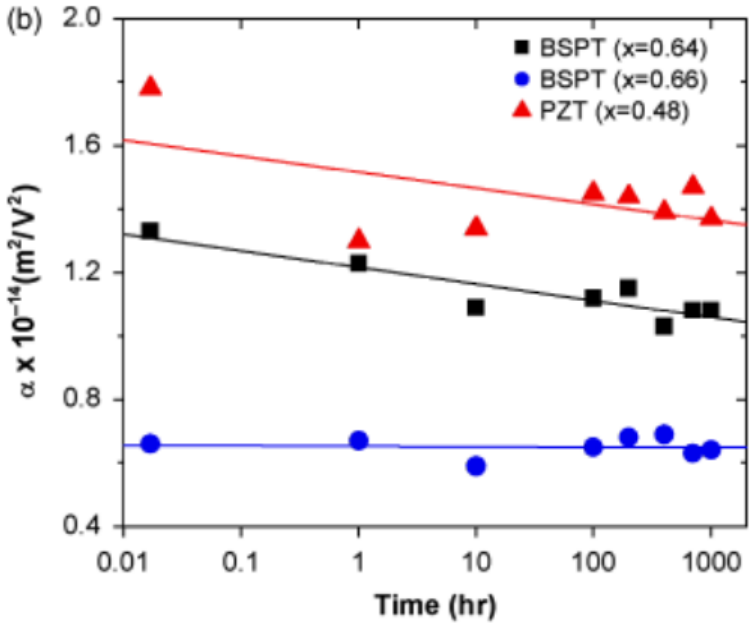

Figure 34: Evolution of domain mobility (α) in BSPT and PZT compositions evaluated by weak-field Rayleigh methodology[98].

3.3 Review

The most prominent feature of merit when dealing with ferroelectric materials is to be certain of what fatigue and ageing are - although both effects can manifest in similar behaviour, the underlying cause can be wildly different.

For fatigue investigations, it is of paramount importance to limit the skew in data that can be achieved as a result of the material ageing considerably. Current trends suggest that 48 hours is sufficient for the majority of ageing to be complete and reliable experimentation be viable - almost all papers report samples left dormant at room temperature for 48 hours before use, with this general consensus regarding ageing, we can draw attention to fatigue investigations.

At first glance there appears significant literature regarding ferroelectric fatigue[b], however there is little in the way of investigating fatigue in multilayer or bulk structures, with reported data concentrating on fatigue behaviour of thin films - current electrode-derived fatigue literature is focussed on the response of thin films, particularly PZT, to novel electrode species, making information ultimately speculative with respect to electrode influence on bulk ferroelectrics, let alone any specificity arising from a particular material system. Considering an understanding of fatigue is critical in the use of ferroelectric materials in any application it seems bizarre that there is little published on fatigue of these heavily used multilayer and bulk configurations, although there is no doubt that commercially sensitive data on these structures exists, their lack of publication is a detriment to the field. Granted thin film fatigue is important with regard to the likes of FeRAM and other ferroelectric data storage technologies, but the use of ferroelectric materials is only recently delving into the micro and nano-structured realm. Furthermore there are many factors contributing to fatigue, some dependent on processing, electrodes etc. - therefore it is difficult to select one key contributor to fatigue as there are so many variables which combine to give differing fatigue responses.

Considering what has been discussed in the prior literature review section, the focus of the research presented henceforth is that of examining the mechanical properties of the BFLPT

[b] 2,606 articles as of 12^{th} April 2013 - Web of Knowledge database search

system under various cycling stresses and fields independently, and comparing these results to the behaviour of equivalent PZT materials.

4 Piezoelectic Materials Test Apparatus

For the likes of fatigue and ageing to be investigated in ferroelectric materials, be it in multilayer or monolith form, the capability to mechanically fatigue the materials and measure them was assessed. As a result of this, the creation of a testing apparatus was deemed necessary – an experimental setup capable of applying a cycling mechanical stress, at temperature while also possessing a modular design to permit augmentation for future experimental requirements. This section discusses the design requirements and objectives of the apparatus, as well as addressing concerns arising from mechanical testing of ferroelectric materials.

4.1 Operating Principle

By investigating material degradation as a function of applied stress and temperature, the key operating principle of the test apparatus is that of the direct piezoelectric effect. By subjecting the materials being tested to a cycling stress, the associated charge produced by the direct piezoelectric effect is measured, alongside a synchronous measurement of the applied stress. The resultant data can be plotted together, giving charge variation as a function of stress - a piezoelectric co-efficient, measured in pC N^{-1}.

4.2 Sample Geometry and Architecture

With mechanical stimulation key in eliciting a degradation of piezoelectric properties[155,159,160], it is of paramount importance before any mechanical cycling can be conducted that not only are the mechanical properties of materials being investigated understood, but the surface properties also.

Several problems arise when mechanically loading a piezoelectrically active sample; dimensional effects[162], mechanical interactions with the apparatus such as clamping effects (Figure 35)[161,163] and contact material[161] all conspire to produce measurements which, in comparison to those from other non-Berlincourt-type techniques, are erroneous. These conditions are disas-

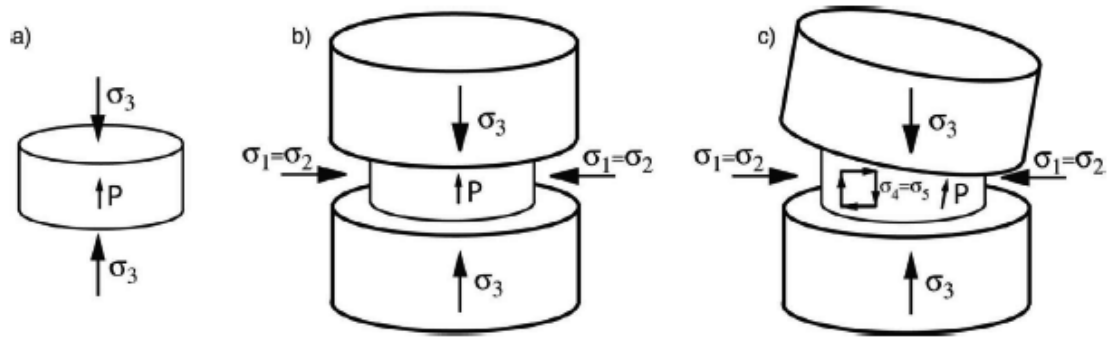

Figure 35: (a) Ideal arrangement for Berlincourt measurements of d_{33}. Only longitudinal pressure σ_3 is present, (b) Due to clamping, lateral stresses $\sigma_1 = \sigma_2$ become significant, reducing the measured d_{33}, (c) Applied stress is not parallel to the poled direction, resulting in both clamping and shear stresses.[161]

trous enough when merely comparing measured d_{33} values, let alone mechanically stimulating materials over many thousands of cycles.

Fortunately, current understanding suggests the discrepancies of these measurements caused by surface contact material and mechanical clamping can be overcome simply by ensuring the material's architecture has a specific dimensionality, originally recommended was having a lateral dimension twice the thickness[163,164], however recent studies[161] have shown that an aspect ratio of at least 1 (Figure 36 & 37) is sufficient. Although highly relevant for understanding fatigue and direct-effect behaviour of bulk piezoelectric ceramics, this is of little significance for multilayer structures where a 1:1 aspect ratio ratio would result in a device that defies convention.

Further to experimental observations of the effects of improper geometries and surface specifications, the British Standards Institution (BSI) and the American Society for Testing and Materials (ASTM) have outlined standard test geometries for compressive testing of advanced ceramics in BS EN 12290:2005 and ASTM C1424-10. Both standards share a common geometry standard (Figure 38) while 12290:2005 permits the use of a simpler second square or circular geometry (Figure 44), while both 12290:2005 geometries are still applicable for testing at high temperature[165].

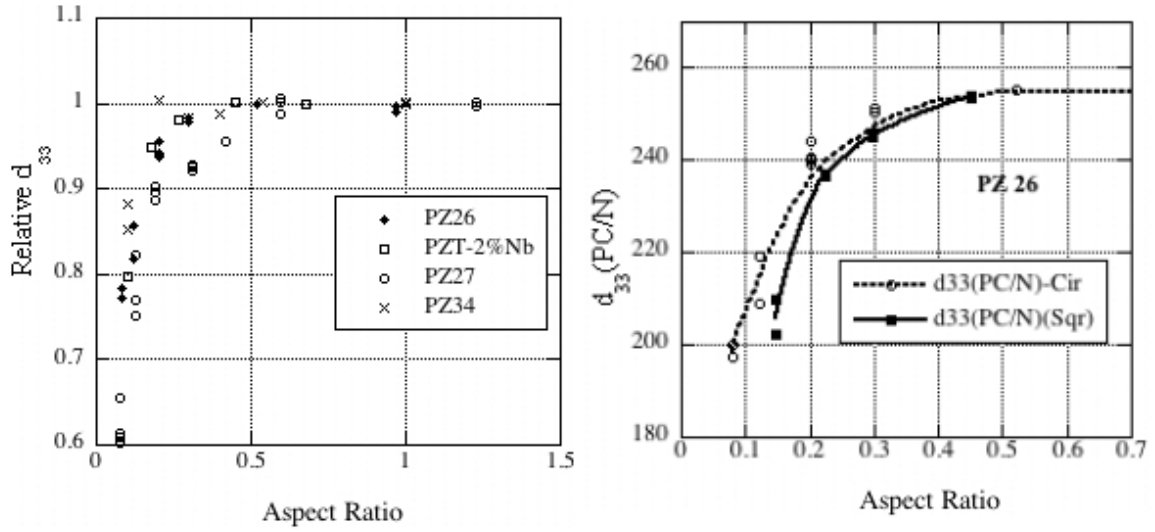

Figure 36: Experimentally determined dependence of; d_{33} on aspect ratio for three types of PZT and a modified PZT ceramic (left) & effect of aspect ratio on d_{33} for different sample geometry (cylindrical & cuboid)[161].

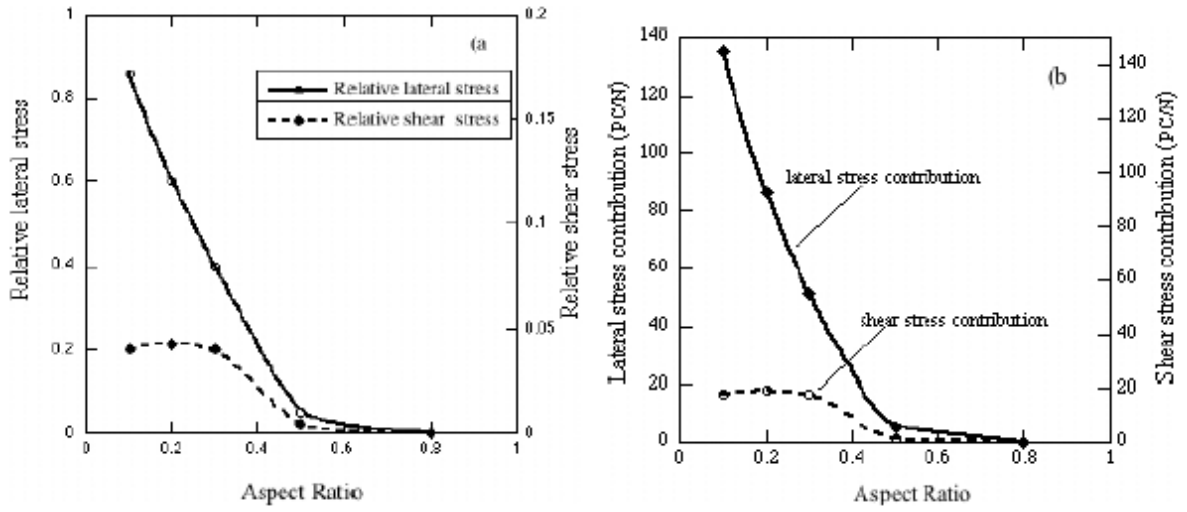

Figure 37: Experimentally determined variations in relative shear and lateral stress (left) and lateral and shear contributions to d_{33} for PZT with a stainless steel metallic contact[161].

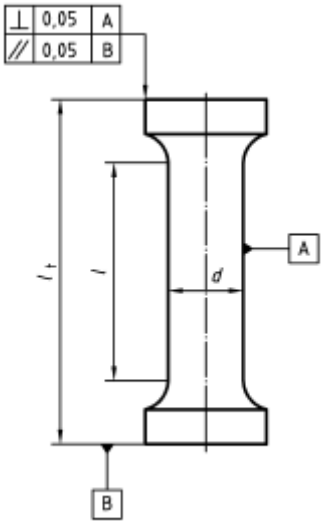

Figure 38: BSI EN 12290:2005 and ASTM C1424-10 shared geometry for compression testing of advanced ceramic materials.[166]

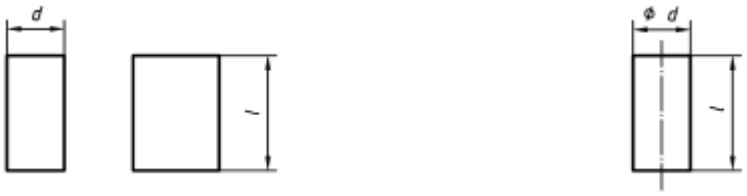

Figure 39: BSI EN 12290:2005 alternative geometry for compression testing of advanced ceramic materials.[166]

4.3 Design Requirements

Several critical design features were realised prior to the final design of the test rig being decided upon:

- Have appropriate fittings to attach to an Instron 3382 frame
- The ability to load samples with minimal shear stresses present
- The ability to heat the sample to 150 °C or higher
- Capacity for displacement transducers for displacement measurements
- Modularity to permit further device augmentation as needs arise

4.4 Designs

4.4.1 Initial Sketch

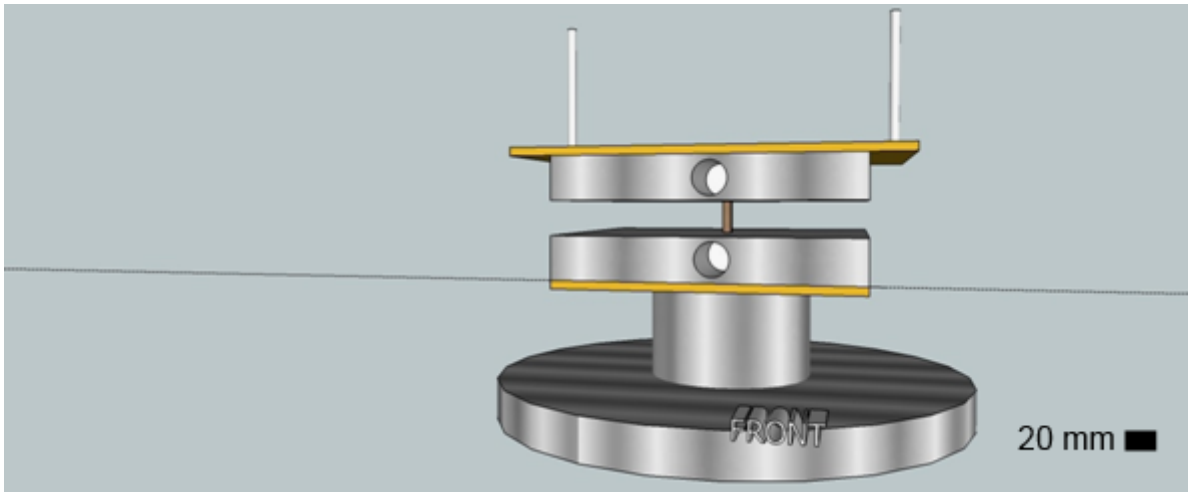

Figure 40: Render of initial design sketch.

The initial design; utilising the pre-existing Instron base and incorporating space for two 20x50mm cartridge heaters, electrical insulation (indicated in yellow) and two optical displace-

ment fibres measuring from the top of the setup. Although adhering to the basic requirements outlined previously, the setup is rudimentary at best.

4.4.2 Design 1

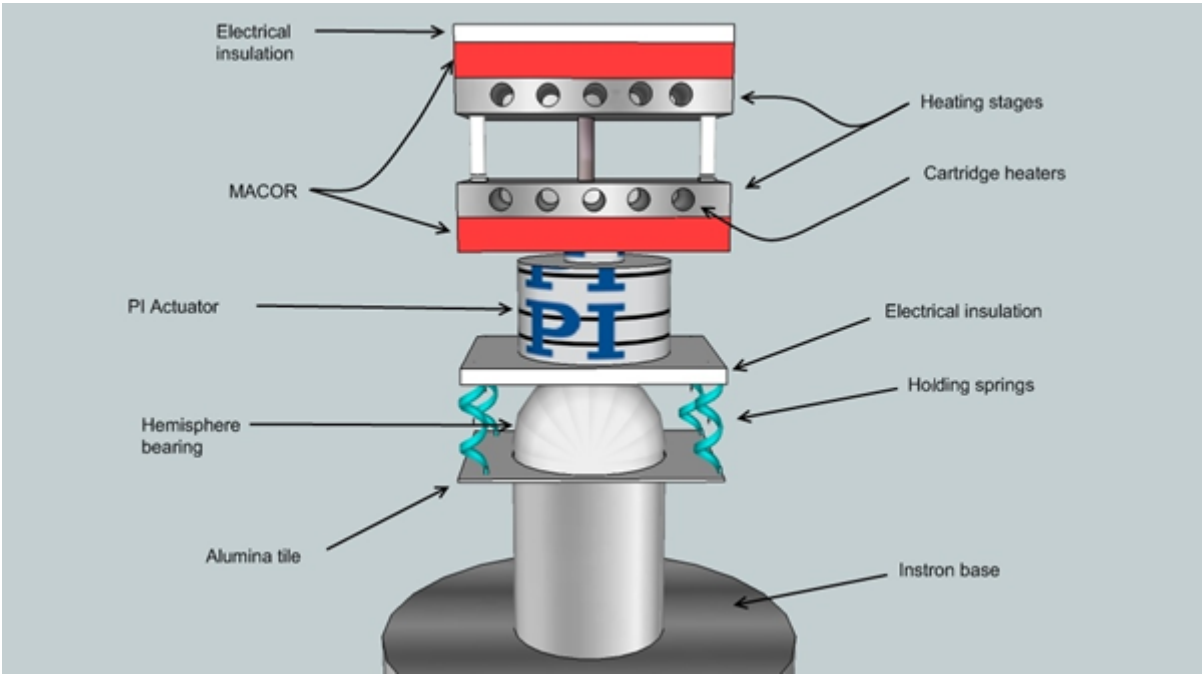

Figure 41: Render of design 1.

By comparison, the first design is considerably more complex than the initial, yet relies upon a compressive load to fix components into position. One key alteration is the incorporation of a hemispherical support near the base as a means of countering any lack of parallel alignment in sample surfaces that would cause a sample to experience shear forces. Several more cartridge heaters have also been added to present a more uniform thermal environment, and the inclusion of a thermal insulation material[c] has been suggested to protect the actuator.

Furthermore, the optical fibres are now encased in thermal insulation material as a protective measure. Much like the initial proposal, this design still requires a compressive load to complete construction.

[c] MACOR

4.4.3 Design 2

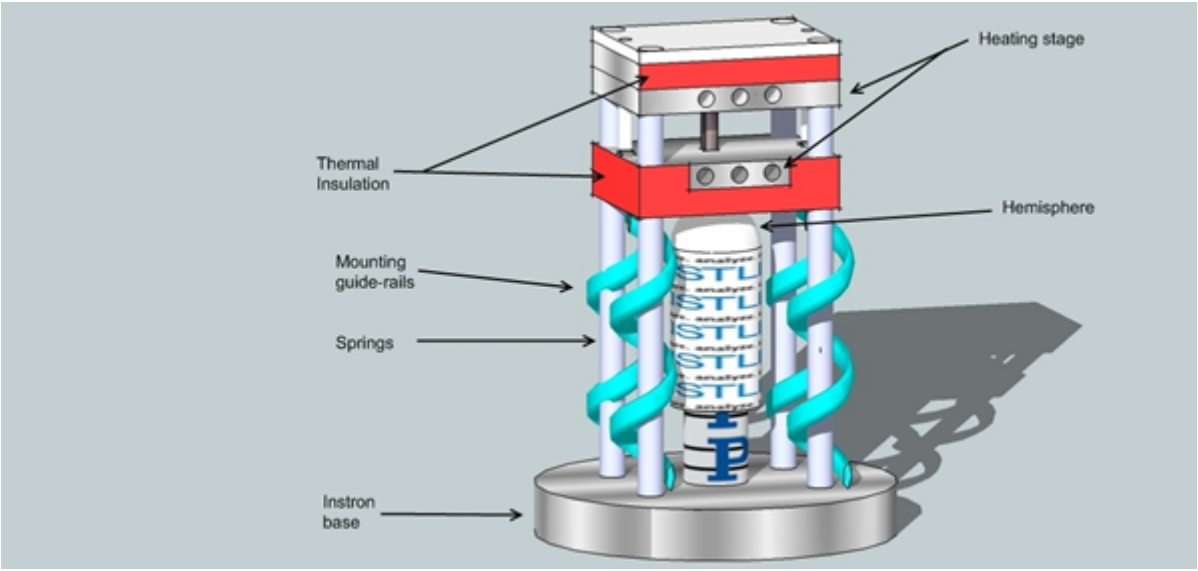

Figure 42: Render of design 2.

As a means to combat the undesirable attribute of prior designs, guiding rails have been incorporated to allow the test stage to be constructed easily and without risk of collapse. Furthermore in addition to the actuator introduced in Design 1, a load cell[d] has been added as an alternative to using the Instron load cell for data collection, with the hemisphere for parallel loading moving further up the setup.

4.4.4 Design 3

Design four, an evolution of Design 3, is significantly more robust in its nature. Evolutionary changes comprise of:

- Increased number of guide rails
- Removal of rail-springs

[d] 9341B Load Cell, Kistler, Winterthur, Switzerland

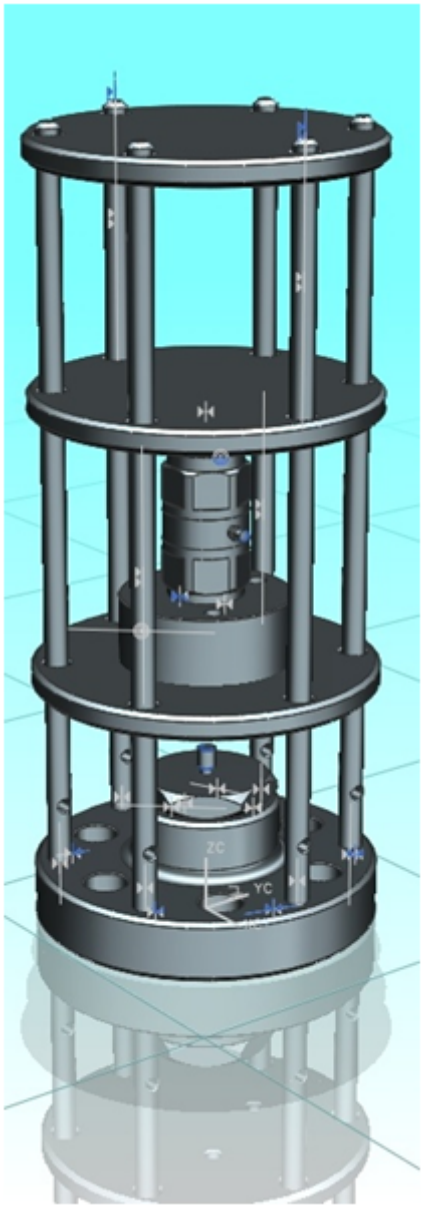

Figure 43: Render of design 3.

- Use of a commercially available load distribution cap attachment for Kistler load-cell in addition to a retention flange
- Threaded attachments for all components to counter any systemic slack; Kistler load-cell, PI actuator

Additionally, investigation into suitable steel grades was undertaken to alleviate any experimental error that may occur as a result of damage to the testing stages from bearing compressive loads. Samples of 303, 316, 431 and 17/4PH steels were procured and tested. Testing consisted of polishing the surface to a smooth finish and using material testing apparatus to compress the load distribution attachment for the load cell into the steel at loads corresponding to the pressures that samples are to be tested to, the surface was then examined for damage and recorded.

All samples except 17/4PH exhibited dimpling, with indentation size directly proportional to compressive load. This is of significant importance as at large loads the sample is expected to displace in the region of tenths of microns, if the surfaces are allowed to deform, the deformation will act as a slack in the system and absorb this displacement - making them unsuitable for high load scenarios. Furthermore 17/4PH poses certain difficulties during machining, increasing the cost of 17/4PH parts dramatically, as such the material is not preferred for creating whole components from.

4.4.5 Final Design

The final design is a steady evolution of design 3, adding several refinements and functionalities.

Platen guide rails

Stage platens are now guided by linear bearing bushes[e] selected to allow smooth motion of the platens when operating the rig at ambient and elevated temperatures utilising corrosion-

[e]Rexroth R065822030, Bosch Rexroth AG, Robert Bosch GmbH

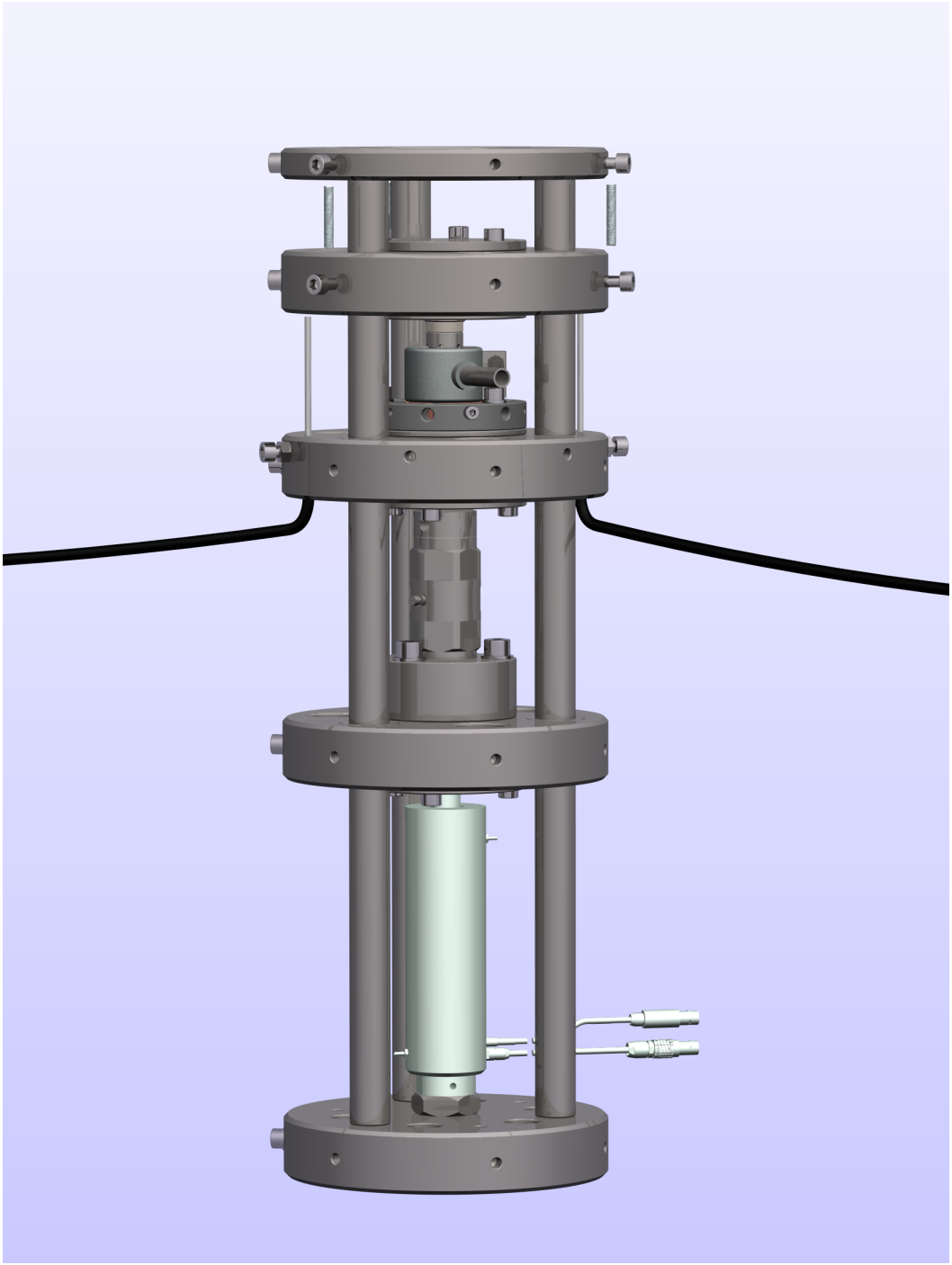

Figure 44: Full view, raytraced render of the final stage of the PTR development incorporating the heater attachment.

resistant anti-friction bearing steel to ISO 683-17/EN 10088. An addition, a locating ring at the top of the rig has been added to ensure guide rail alignment.

Table 5: Specification of linear bushings.[167]

Operating Range (°C)	Velocity (ms^{-1})	Acceleration (ms^{-2})	Breakaway Force (N approx.) .
-20 to 100	5	150	6

Optical displacement probes

Optical probes[f] are finalised as the sensor of choice for strain field and deformation measurements due to their exceptional performance:cost ratio outperforming equivalent cost laser, eddy current and LVDT displacement transducers. Six possible mounting positions for the probes are available to accommodate for any future modification to the apparatus, with an under-cut insert to allow for adjustment such that the probes are within the correct operational distance margins (Figure 45). The probes use an 880 nm LED with a resolution of 20 nm at 20 kHz, possess a continuous tip operating temperature range of -55 to 175 °C[168], far exceeding the operating temperature of the steel platens when the heater attachment is in use, and contain ambient light rejection eliminating interference that may be caused by external lighting around the apparatus.

Sample stand-offs

Sample stand-offs consisting of a zirconia[g] stand (10mm ϕ, specification Table 6) embedded in one of two 316L stainless steel structures bolted centrally to the apparatus as electrical isolation for the sample, while also permitting a sample height of 2 or 8 mm (Figure 46).

Heater attachment

A key design parameter of the rig is the ability to heat samples. Thanks to the modular nature of the final design, a heater can be attached with relative ease and minimal modification.

[f] D63 analog sensor with ambient light rejection, Philtec Inc.
[g] Y-TZP (Yttria-stabilized polycrystalline tetragonal zirconia), Dynamic Ceramic, Crewe, UK

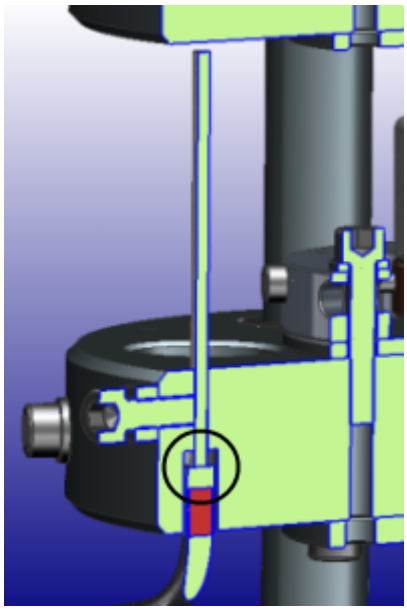

Figure 45: Close-up render of the positioning of optical probes (black circle highlight) in the final design.

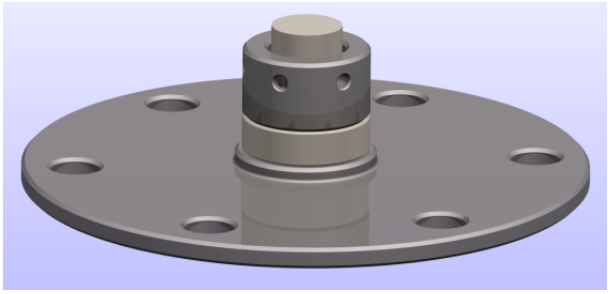

Figure 46: Close-up render of the sample stand-off in the final design.

The attachment is comprised of (Figure 48):

- Zirconia insulation discs to thermally isolate the assembly from the rest of the rig and aid sample heat-soak[h]
- Further Zirconia stand-off for further thermal isolation from the rig
- Electrode stub (316L stainless steel) to allow an electrical connection to samples with electrodes as contact surfaces
- Copper thermal conduction cores to aid heat transfer between the heater and the sample base
- Solid steel sample base with radial threaded holes for electrical connection and thermocouple placement
- Mica insulated band heater[i] rated to 150 W, 5.89 W cm^{-2} controlled externally

Table 6: Specification of Technox 1000.

Hardness	Compressive Strength (MPa)	Thermal Conductivity (Wm^{-1} K)
1400	2000	2

Sacrificial plates on contact surfaces allowing for modular test areas and the removal of the heater attachment when not required as well as replacement of damaged surfaces at a later date with plates machined from 17/4PH steel.

Earthing points on all stages as a safety precaution in the event of sample arcing earth ribbons connected to the earthing point available on the 3382 frame.

[h] Technox 1000, 3Y-TZP, Dynamic Ceramic, Crewe, UK
[i] MBH-1210150B/120, Omega Engineering Ltd

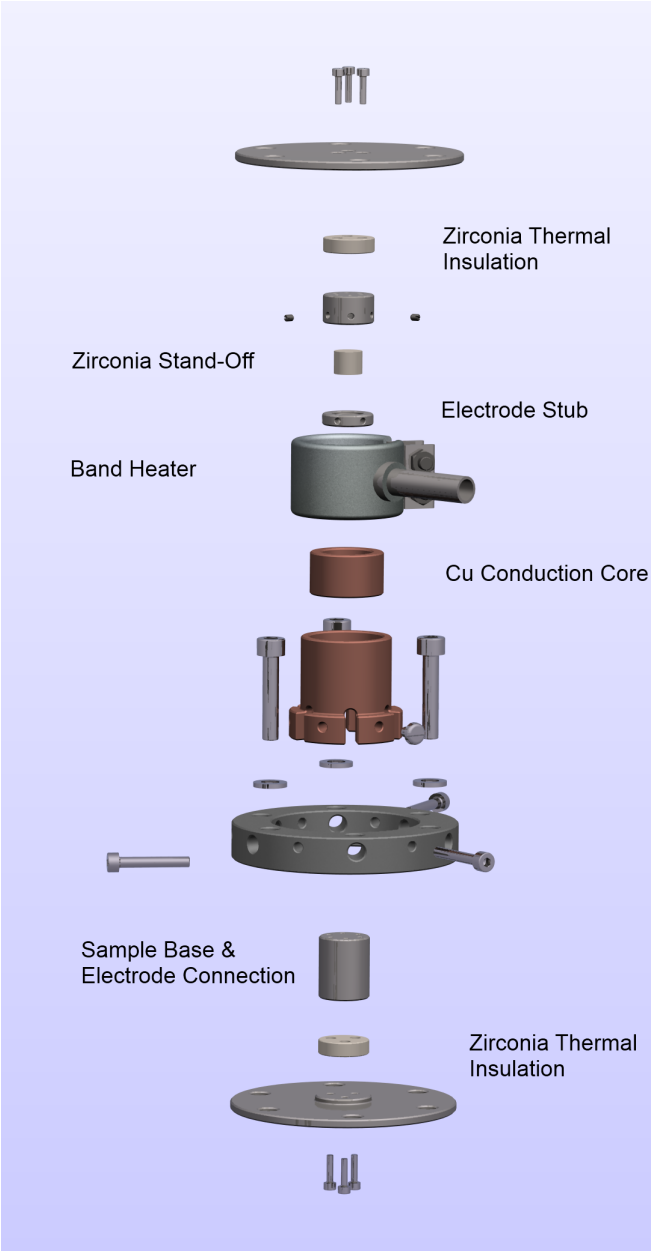

Figure 47: Exploded render of the heater attachment components.

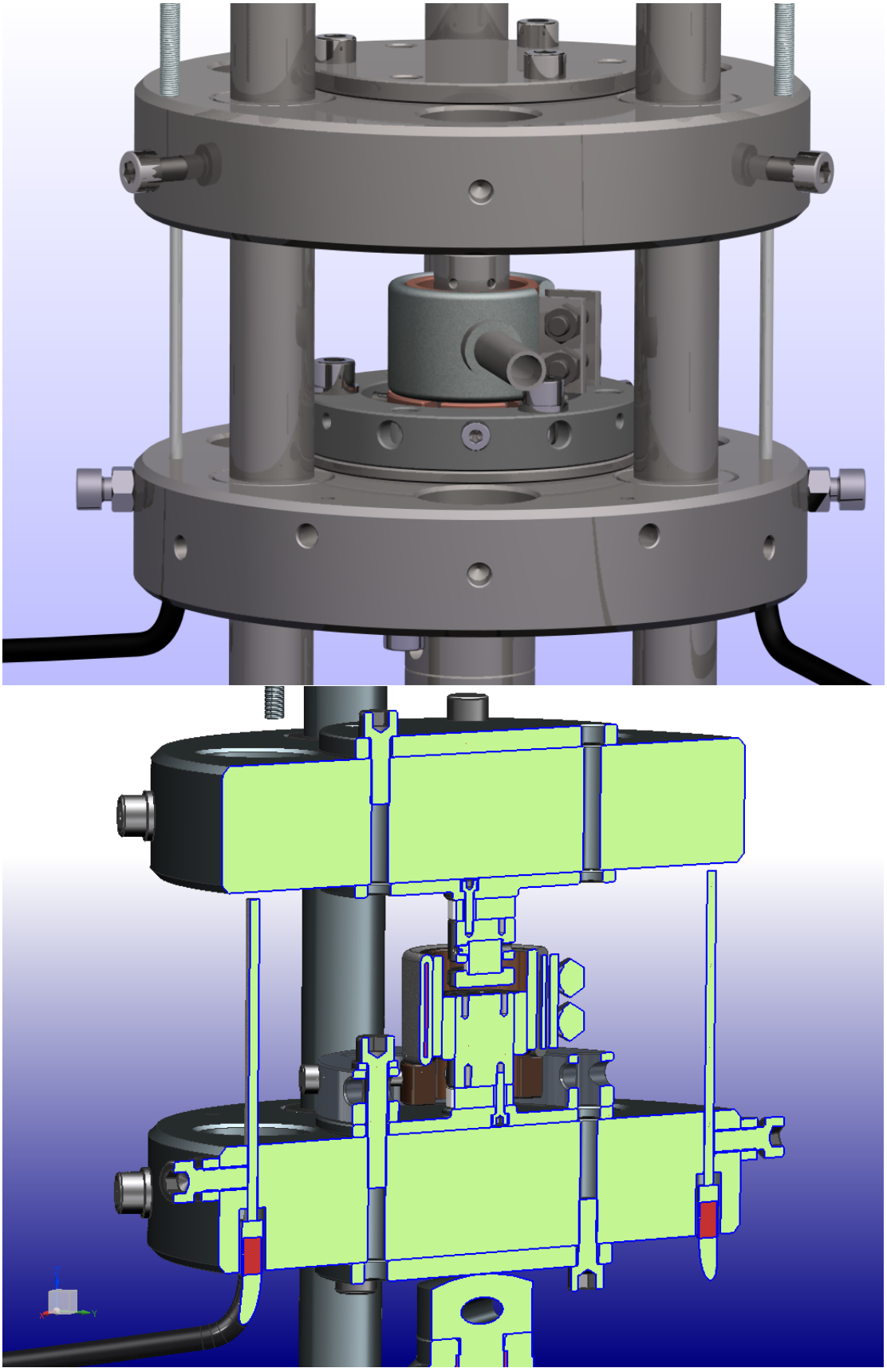

Figure 48: Heater attachment and cross-section.

4.5 Control and Data Acquisition

For the control and data acquisition of the apparatus, two solutions are employed.

Bluehill

Data collection and system control of the Instron is handled by the supplied Bluehill software package as no outside control is possible using the Bluehill API.

LabVIEW

The LabVIEW environment was selected for the inherent robust architecture, multithreaded operation, versatility and the capability to handle large amounts of data along with rapid signal acquisition and generation rates. Acquisition is handled by a cDAQ 4-slot chassis using a USB interface to a host computer, outfitted with:

- NI 9215 card - chosen for its operational range of ±10 V across four input channels capable of a sampling rate of 100 kS sec^{-1}
- NI 9263 card - complimentary to the 9215 this card is capable of ±10 V signal output across four channels with a sampling rate of 100 kS sec^{-1}, aiding synchronisation between output and acquisition of signals
- NI 9211 card - typical thermocouple input module, high accuracy, but with a sampling rate of 14 S sec^{-1} as a fast sampling rate was deemed excessive for thermal monitoring
- NI D I/O card - a digital I/O module for potential requirements to receive or generate TTL (or similar) triggers

Table 7: National Instruments DAQ Configuration

Device	Channel 1	Channel 2	Channel 3	Channel 4
NI 9215	Kistler Load Cell	Optical Probe 1	Optical Probe 2	d_{33}
NI 9263	Actuator Control	Optical Probe 1 Offset	Optical Probe 2 Offset	–
NI 9211	Actuator Temp.	Control Temp.	Sample Temp. 1	Sample Temp. 2

5 Experimental

This section outlines the experimental methodologies used, sample preparations and experiments throughout the research.

5.1 La-doped Bismuth Ferrite Lead Titanate Material Synthesis

3% BFLPT monolithic ceramics were prepared by a conventional solid state reaction method. Laboratory reagent grade oxide powders[j] were weighed in the correct stoichiometric ratios as to fulfil the formula (1-x)($Bi_{1-y}La_y$)FeO_3-x$PbTiO_3$. Once dried overnight, appropriate quantities of powders were attrition milled for 1 hour[k] in 2-propanol, the resultant slurry dried, sieved and calcined at 800°C for two hours in covered alumina crucibles. After calcination, the powders were again sieved, 1% (wt.) methacrylate binder added before a further milling, drying and sieving step. Cylinders were then uniaxially die pressed (2 kN) from the resultant powder before isostatic pressing to 320 MPa. Sintering was carried out in a powder bedded crucible according to a regime of:

- Heating to 500 °C at a rate of 50 °C hr^{-1} (binder burn-off)
- Heating to 1050 °C at a rate of 300 °C hr^{-1}
- Dwell at 1050 °C for 30 minutes
- Cool to 700 °C at 300 °C hr^{-1}

[j] Sigma-Aldrich, St. Louis, USA
[k] Dynomill, WAB, Switzerland

- Cool to room temperature at 50 °C hr^{-1}

The inclusion of a powder bed during final sintering reduces weight loss in pressed powders by virtue of an increased partial pressure of lead and bismuth volatiles.

Once sintered the cylinders were then ground and polished using silicon carbide papers from P320 down to P2500 grit to remove surface contaminants and provide a smooth surface for electrodes. Silver electrodes were painted onto opposite faces of the cylinders, fired-on at 600 °C and polished to a smooth finish with P2500 papers before poling, submerged in silicone oil, at 7 $kVmm^{-1}$ for 1 minute at room temperature with field applied in accordance with BS EN 60243-1:1998.

5.2 Piezoelectric Measurements

As mentioned previously (Section 1.2) the value of d_{33} is defined as the charge produced due to an applied force or the change in force due to an applied field, resulting in two possible ways of determining the d_{33} coefficient of prepared materials; one direct and one indirect. Thanks to the wide range of sample geometries that can be measured, the direct (Berlincourt) method is preferred, in comparison to electrical resonance measurements where the sample must possess an ideal resonance mode to be accurate.

Measurement of piezoelectric coefficients were made by virtue of the Berlincourt method using a commercial meter[l]. The meter operates in a quasi-static mode whereby a small oscillating force (0.05-0.5 N)[169] is applied to the sample and the resultant charge is measured and divided by the amplitude of the applied force to give a measure of d_{33} in pC N^{-1}.

5.3 Impedance Analysis

Impedance analysis was conducted using an impedance analyser[m], controlled over GPIB by the PRAP[n] software package.

[l] PM300, Piezotest Ltd., London, UK
[m] HP4294a, Hewlett-Packard Company, California, USA
[n] Piezoelectric Resonance Analysis Program, TASI Technical Software Inc., Ontario, Canada

5.4 Permittivity-Temperature

Permittivity-temperature (PermT) measurements were possible by use of one of two analogous PermT apparatus setups, controlled in a LabVIEW environment, using one of two impedance analysers[o] applying an excitation voltage of 1 V, temperature measurements were recorded by a thermocouple controller[p] at 30 second intervals.

5.5 Thermally Stimulated Depolarisation Current Measurement of Pyroelectric Effect and Depolarisation Temperature

Mentioned previously (Section 1.3.4), certain materials possess the capability to produce a change in polarisation as a result of heat input (or extraction) - the *pyroelectric effect*.

Measurements of the pyroelectric effect were made using an eletrometer[q] controlled via a general purpose interface bus (GPIB) connection, temperature logging by a USB thermocouple interface[r], and thermal variation by a tube furnace[s] with a heating rate of 10 °C min^{-1}, with acquisition and data capture in a LabVIEW environment. To ensure a stable measurement, the electrometer was left switched on for a minimum of 6 hours before measurements, as recommended by the manufacturer. The collected charge data is integrated over time to give a result correlating polarisation to temperature, allowing the determination of an approximate depolarisation temperature.

5.6 Strain–Field Measurement

Strain–field measurements were possible by use of an experimental setup consisting of an optical fibre displacement sensor[t], data acquisition hardware[u] controlling a 5 kV amplifier source[v]. The

[o] 428XA (10-1 MHz) or 4192A (10-10 MHz), Hewlett-Packard Company, California, USA
[p] TC–01, National Instruments Corporation, Austin, TX
[q] 614 Electrometer, Keithley Instruments Inc., Cleveland, OH
[r] TC–01, National Instruments Corporation, Austin, TX
[s] Pyro Therm Ltd., UK
[t] MTI-2100 Fotonic, MTI Instruments, Albany, NY
[u] Precision LC, Radiant Technologies, Albuquerque, NM
[v] Model 5/80, Trek Inc., Medina, NY

aforementioned devices were controlled by a proprietary software package[w] capable of field signal generation and polarisation hysteresis measurements.

[w]Vision, Radiant Technologies, Albuquerque, NM

5.7 Synchrotron Diffraction

Synchrotron diffraction results were collected on beamline i15, the extreme conditions beamline for studying materials subject to temperature and stress variations, at Diamond Light Source. Samples of material, no thicker than 1 mm were irradiated with X-ray radiation. The advantage of using a synchrotron source for X-ray diffraction is the increased penetration depth - enabling a diffraction spectra more indicative of the material bulk, than the surface interaction observed with laboratory-based X-ray diffractometers.

Material for irradiation was prepared by polishing to give as smooth a finish as possible to prevent any destructive interference caused by interaction with the face of the material. Samples were subsequently submerged in silicone oil and heated using two 35 W cartridge heaters, controlled by a LabVIEW programme (Figure 49).

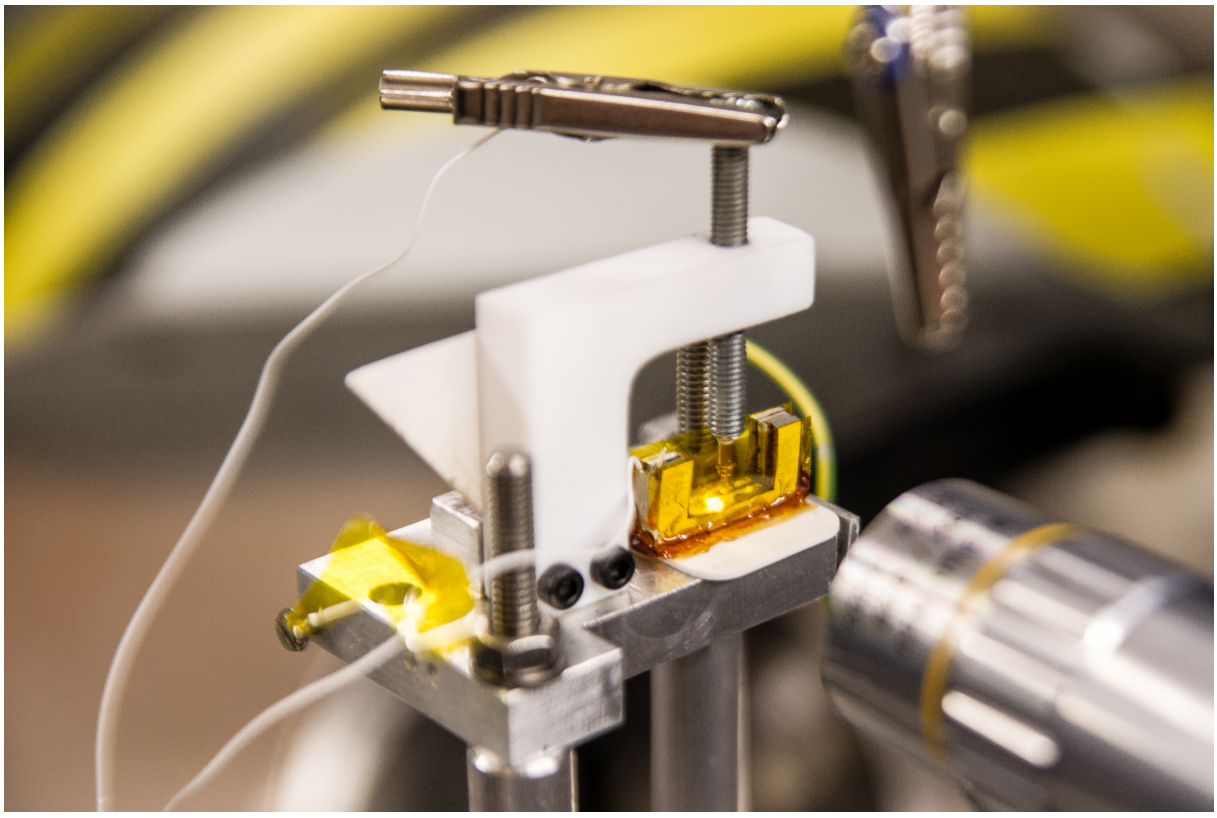

Figure 49: Sample apparatus used at i15, Diamond Light Source.

The resultant exposures were processed in Fit2D to produce spectra that were further analysed in WinPLOTR.

5.8 Fatigue

5.8.1 Mechanical Fatigue

Samples were mechanically fatigued in one of two separate methodologies:

Using the Piezoelectic Materials Test Apparatus (Frequency $\leq$20 Hz, Load $\leq$2.8 kN)

- Sample loaded into piezo test rig
- Sample pre-stressed to 10 MPa by Instron 3382 frame
- Cycling stress applied by PI actuator, controlled in LabVIEW environment. Data collection from all available instruments

For pre-stress cycling, above 2.8 kN, an offset DC load must be applied by the Instron frame.

Using the Instron 3382 Frame (Frequency $\leq$0.2 Hz[x], Load $\geq$12 kN)

- PI actuator removed from test apparatus
- Sample pre-stressed to 10 MPa by Instron 3382 frame
- Cycling stress applied by 3382 frame, controlled in Bluehill environment. Data collection from all available instruments controlled by LabVIEW

All experimental monolithic samples were checked for dimensionality to ensure an aspect ratio of 1 or greater. For MLAs these geometric requirements were ignored for reasons discussed previously (Section 4.2). After each regime impedance, d_{33} and capacitance measurements were made.

[x]Dictated by frame specifications

5.8.2 Electrical Fatigue

This methodology involved the use of a computer-controlled signal generator written in LabVIEW, outputting to an amplifier (Trek) via a NI cDAQ 9263 module to fatigue a sample. Samples were pre-stressed with a 5 MPa load to reduce the likelihood of the sample being in tension during cycling

Fatigue cycles involved actuations from 1000 cycles increasing to a maximum cumulative number of actuations with impedance, d_{33} and capacitance measurements made after each cycle run.

The electrical fatigue of monolith structures did not take place as suitable equipment that would provide in excess of the material's E_C was unobtainable.

5.9 Ageing

For ageing, samples were poled at their prescribed fields and temperatures for a predetermined amount of time. Initial Berlincourt measurements of d_{33} were made shortly after poling, followed by subsequent measurements using Berlincourt and impedance analysis at poling +48 hours before any experimental procedures could be carried out.

Where further ageing has been required, samples were left for a further month after initial experimentation at poling +48 hours.

5.10 Rayleigh Measurements

Rayleigh measurements involved the use of the materials test apparatus and samples with correct geometry (Section 4.2). Experimental protocol was thus:

- Pre-stress to 10 MPa by 3382 frame
- Cycling of PI actuator at 0.1 Hz and 20 μm displacement and re-stress to 10 MPa by 3382 frame to remove slack from the system

- Cycling of PI actuator at 2.5 – 20 μm in 2.5 μm increments at 1 Hz - applying the AC stress

Material response was measured by virtue of a charge amplifier (5011B, Kistler) connected directly to the material under test - the subsequent charge amplifier output recorded using data acquisition equipment previously outlined (Section 4.5) sampling at 1 kS sec^{-1}. Compressive load was measured using the quartz load cell component of the test apparatus via an identical charge amplifier output to aforementioned data acquisition hardware, with acquisition across all channels synchronised to 1 ms.

For experiments where heating was required, all pre-stress was removed from the sample before heating began. Heating was monitored by use of the actual sample's pyroelectric response - experimentation did not commence until thermal drift from the sample was negligible, before the routine outlined previously was conducted.

The collected data was then analysed in DIAdem[y] to produce a charge-stress hysteresis loop, to which a linear regression was fitted giving values for d_{init} and α (domain wall activity).

[y]National Instruments Corporation, Austin, TX

6 Base Materials Information

This section presents experimentally determined data regarding the ferroelectric ceramics being investigated in subsequent chapters. Coercive field results are quoted from the x-axis intercept, and were measured on poled materials at room temperature, averaged over 3 sinusoidal loops applied at 1 Hz with a 1000 ms wait between each loop – fitting with the remit of this research investigating behaviour of poled ferroelectrics.

6.1 3% La-doped BFPT

6.1.1 Coercive Field

Measurement of E_C on 3% lanthanum doped BFPT yields a value of 5.1 kV mm^{-1} from a 10.5 kV mm^{-1} applied field, at a frequency of 1 Hz (Figure 50).

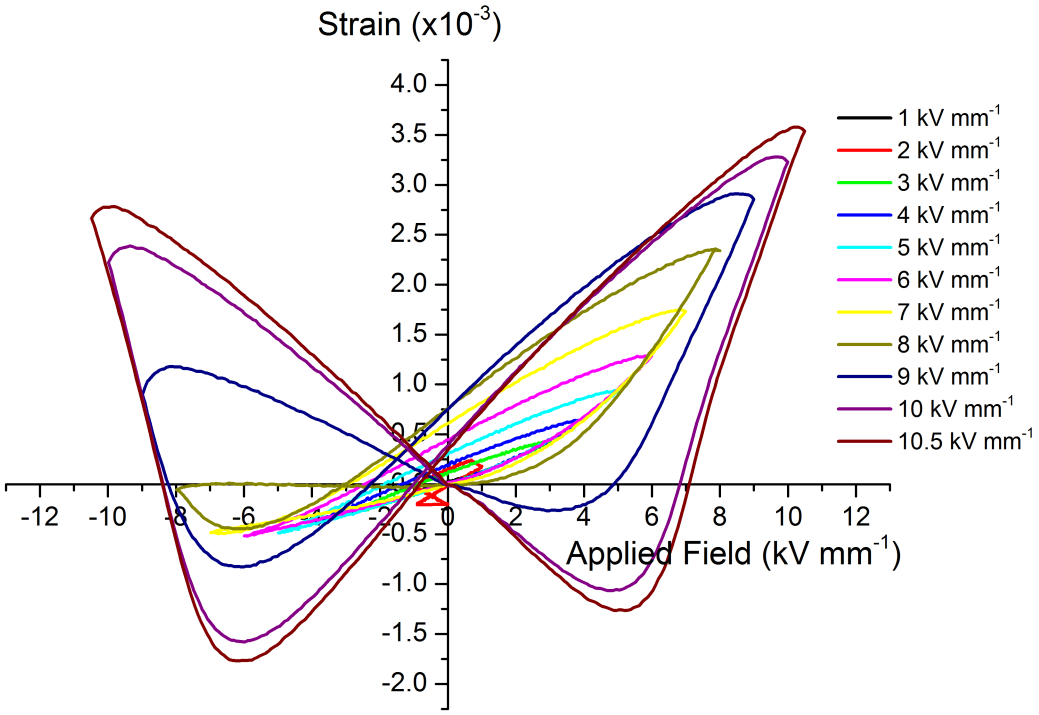

Figure 50: Strain–field measurements for a 470 μm thick 3% La-doped BFPT pellet.

6.1.2 Depolarisation Temperature and T_C

Using the methodology outlined in Section 5.5, thermally induced current measurements were performed on virgin, poled, 48 hours aged 3% BFLPT pellets to determine depolarisation temperature. Furthermore permittivity-temperature (Section 5.4) measurements were performed.

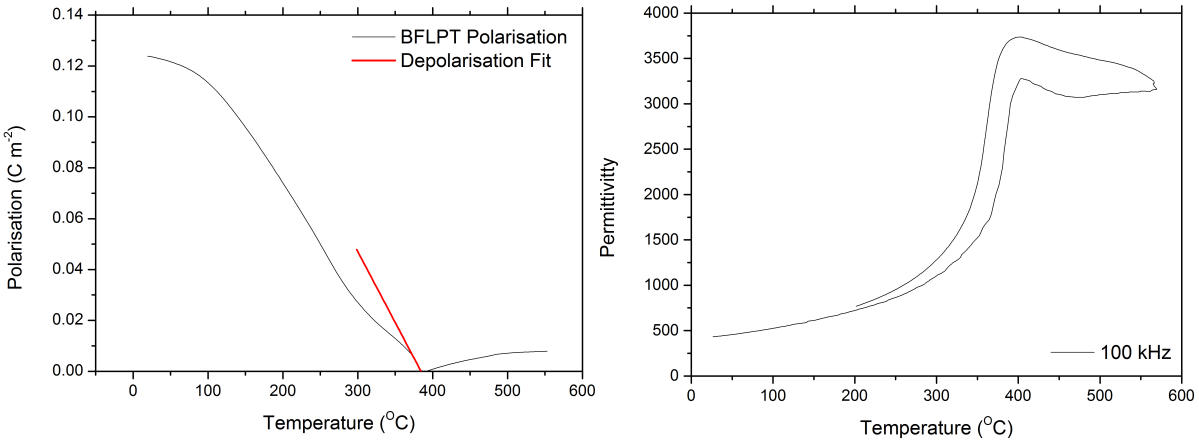

Figure 51: Left: Depolarisation charge response of a BFLPT pellet. A linear fit to the highest polarisation decay in the data yields a depolarisation temperature of 384.45 °C. Right: Permittivitty-temperature results for a 3% La-doped BFPT pellet at 100 kHz with an excitation of 1 V.

The current response produced a depolarisation temperature (T_{depole}) of 384.45 °C (Figure 51). While permittivitty–temperature results yield a T_C of 394 °C (Figure 51).

6.2 PZT Compositions

The PZT compositions discussed henceforth are equivalent to:

Table 8: PZT Nomenclature

PZT Equivalent Composition Nomenclatures				
	Navy Type	EN 50324-1	NCE	PIC
Hard	I & III	100		181
Soft	II	200		255
	VI	600	55	

6.2.1 Coercive Field

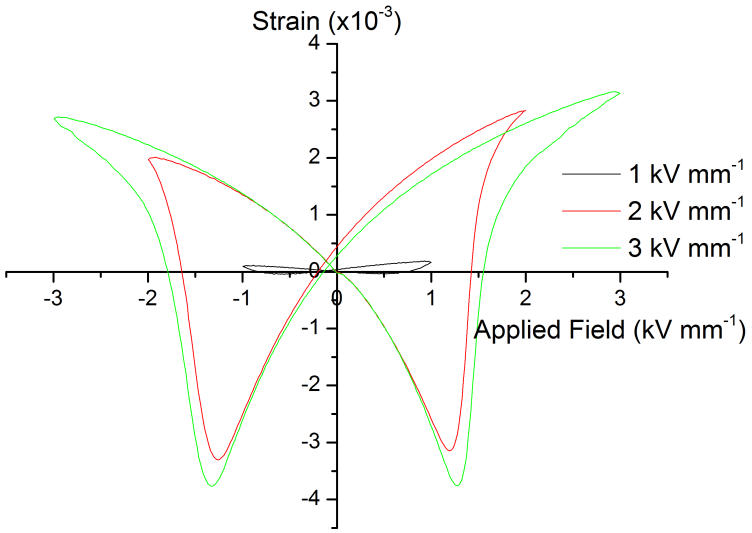

Figure 52: Strain–field measurements for a 924 μm thick PIC255 pellet.

Measurement of E_C on 3% PIC255 yields a value of 1.25 kV mm^{-1} from a 3 kVmm^{-1} applied field, at a frequency of 1 Hz (Figure 52), while 1.18 kV mm^{-1} is achieved for PIC181 (Figure 53, higher field was applied and lead to dielectric breakdown), while NCE55 has E_C of 1.1 kV mm^{-1} (Figure 54).

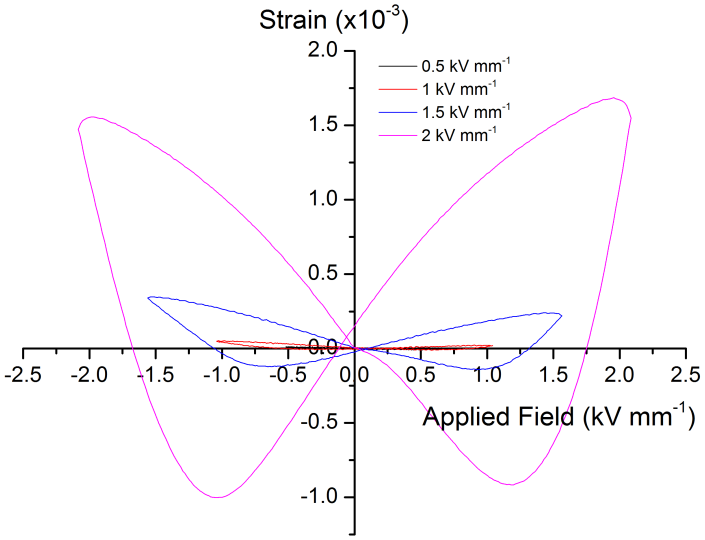

Figure 53: Strain–field measurements for a 2048 μm thick PIC181 pellet.

6.2.2 Depolarisation Temperature and T_C

A linear fit to the highest polarisation decay in the data yields a depolarisation temperature of 278.74 °C for PIC181, 301.55 °C for PIC255 (Figure 55). Meanwhile NCE55 appears to depole at 164.73 °C (Figure 55). While the Curie temperature for the PZT materials (Figure 56) are 210 °C (NCE55), 350 °C (PIC255, approx.) and 360 °C (PIC181).

6.3 Summary

Presented are all base material results in tabulated form for later reference.

Table 9: Base Materials Information

Material	E_C (kV mm^{-1})	T_{depole} (°C)	T_C (°C)
BFLPT	5.1	384	394
NCE55	1.12	164	210
PIC255	1.25	301	350 (approx.)
PIC181	1.18	278	360

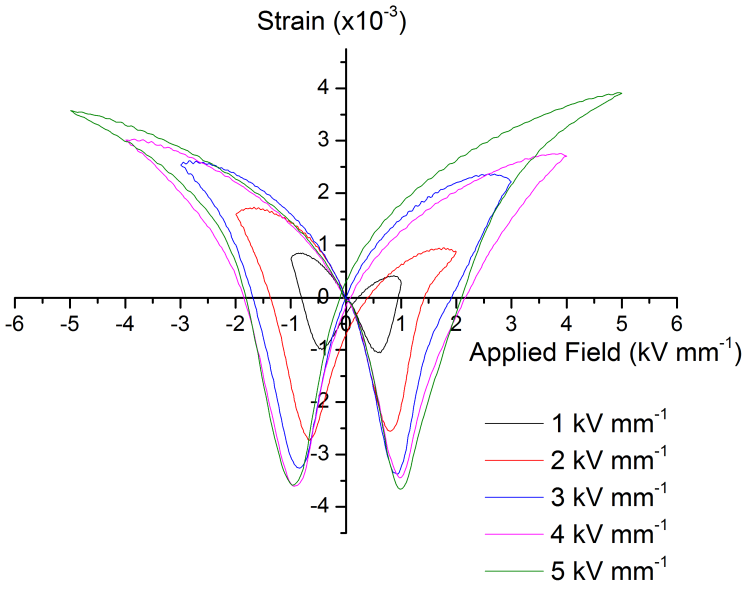

Figure 54: Strain–field measurements for a 508 μm thick NCE55 pellet.

7 Fatigue of 3% La-doped Bismuth-Ferrite Lead-Titanate Multilayer Actuators

7.1 Sample Fabrication

3% BFLPT and PZT multilayer devices were prepared by tape casting methods outlined previously (Section 1.8) by Noliac A/S, Denmark, resulting in MLA elements of dimensions 5x5x2 mm consisting of 67 μm ceramic layers between 2 μm interdigitally configured platinum electrodes (Figure 19 & 57).

Table 10: Variability of MLA Devices

Material	Avg. Effective d_{33} (pC N^{-1})	d_{33} (pC N^{-1})	Avg. Cap. (nF)	Std. Dev.
BFPT	2869.8	95.6	24.04	37.23 / 0.45
CMAP07 (PZT)	8233.89	274.4	106.93	257.67 / 1.59
CMAP11 (PZT)	6498.28	216.6	79.56	160.06 / 1.40

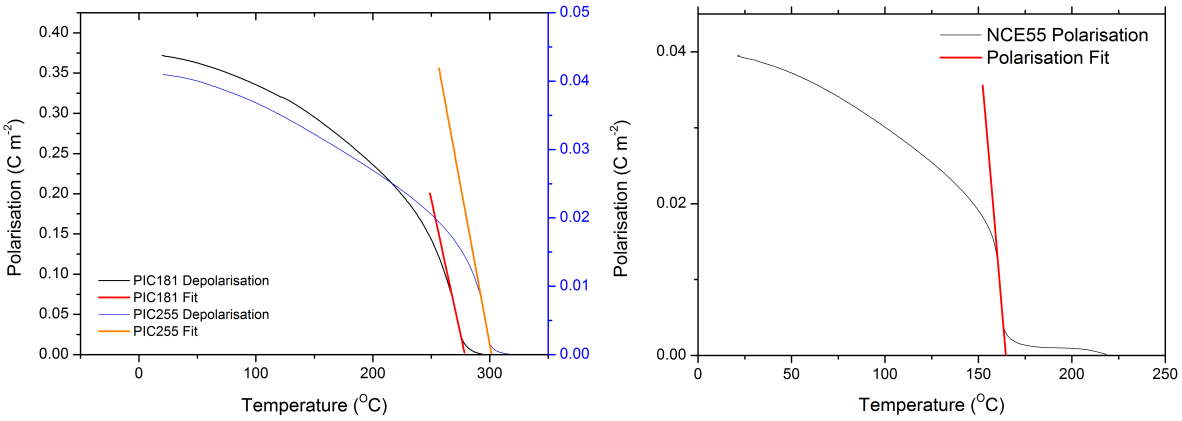

Figure 55: Depolarisation charge response of PIC181 and PIC255 PZT compositions in pellet form (left) & NCE55 (right).

A randomly selected sample of BFLPT and PZT (both compositions) MLAs were checked for variability and found, in the case of BFPT to be manufactured within instrumental errors (Figure 58) while PZT showed a larger spread in both capacitance and effective activity[z] (Figure 59). The d_{33} reported are extremely high because what is being measured is the *effective* activity of the multilayer element – i.e. the total piezoelectric effect of each individual layer that makes up the multilayer element (Section 1.8). Another variable to note is that of ageing time – the PZT elements were aged for a minimum of a month (per industry adopted standard) and were not made to order but picked off the shelf, conversely the BFLPT elements were made to order and were allowed to age for at most a week before these initial measurements took place.

7.2 Mechanical Testing

7.2.1 Preliminary Mechanical Testing

Initial investigation involved a simple test applying a linearly increasing compressive stress (100 MPa min^{-1}) until destruction of the multilayer elements – three elements of each composition were tested, with results averaged. Observed results show that BFLPT is considerably mechanically stronger than the CMAP07 (hard) and CMAP11 (soft) counterpart PZT elements - with

[z] *Effective activity* is used with regard to multilayer structures and is the total response of the whole structure

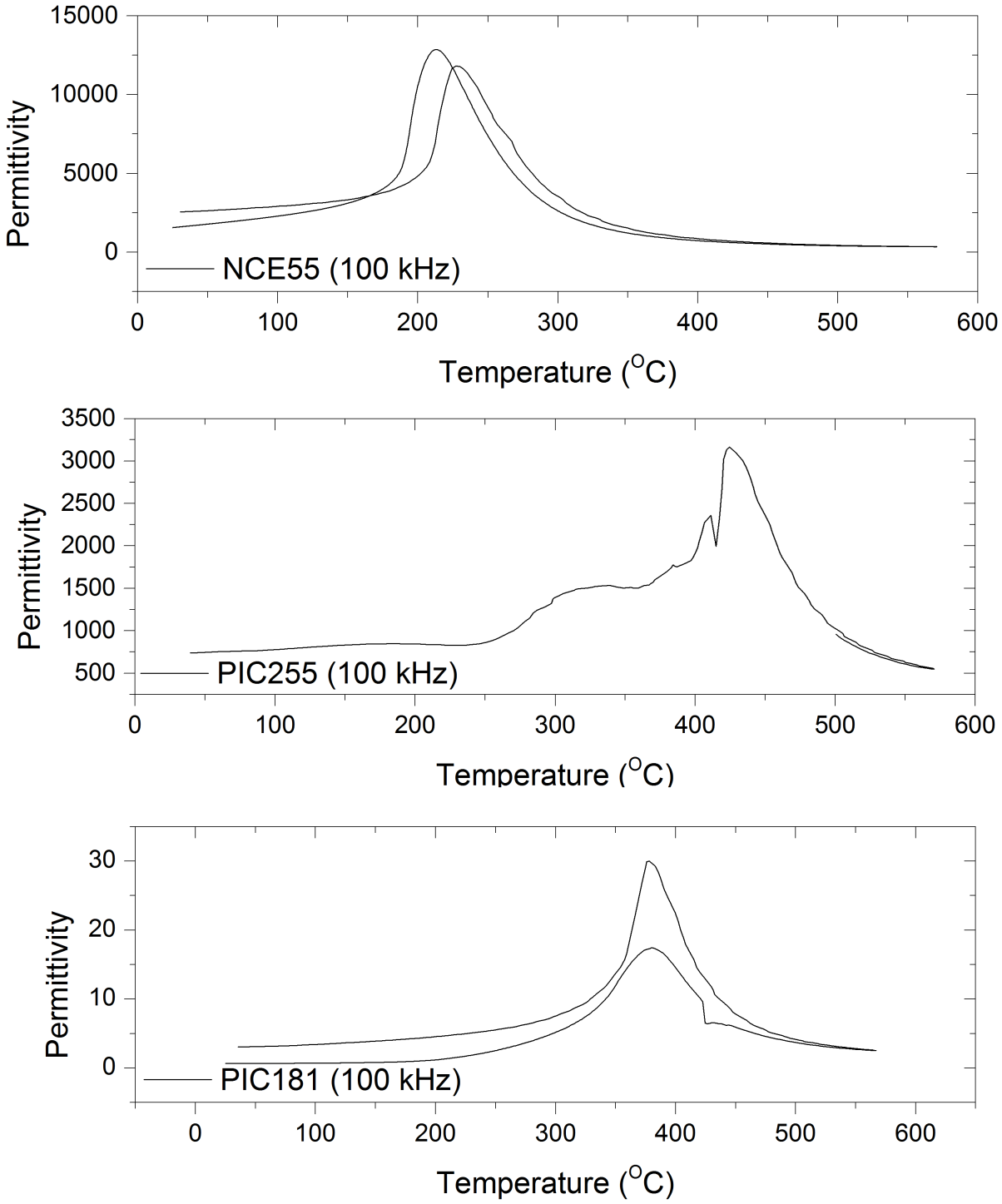

Figure 56: Permittivitty-temperature response of NCE55, PIC255 & PIC181 PZT compositions in pellet form.

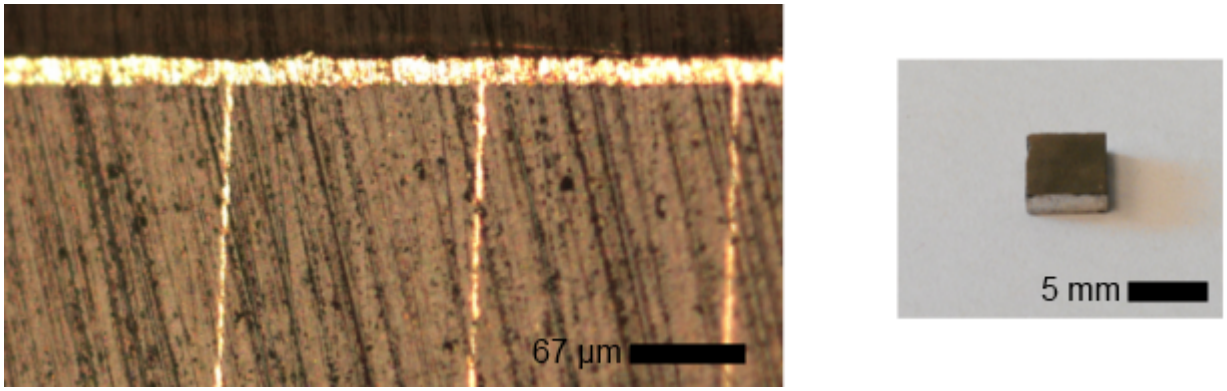

Figure 57: Micrograph of interdigital electrodes in BFLPT MLAs prepared by Noliac A/S (left) and a photograph of an MLA (right).

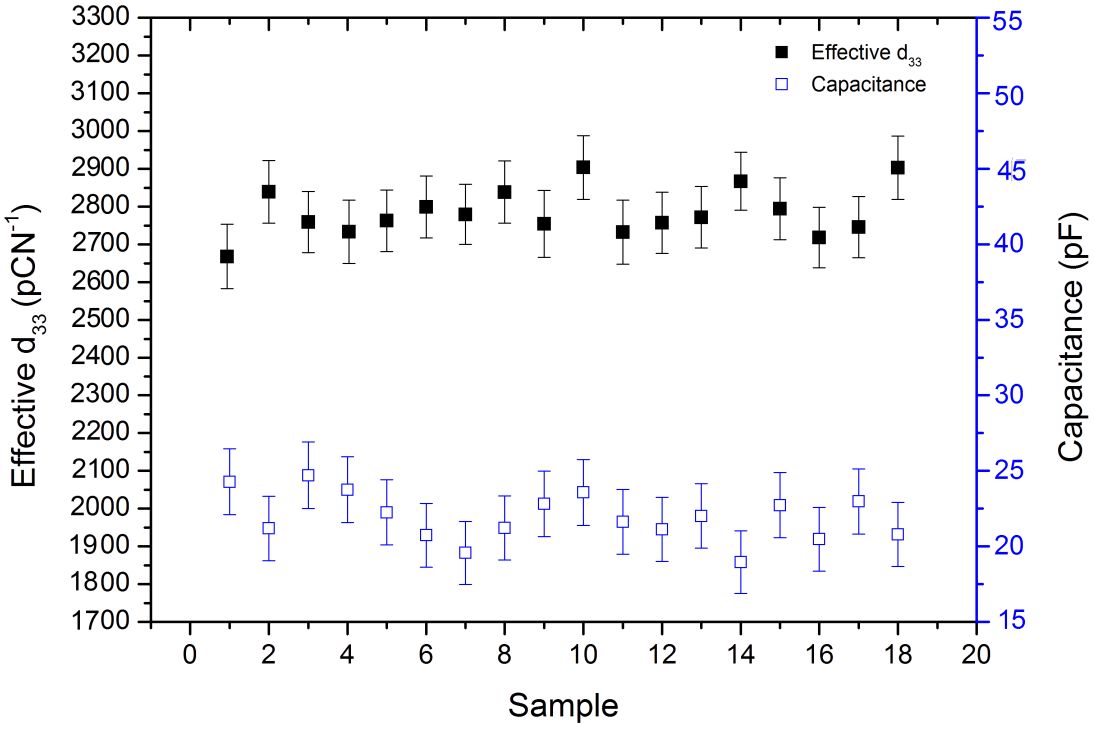

Figure 58: Variability of prepared BFPT MLAs. Error bars represent instrumental error contributed by the Berlincourt meter.

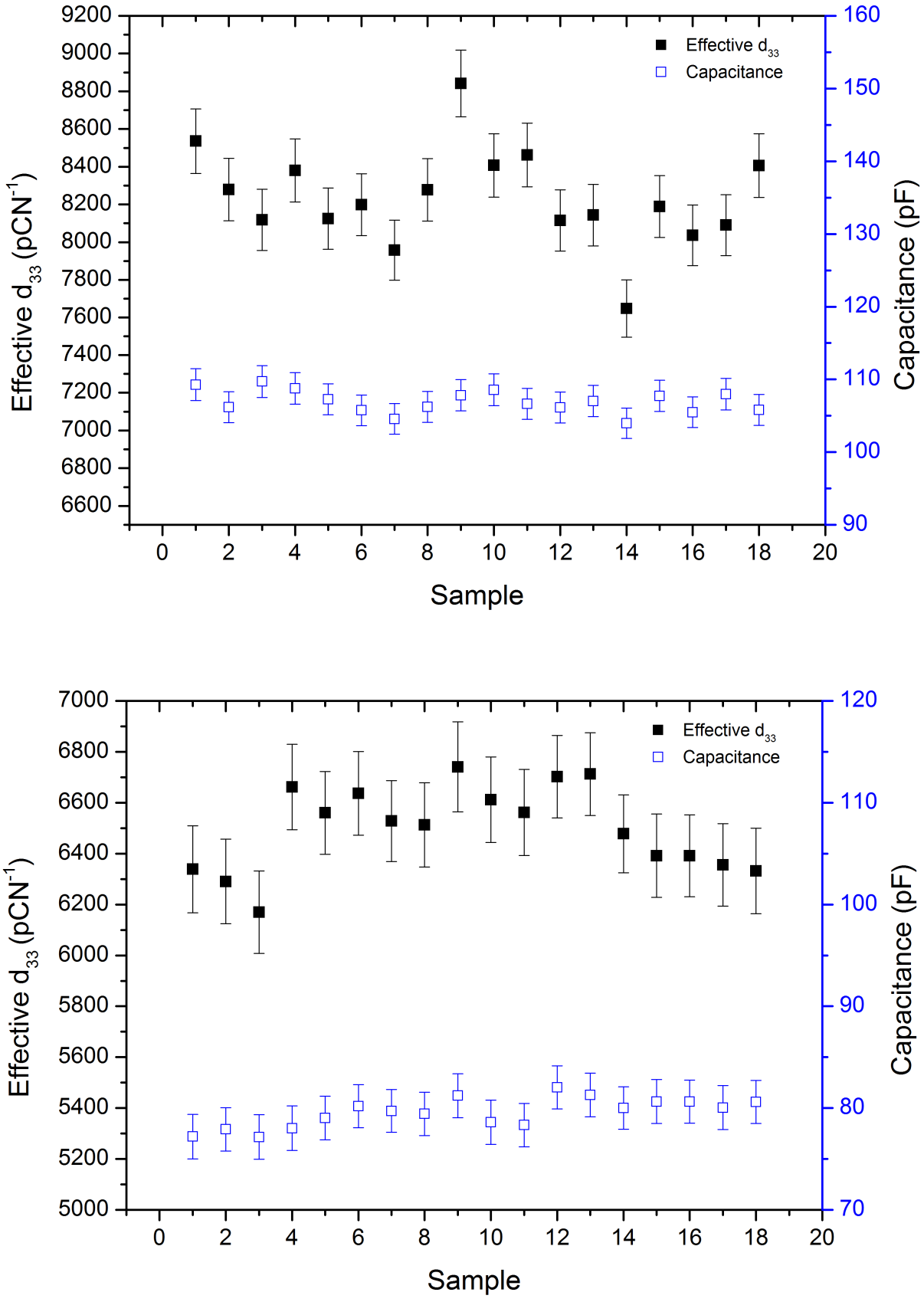

Figure 59: Variability of prepared CMAP07 (top) and CMAP11 (bottom) PZT MLAs. Error bars represent instrumental error contributed by the Berlincourt meter.

a yield stress of 110 MPa and 170 MPa for CMAP11 and 07 respectively (approximately similar to that of bone), while the BFLPT multilayer element begins to yield approaching 800 MPa (Figure 60) – in excess of high strength A514 steel.

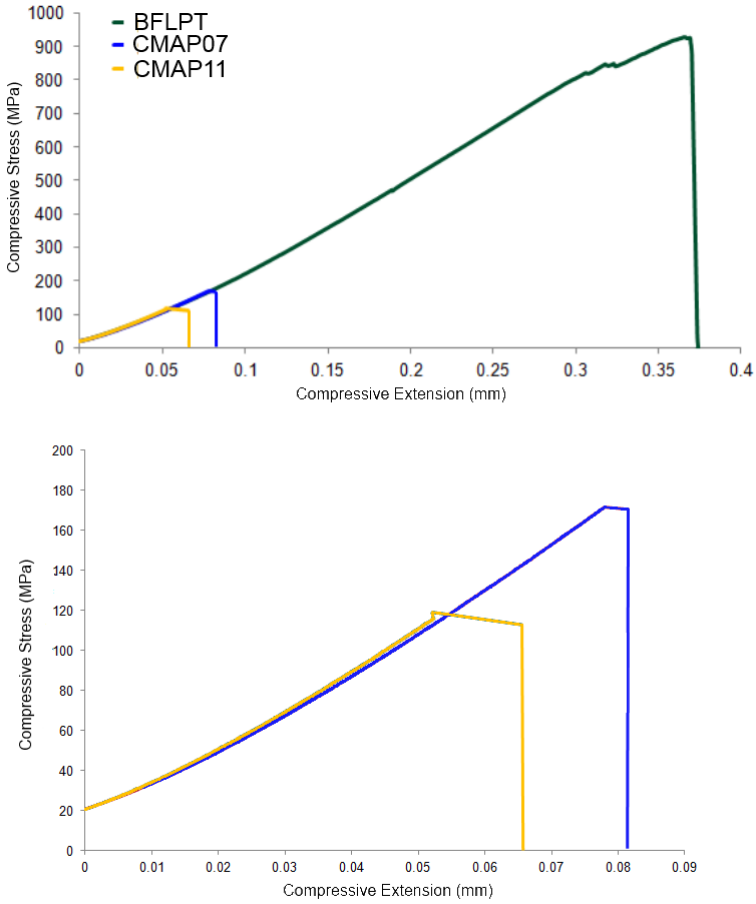

Figure 60: Mechanical testing of BFLPT and PZT multilayer elements to destruction.

Coercive stress measurements did not form part of the preliminary testing due to the complexity of such measurements and the requirement for a substantial enough sample size for a meaningful result to be obtained, additionally it is likely that the multilayer elements would undergo a mechanical failure at a lower stress than they would depole.

7.2.2 Preliminary Stress Cycling

Using this information, figure 60, an outline for the mechanical cycling of these materials can be made with regard to minimising any physical destructive effects that may arise from mechanical cycling for BFLPT – i.e. that of remaining below the proportionality limit stress beyond which the materials do not conform to Hooke's law.

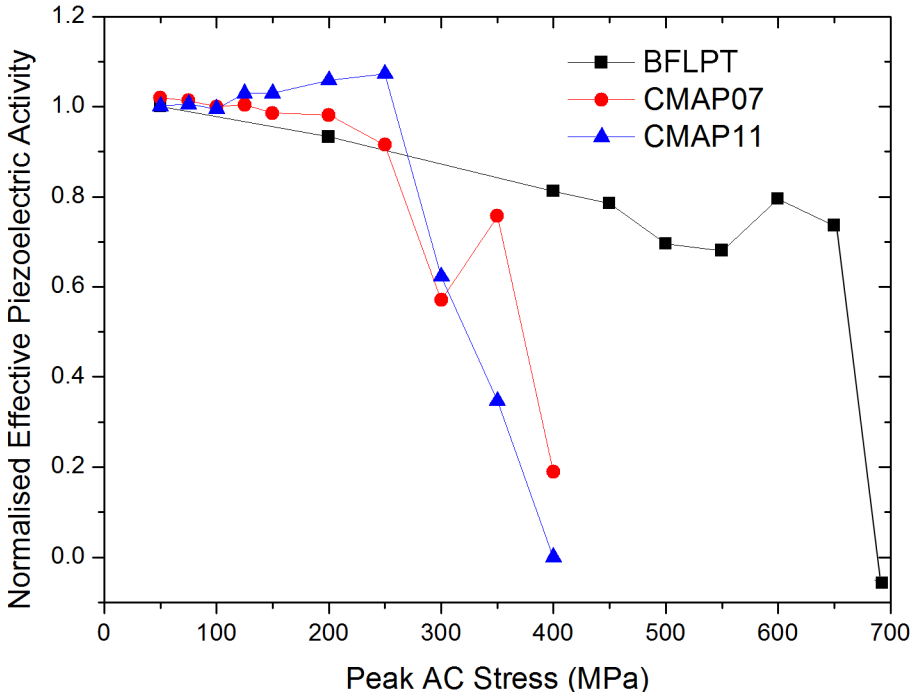

Figure 61: Response of MLAs to stress cycling. Each data point represents an individual sample subject to 1,000 cycles.

Fresh samples of the three compositions were cycled at increasing stresses for 1,000 cycles at 0.2 Hz to gain an understanding of material behaviour at increasing applied alternating stresses, after cycling the elements were left for 24 hours before measurement of activity. The data (Figure 61) shows that when cycling stresses are applied in excess of the yield stress, piezoelectric activity is still present for all compositions. PZT undergoes an enhancement in activity, as predicted by current literature, before a very gradual loss in activity, due to the slow mechanical failure of the elements. However the mechanical failure of the BFLPT elements takes place instantly,

showing a linear degradation of activity coherent with conventional ferroelectric ageing, before a catastrophic failure and no significant element structure remains.

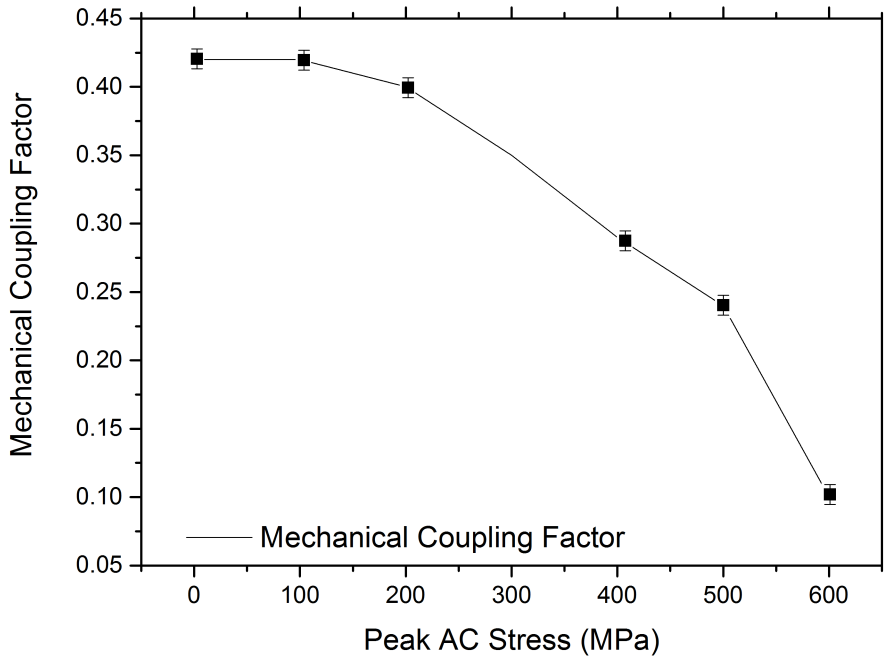

Figure 62: Evolution of k, mechanical coupling factor, for La-doped BFPT multilayer elements cycled for 1,000 cycles at 0.2 Hz.

Fitting with the logarithmic degradation in piezoelectric activity, the mechanical coupling factor k can be observed degrading from an initial value of 0.42 for all elements before cycling (Figure 62).

Furthermore, BFLPT was examined using a synchrotron X-ray source (Section 5.7) as a function of temperature. The resultant diffraction patterns were peak fitted for both rhombohedral and tetragonal phases (Figure 63), with the 2-theta positions transformed into d-spacings by virtue of Bragg's Law and subsequent unit cell dimensions allowing the calculation of unit cell volume – showing a volume change for both phases, varying with temperature (Figure 64).

There is an observed shift in concentration of tetragonal and rhombohedral crystallographies

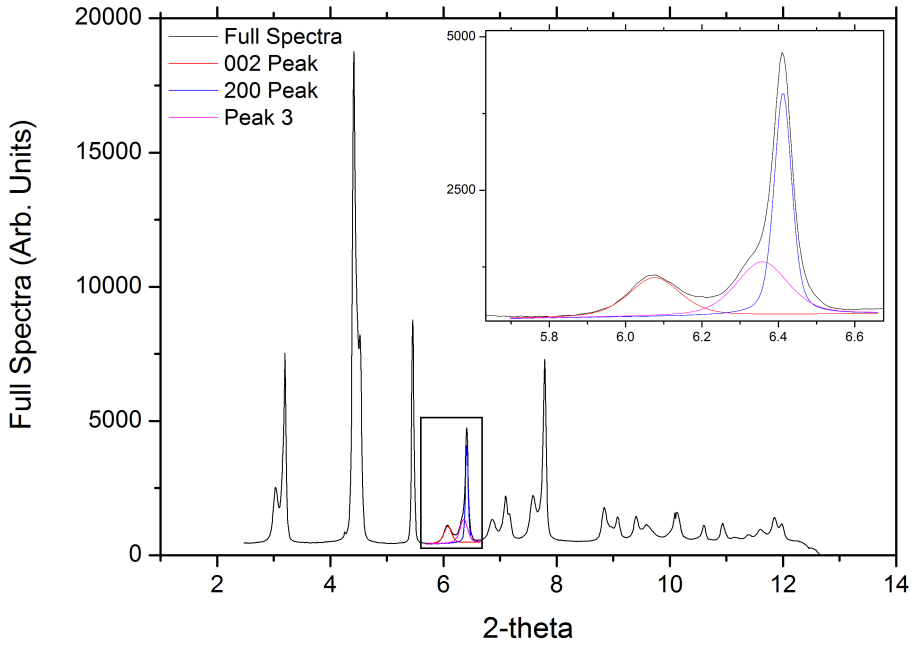

Figure 63: Example of peak fitting for a BFLPT sample subject to synchrotron irradiation.

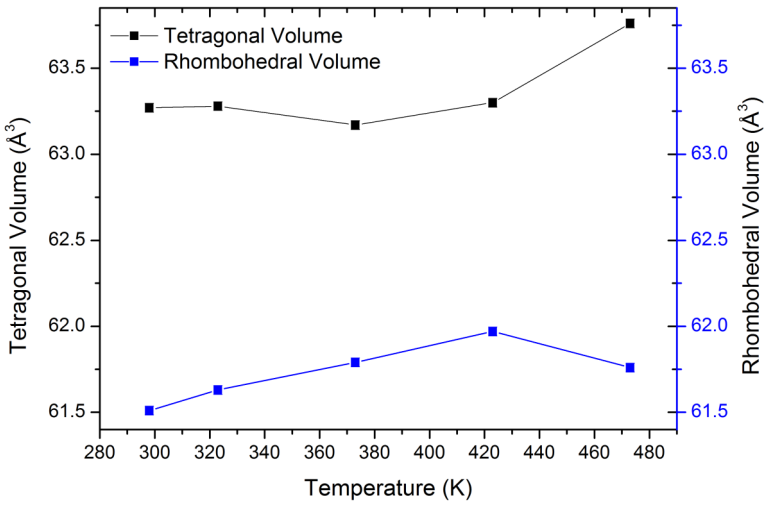

Figure 64: Variation in volume of rhombohedral and tetragonal phases in La-doped BFPT over a temperature range of 25-200 °C.

over the experimental temperature range, suggesting the presence of transformation toughening (Figure 73) in addition to the previously mentioned crystallographic volume change.

7.2.3 Continuous Stress Operation

Using Section 7.2.2 as a roadmap, a single fresh BFLPT element was cycled mechanically with 400 MPa peak AC stress for 10^6 cycles at 0.2 Hz – simulating operation in a harsh environment. The 3% La-doped BFPT element shows a general linear trend in the degradation of piezoelectric activity (Figure 65) to 100,000 cycles, suggesting this is due to conventional ageing of the material. While further cycling causes a logarithmic reduction in activity, suggesting a phenomenon, such as a microcrack or other mechanical effect, is present other than conventional ageing is degrading the activity of the material.

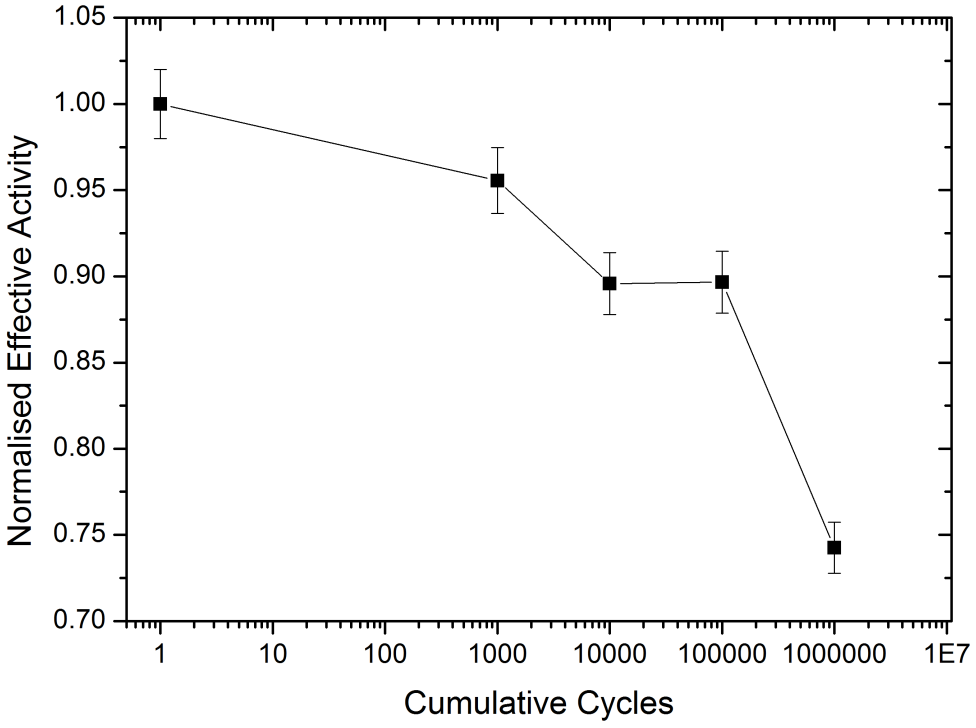

Figure 65: 400 MPa peak cycling of BFLPT multilayer element at 0.2 Hz with 10 MPa pre-stress.

The only viable way of verifying the hypothesis that a mechanical effect is the cause of the drastic loss of activity is by actively searching for any mechanical defects using a microscope. Without an approximate location of the crack, this would be extremely difficult to accomplish as the likelihood of a microcrack being embedded in a section cut from the element is high. Therefore a reasonable method for verifying the formation and approximate location of microcracks would be using a stereoscopic acoustic emission setup at opposing faces of the element – using a glass rod, connected to a PZT sensor, crack events could be detected. Further the time difference in the arrival of the emission event at each sensor, combined with the speed of sound in the element could be used to give an approximate location for the crack.

Other methods exist for examining this sample to see what happened to it:

- Hysteresis measurement – this would show pinching of the polarisation-field loop. However it would also cause the material to change as driving it to high field would effectively be re-poling the depoled areas.
- X-ray diffraction - would only penetrate a small depth into the sample and would not give any conclusive bulk result for the sample.

The method chosen was that of sectioning the fatigued element, and a virgin element, into 1 mm thick sections and examining it using synchrotron radiation as these high-energy x-rays would penetrate the sample and give a bulk crystallographic representation of the element. Unfortunately the results showed no change.

7.3 Electrical Cycling

7.3.1 Preliminary Field Cycling

Exploiting the converse piezoelectric effect – materials were subject to cycling (Figure 66) by applying increased unipolar field until zero d_{33} was observed. Separate elements were used for each field, and cycled for 1,000 cycles at 100 Hz, a 5 MPa pre-stress was in effect to prevent the elements being in tension during cycling as tension effects can lead to the mechanical failure of ceramic materials very rapidly.

The data collected substantiates the theory previously discussed (Section 3.1.1) regarding electronic fatigue being more apparent at fields approaching and exceeding the material E_C. PZT shows complete failure around E_C due to dielectric breakdown (Figure 66, highlighted) while BFLPT continues to operate above E_C (5.1 kV mm^{-1}) with only slight degradation of activity.

7.3.2 Continuous Field Operation

With a key contributor to the investigation of BFLPTs long term behaviour and stability being the potential application of the material in an environment with strict power demands, the multilayer elements were subject to field cycling at an appropriate voltage (considering the desired application environment), thus cycling occurred well below E_C with minimal fatigue observed until in excess of 2,000 million cumulative cycles (Figure 67) – far in excess of observed 10^8 cycles for PZT presented in section 3.1.1. A possible explanation for this is the reduction in capacitance from 24.08 nF to 22.03 nF after the complete cycle run – this suggests that the reduction in activity is due to electrode damage, depolarisation or conductive pathways being formed, either way resulting in a reduction of the amount of dielectric medium available to polarise.

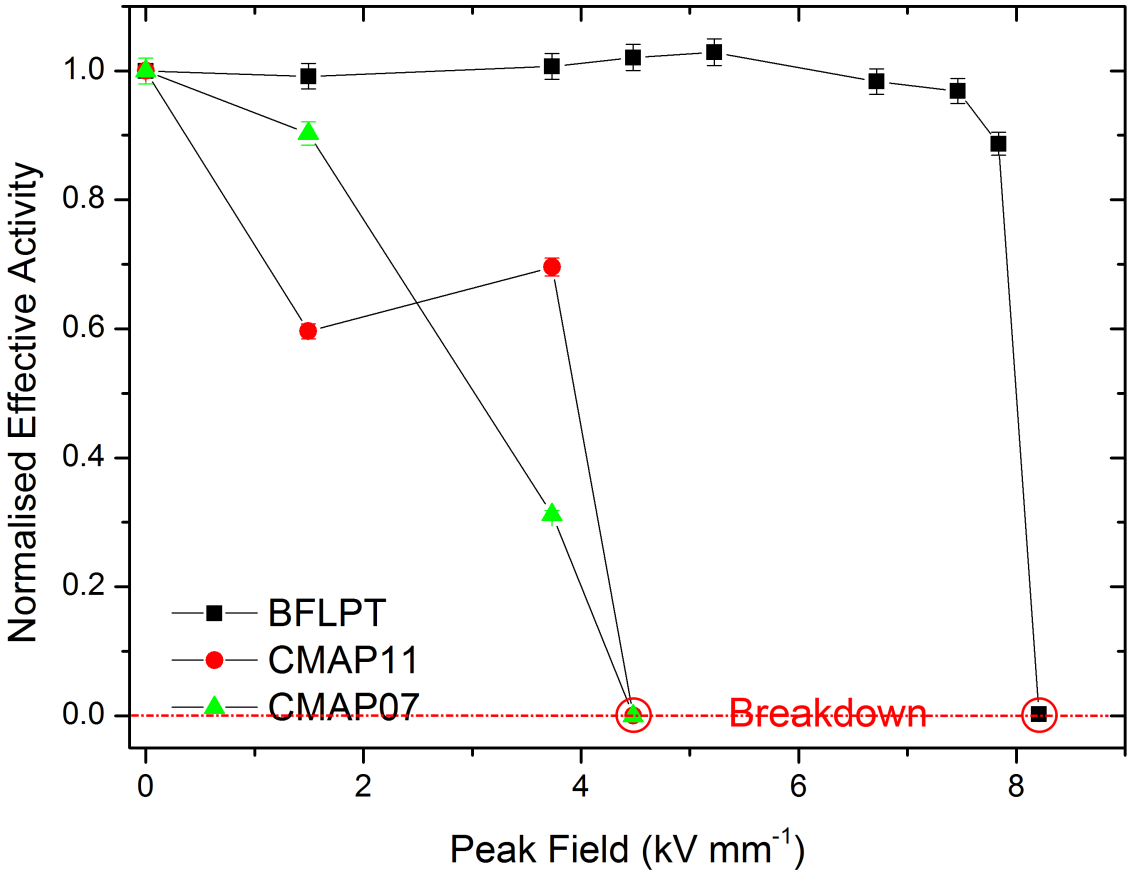

Figure 66: Activity evolution of BFLPT and PZT multilayer elements subject to 100 Hz field cycling at differing applied fields and 5 MPa pre-stress. Each data point represents an individual element being tested

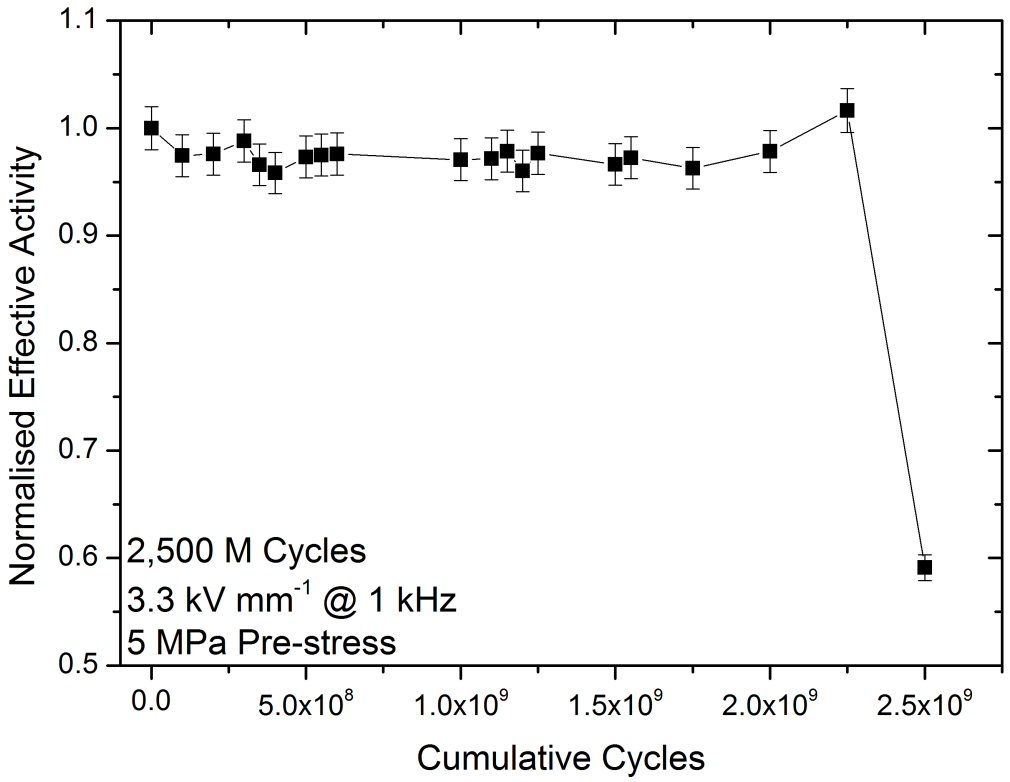

Figure 67: Activity evolution of a BFLPT multilayer element subject to 1 kHz field cycling at 3.3 kV mm^{-1} and 5 MPa pre-stress.

7.4 Conclusions

Obvious conclusions can be made from the presented data with respect to the implied longevity of BFLPT multilayer elements, namely the considerably larger mechanical stresses the material is capable of withstanding in comparison to PZT (Figures 60 & 61). Furthermore, these elements are capable of some operation above E_C (5.1 kV mm^{-1}, Section 6.1.1) – presented in figure 66, with headroom in operating field before a total loss of activity is manifested. The calculated displacement of the BFLPT elements at 200 V applied, is in the region of 500 μm compared to the approximate 1,600 μm calculated displacement from CMAP07 at the same applied voltage shows some disadvantage, but coupled with the differing mechanical properties BFLPT makes a viable option for a scenario where actuation is required in high stress environments.

8 Direct-Effect Rayleigh Behaviour in Bismuth Ferrite Lead Titanate

The use of the Rayleigh law (Equation 8) allows us to use a small cycling stress, exploiting the direct piezoelectric effect, in order to measure the combination of intrinsic (polarisation, reversible domain wall motion) and extrinsic (irreversible domain wall motion) contributions to the response of a poled ferroelectric. However a critical assumption is made in order to apply the Rayleigh law - the applied stress does not cause any domain volume change.

8.1 Room Temperature

With literature confirming PZTs Rayleigh behaviour (Section 2) at room temperature, the first investigation was into the applicability of Rayleigh theory to BFLPT.

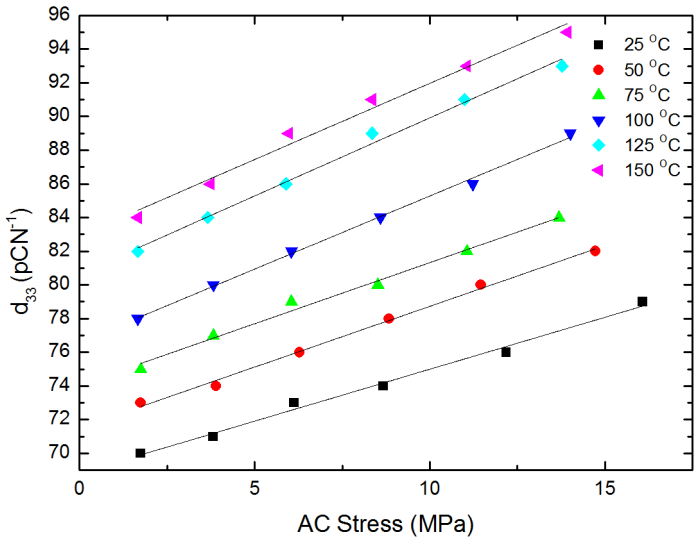

Figure 68: Linear response of BFLPT to a weak AC stress.

Using the test apparatus (Section 4), a poled BFLPT cylinder with a 1:1 aspect ratio as per section 4.2 was subject to a 10 MPa pre-stress and an increasing 1 Hz cycling stress at room temperature (25 °C, Figure 68). Measurements are possible by a combination of the charge produced by the sample and the applied stress, plotted together to give a charge-stress loop

(Figure 69), a linear regression is then calculated for the loop giving coefficients coherent with equation 8. After processing the charge and stress data, a clear linear trend is apparent for BFLPT throughout the experimental stress range.

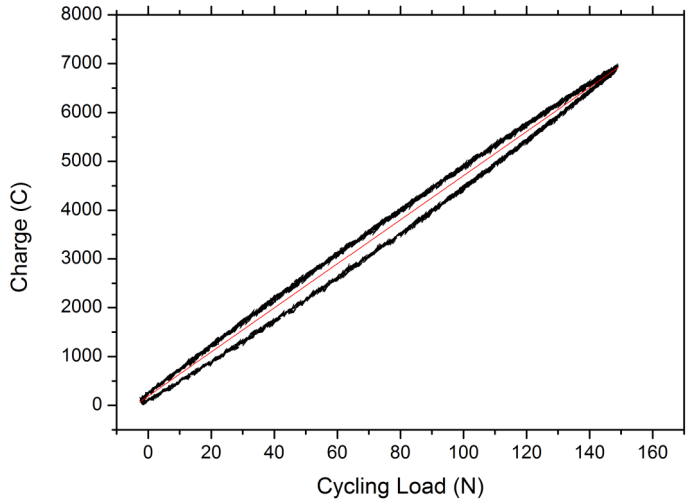

Figure 69: Example of processed direct-effect Rayleigh data, showing charge increase with increasing cycling load and linear regression fit.

8.2 Elevated Temperature

Following on from the observation of Rayleigh-like behaviour in BFLPT at room temperature, the same experimental practice exploiting the direct piezoelectric effect, was employed to observe Rayleigh behaviour as a function of temperature (Figure 68). The behaviour observed shows a strong positive temperature dependence of d_{init} and α (Figure 70) – intrinsic contributions (polarisation) and extrinsic (domain wall motion) to the piezoelectric response of BFLPT.

$$d_{33} = 2Q\varepsilon P_S \tag{9}$$

This strong temperature dependence of both contributions – 16% for d_{init} - the combination of polarisation and reversible domain wall motion, and 31% for α - irreversible domain wall motion, means that therefore the response of the material solely as a result of polarisation needs

to be found.

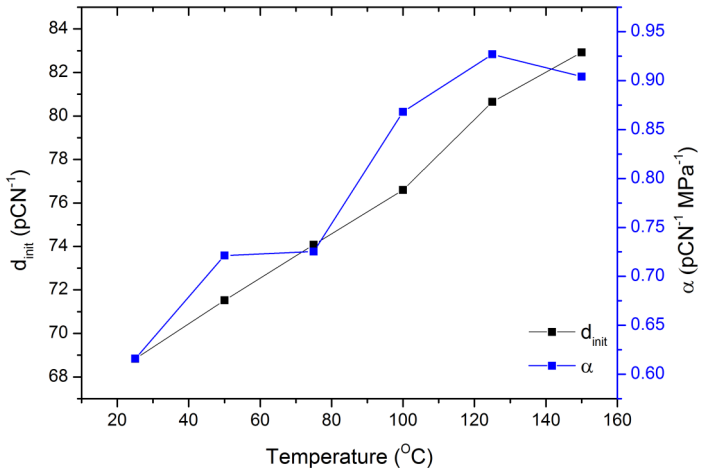

Figure 70: Temperature dependence of d_{init} and α for BFLPT.

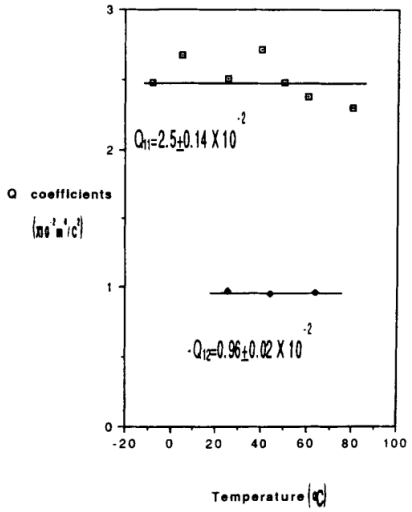

Figure 71: Temperature independence of electtrostiction co-efficient Q.

By virtue of equation 9 and the assumption that Q is temperature independent [170] (Figure 71), permittivity-temperature and thermally stimulated depolarisation current measurements were taken across the Rayleigh experimental temperature range (25-250 °C) on samples of BFLPT aged for 48 hours.

These two measurements were then combined to result in the data presented in Figure 72.

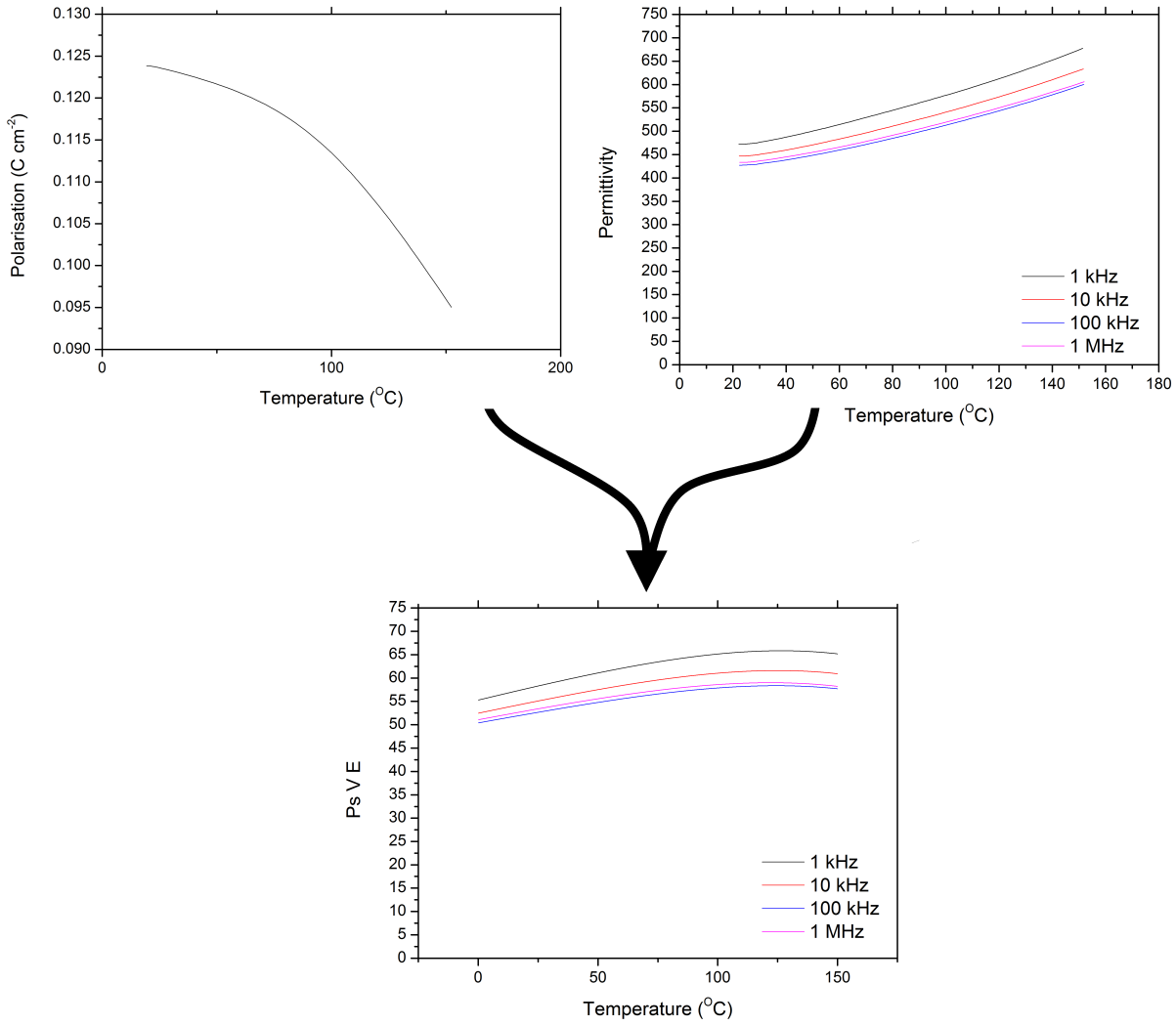

Figure 72: Temperature dependence of polarisation and permittivity for BFLPT throughout the Rayleigh experimental temperature range.

What this shows is that across the temperature range of the Rayleigh experiment, polarisation (P_r) is highly temperature dependent – accounting for a 12% change in pure intrinsic contributions.

These results quantify the dominance of polarisation in the intrinsic response of BFLPT in this temperature range. Further information provided by temperature-dependent synchrotron data shows a corresponding reduction in tetragonality (Figure 74), coherent with results by Kounga *et al.*[34] for a morphotropic phase boundary PZT composition, considering that the BFLPT composition used throughout this thesis also resides within the BFPT MPB region these results mean that there is a definitive change in phase concentrations present (Figure 73), this means that the total response of BFLPT as a function of temperature can be broken down into:

Table 11: BFLPT Contribution Temperature Dependence

Material	d_{init}	α	d_{33} Intrinsic	d_{33} Reversible Domain Walls
BFLPT	16%	31%	12%	4 %

However there is a caveat to these calculated results, they are only completely valid in a situation where phase concentrations are not changing – in the BFLPT system, it is clear from the synchrotron data (Figure 73) that a change in phase concentrations is occurring as a function of temperature.

Although this calls into question the definitive values of the change of contributions as a function of temperature, the question of why this happens can still be answered by considering several factors.

First, the polarisation response (d_{33} intrinsic) increases as a function of temperature. Secondly, the MPB is not a defined concentration point for a mixed phase material but a wide concentration range (Section 1.5.1). Third the nature of an MPB composition is that of a temperature dependent co-existence of rhombohedral and tetragonal phases, thus a sufficiently large temperature change in the system will elicit a phase change to a phase of lower entropy – this

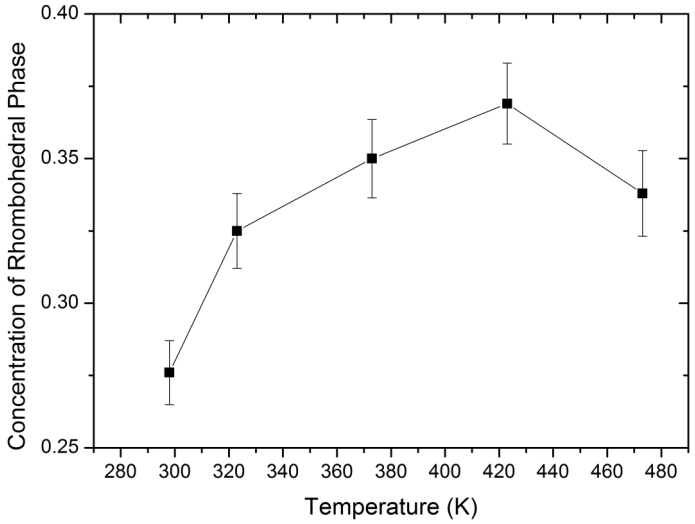

Figure 73: Observed increase in rhombohedral phase concentration in La-doped BFPT over a temperature range of 25-200 °C.

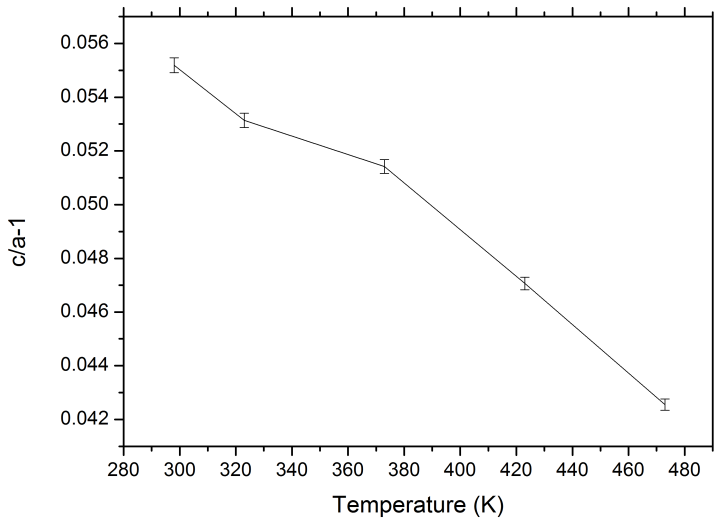

Figure 74: Observed decrease in tetragonality in La-doped BFPT over a temperature range of 25-200 °C.

phase concentration temperature dependence is clearly observed (Figure 74). Further in order for large strain, caused by a reduction in tetragonality and increased extrinsic contributions, to occur we must consider the material as a tetragonal:rhombohedral composite where an abundance of rhombohedral phases are required for tetragonal extrinsic contributions to dominate, as reported by Kungl *at al.*[171]. Finally, considerations must be made with respect to the energetics of polarisation reorientation taking place, better shown in terms of activation energies (E_a) in figure 75.

What is happening in terms of reversible extrinsic contributions (reversible domain motion that contributes to the d_{init} value) is that at room temperature, and above, there is sufficient thermal energy for the polarisation rotation to occur completely - ie. all reversible domains change polarisation orientation. While for irreversible extrinsic contributions (irreversible domain motion that is the sole contributor to the α value) the activation energy at room temperature of the re-orientation (E_{aRT}) is significantly larger than kT, causing no or minimal irreversible extrinsic contributions as it resides in an energetic minima (Figure 75, inset). Thus considering the material as a tetragonal:rhombohedral composite we can adopt Kungl's theory that the increase in rhombohedral phase concentration from intrinsic contributions permits the dominance of extrinsic contributions by lowering the activation energy at elevated temperatures (E_{aHT}).

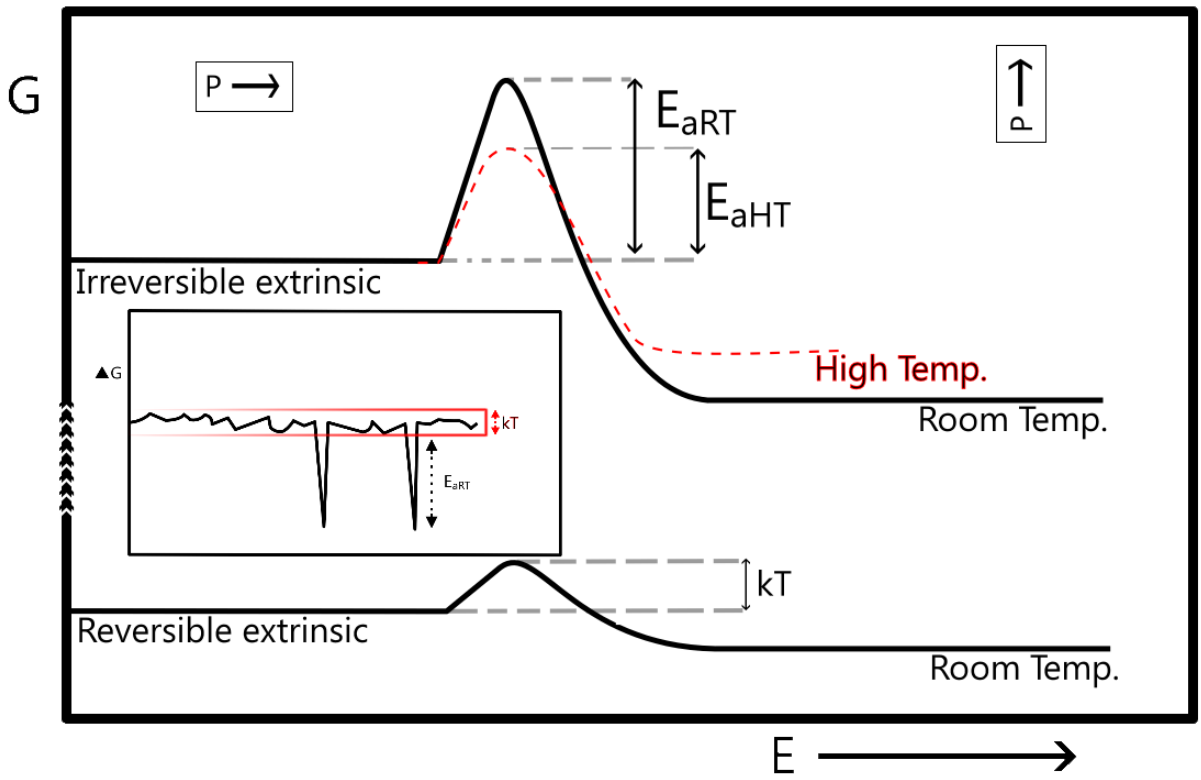

Figure 75: Theorised energetic changes occurring during heating of BFLPT, eliciting a polarisation re-orientation where sufficient thermal energy (kT) is applied to the system. The assumption is made that because polarisation response is measurable at room temperature, kT at room temperature must be equivalent or greater than E_a for polarisation re-orientation in reversible domain wall motion.

9 Rayleigh Behaviour as a Function of Ferroelectric Ageing in Bismuth Ferrite Lead Titanate & Lead Zirconate Titanate

Conventional thinking (Section 3.2) suggests that 48 hours is sufficient for a ferroelectric material to age to a point at which its character is largely constant and is open to experimentation without the effects of ageing causing skew in data collected at a later date, thus using Rayleigh methodology (Section 5.10) we set out to examine the changes in contributions responsible for the direct piezoelectric effect in BFLPT and soft (Navy Type VI), hard (Navy Type I) and an intermediate Navy Type II PZT. These measurements were conducted up to a maximum of 200 °C for BFLPT samples and 150 ° for all PZT materials in a single experimental run. Presented for discussion are the results obtained from BFLPT and Type II (PIC255) PZT .

9.1 48 Hours After Poling

Upon verification of correct dimensionality, all materials were poled - 7 $kVmm^{-1}$ for 1 minute at room temperature for BFPT, and 2.25 $kVmm^{-1}$ for 10 minutes at approximately 70 °C for PZT material. The values for poling are concurrent with those observed in academic and industrial literature.

9.1.1 PZT

The differing PZT compositions gave interesting results (Figure 76 & 97).

- The softest, NCE55 (Type VI), appears to already be showing its character - expressing a linear stress response early throughout the entire temperature range. However, counter-intuitively temperature dependence is heavily negative with a value of -1.74 pCN^{-1} $°C^{-1}$, countering what would be expected based on current literature – domain wall mobility and polarisation contributions should have a positive temperature relationship.

Results for Type VI (NCE55) and Type I (PIC181) are presented in the appendix

- Similarly the hardest material, PIC181 (Type I) shows strong linearity in stress response (Figure 97), along with an almost non-existent temperature dependence of intrinsic contributions (0.041 pCN^{-1} $°C^{-1}$).

With the most interesting results arising from the intermediate Type II composition with non-Rayleigh behaviour observed – i.e. not displaying a linear response to applied stress, and showing strong temperature dependence of both intrinsic (d_{init} – y-axis intercept) and extrinsic (α – gradient) contributions to piezoelectric activity, this material's ageing behaviour will be focussed on in detail.

Distinctly non-Rayleigh in behaviour until elevated temperatures (Figure 76), evident in the distinct lack of clear linearity until 75 °C, Type II PZT (PIC255) also exhibits a strange trend of a negative temperature dependence of d_{init} (polarisation and reversible domain contributions) to the order of -0.19 pCN^{-1} $°C^{-1}$ and negative extrinsic contribution dependence (Figure 80). Further analysis shows a second order polynomial fits PIC255 data throughout the entire temperature range, giving an expression for room temperature behaviour of:

$$d_{33} = 328.8 + 26.5X_{max} - 1.3X_{max}^2 \tag{10}$$

9.1.2 BFLPT

BFLPT however exhibits Rayleigh behaviour at 48 hours after poling, while exhibiting strong temperature dependence throughout the range of applied stress (Figure 77) to the order of 0.11 pCN^{-1} $°C^{-1}$ as already noted in Section 8.

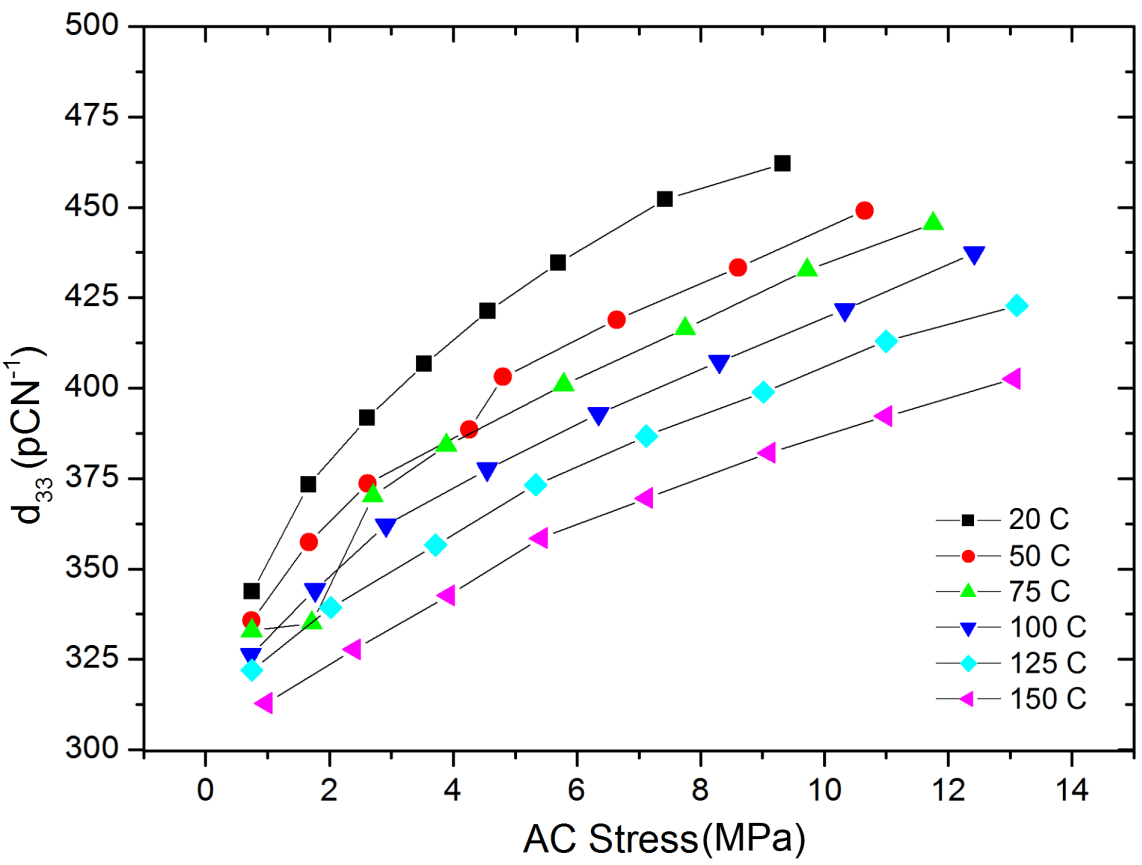

Figure 76: Direct-effect response of PIC255 48 hours after poling.

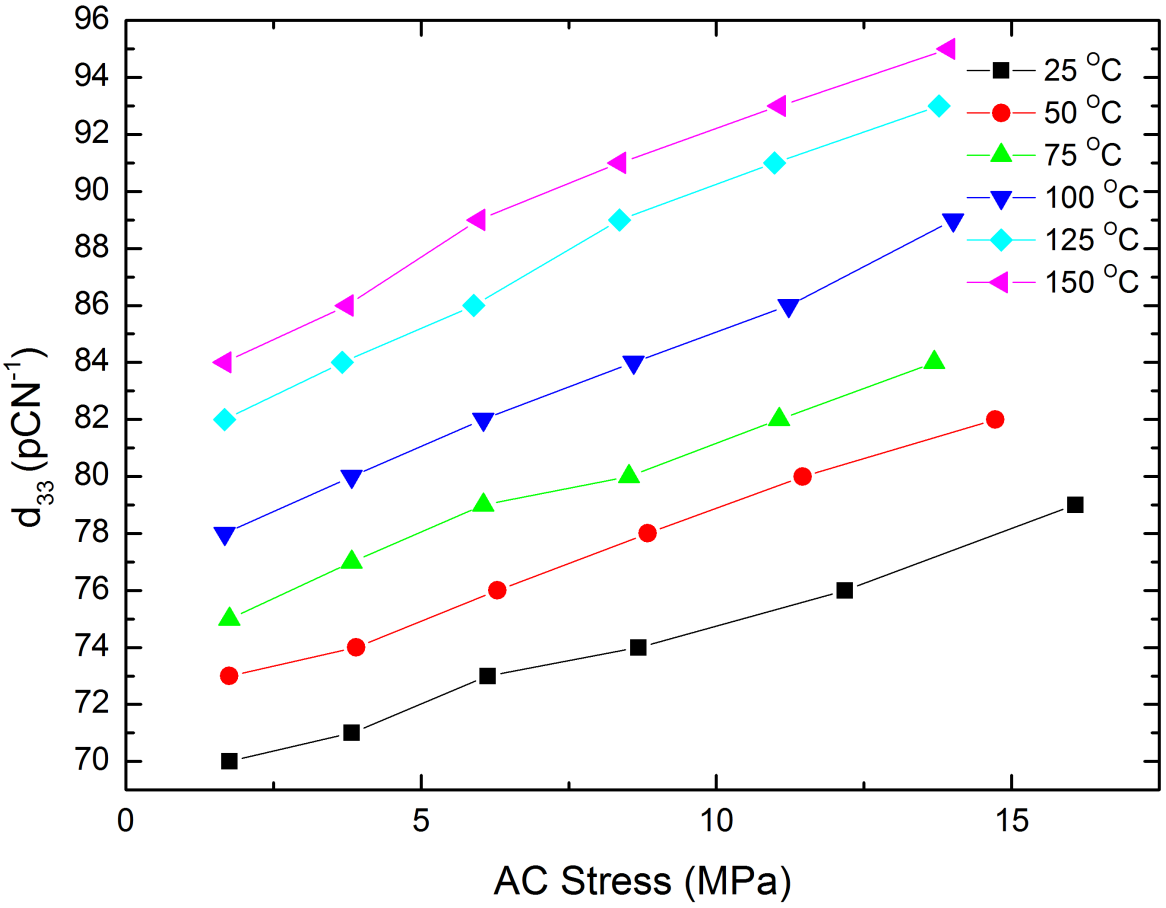

Figure 77: Direct-effect response of 3% La-doped BFPT material 48 hours after poling.

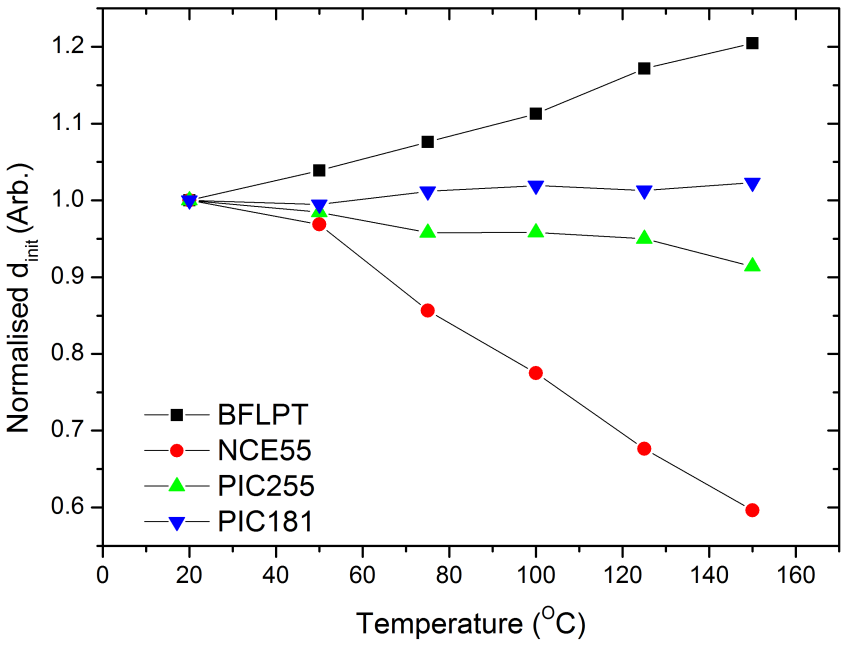

Figure 78: Normalised temperature dependence of d_{init}.

9.2 1 Month After Poling

Subsequent repeat measurements were taken after 1 month ageing at room temperature and humidity.

9.2.1 PZT

The one month ageing period has caused all materials to become Rayleigh-like in their behaviour - linear stress responses are observed for all three compositions (Figures 79, 96 & 98) throught the experimental temperature range.

Further, the previously observed temperature dependence of the PIC255 (Type II) material has been significantly reduced, something figure 80 helps visualise the stark change in the behaviour of intrinsic (d_{init}) and extrinsic (α) contributions in the intermediate PIC255 (Type II) PZT – losing most temperature dependence in intrinsic contributions (Figure 80) but still retaining a slight negative trend (-0.05 pCN^{-1} $°C^{-1}$), suggesting a significant amount of change

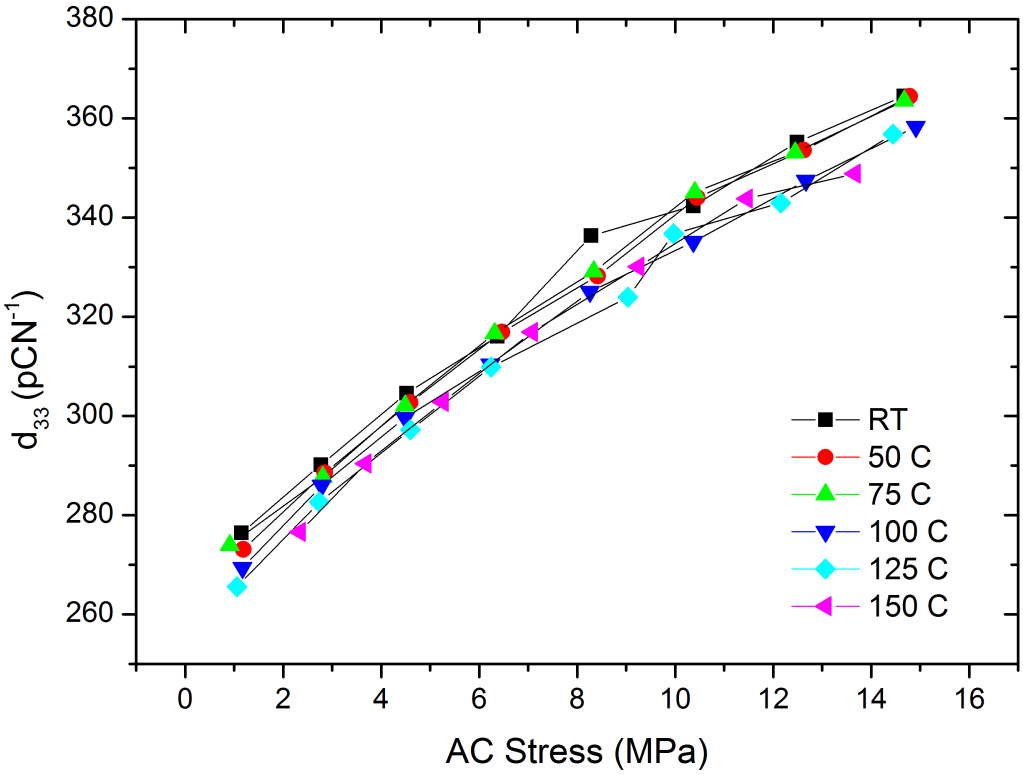

Figure 79: Response of 1 month aged PIC255 to alternating stress.

has occurred since the initial 48 hour ageing period, and appearing analogous in behaviour to hard PZT at 48 hours after poling (Figure 97, appendix).

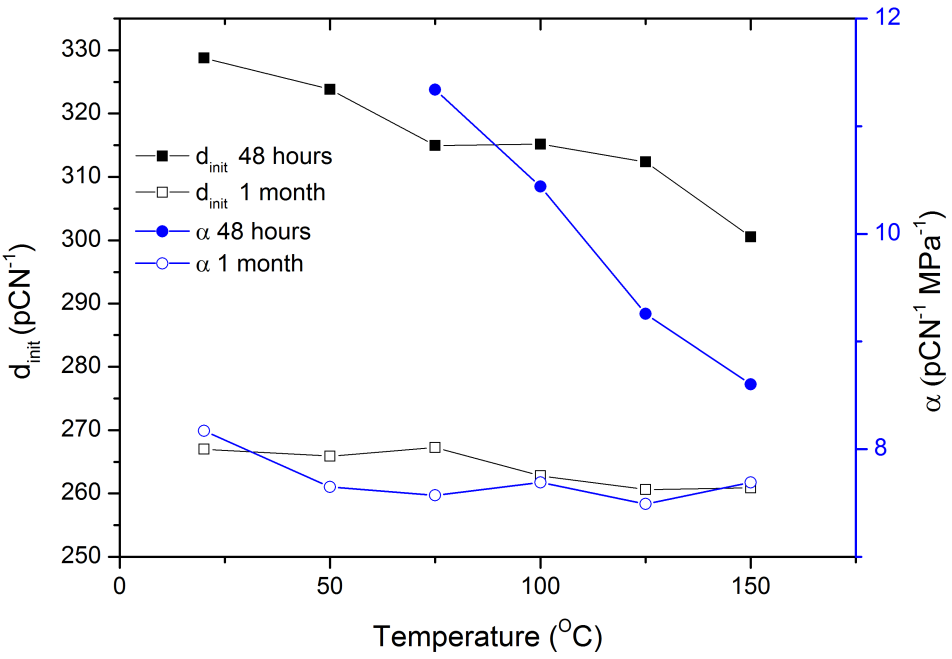

Figure 80: Rayleigh parameters α and d_{init} as a function temperature for PIC255 calculated from data shown in figures 76 and 79. At 48 hours aged, d_{init} has been calculated from a second order fit.

Using equation 11 we can extract the contributions to the material response that arise from non-switching domains. Whereby α is the Rayleigh coefficient, and X_O is the total stress applied.

$$Irrev.Contributions = \frac{\alpha X_O}{d_{init} + (\alpha X_O)}.100 \tag{11}$$

Figure 81 correlates with the observed temperature behaviour of intrinsic contributions in PIC255, showing negative temperature dependence in irreversible domain contributions. By comparison, PIC181 ages to form negligible temperature dependence in these contributions (Figure 99).

With an arguably significant change occurring in PIC255 (Type II) material, the temperature

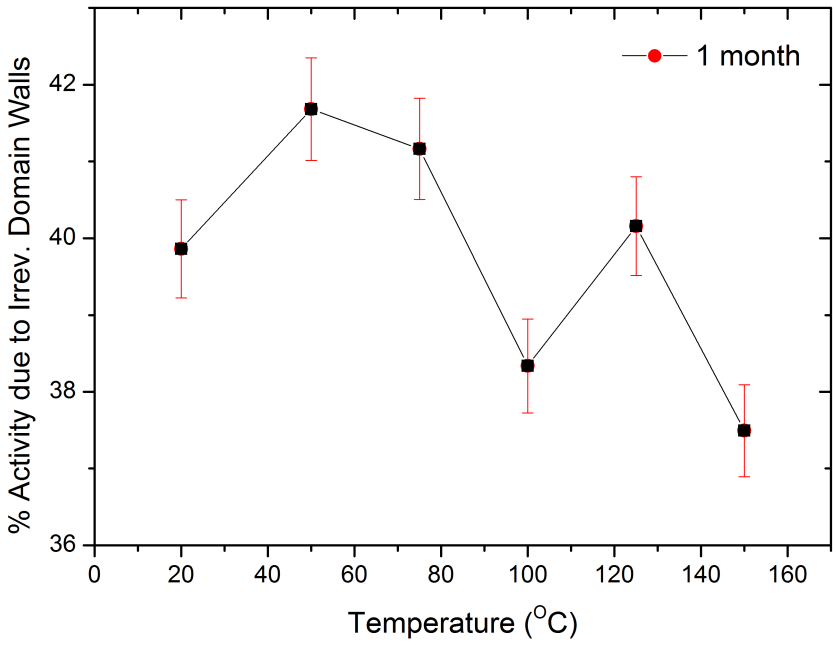

Figure 81: Calculated activity in PIC255 arising from irreversible domain wall contributions 1 month after poling.

dependence of other contributors was examined as a means of eliminating other extraneous phenomena that may have influenced the ageing of the materials over the experimental temperature range previously used (25–150 °C). To do this, discs of the same material as the cylinders tested previously were examined for permittivity and polarisation change as a function of temperature 48 hours after poling. This data was then subject to a 3rd order fitting for both polarisation and permittivity. The resultant data presents negligible temperature dependence in PIC255 (Type II) material across the experimental temperature range.

9.2.2 BFLPT

However the BFLPT material, although still exhibiting a Rayleigh response to stress, is still showing temperature dependence throughout the stress range albeit a dependence approximately have that observed at *poling + 48 hours* (Figure 83) 0.05 pCN^{-1} $°C^{-1}$ to 0.11 pCN^{-1} $°C^{-1}$. With 3 months ageing, BFLPT has also become mechanically stiffer (Figure 84, bottom).

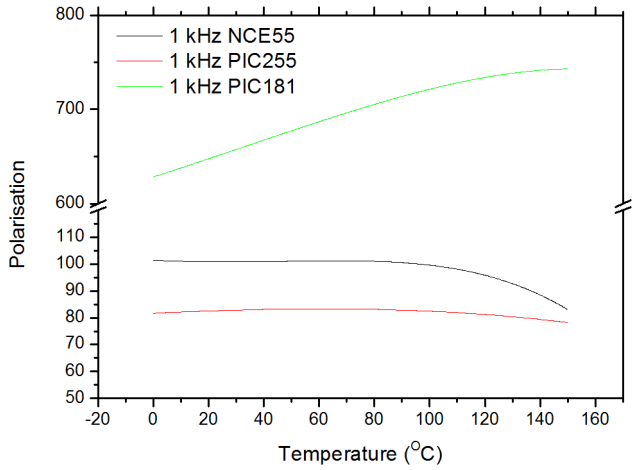

Figure 82: Calculated values from experimental permittivity and polarisation fits as a function of temperature for NCE55, PIC255, PIC181 throughout the experimental temperature range.

9.3 Conclusions

The softest PZT (NCE55) ceramic on test exhibited behaviour which corroborates the 48 hour theory. The material response remains largely unchanged after 48 hours and 1 month post-poling, however temperature dependence drops by 20%.

Similarly, the hardest PZT tested (PIC181) is applicable to the 48 hour ageing theory – temperature dependence is extremely minimal at 48 hours, with a strong linear Rayleigh-like response to stress. 1 month ageing results in an already inconsequential temperature dependence (0.041 pCN^{-1} $\circ C^{-1}$) of intrinsic contributions reducing further and extremely linear response to applied alternating stresses. PIC181s loss of temperature dependence is also apparent in the extrinsic contributions – observed as the near constant gradient across all temperatures representing the α co-efficient in figure 98. Combined with the increase in contributions due to irreversible domain walls, suggesting domain wall pinning is the key contributor to ageing in the ceramic (Figure 99, appendix).

The greatest interest lies with PIC255 (Type II), it shows no conformity to the notion of 48 hours being sufficient time for complete, or even a large proportion of ageing to have taken

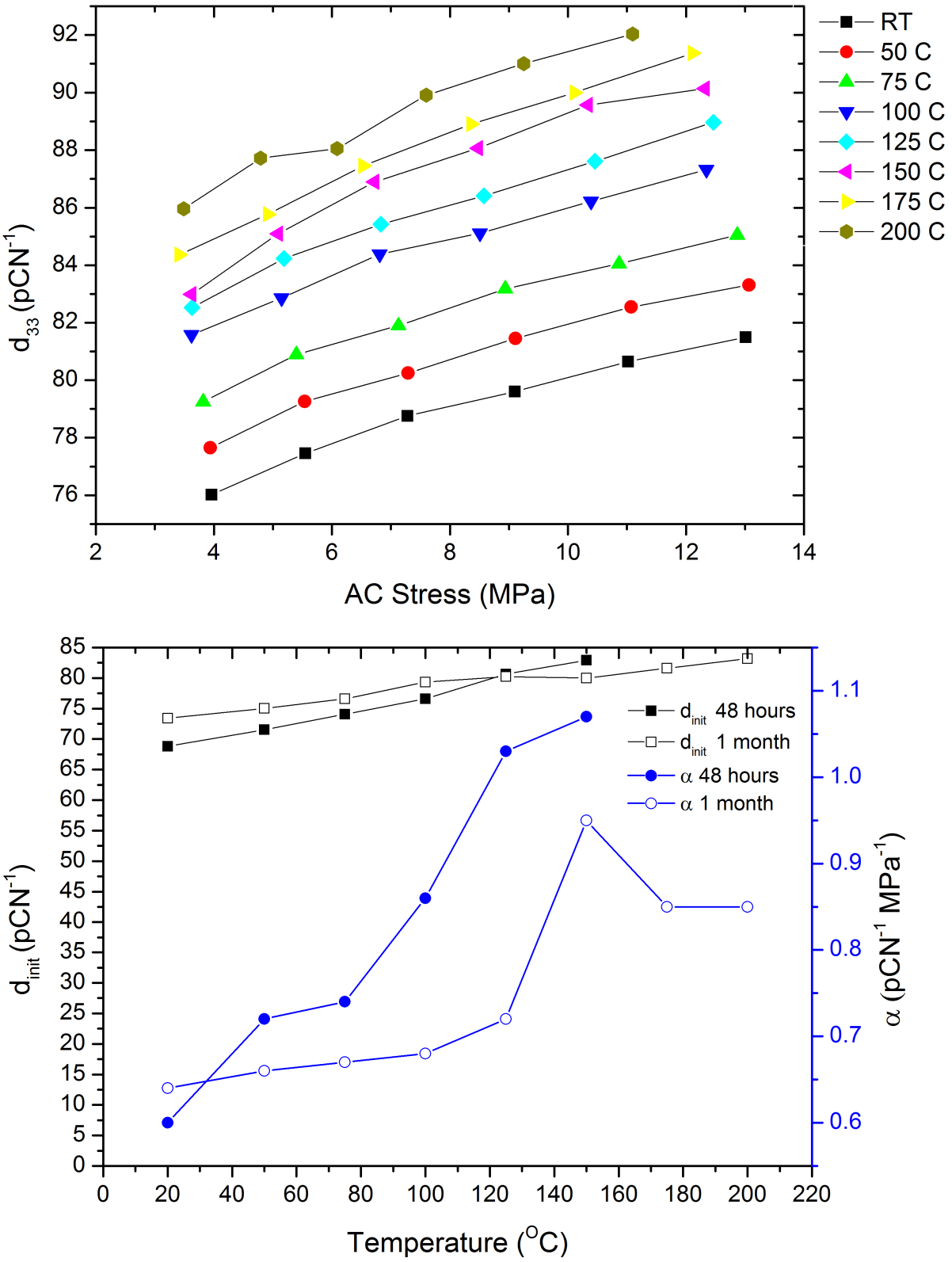

Figure 83: Response of 1 month aged BFLPT material to alternating stress.

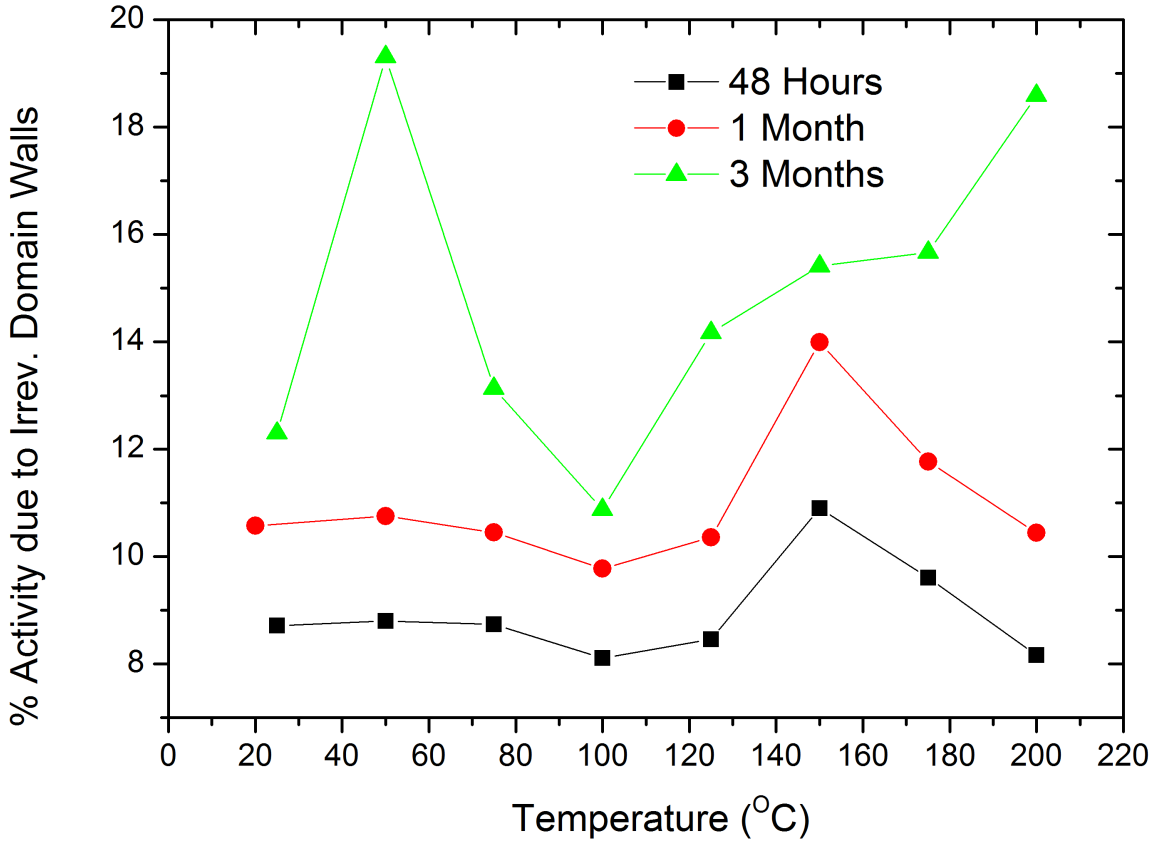

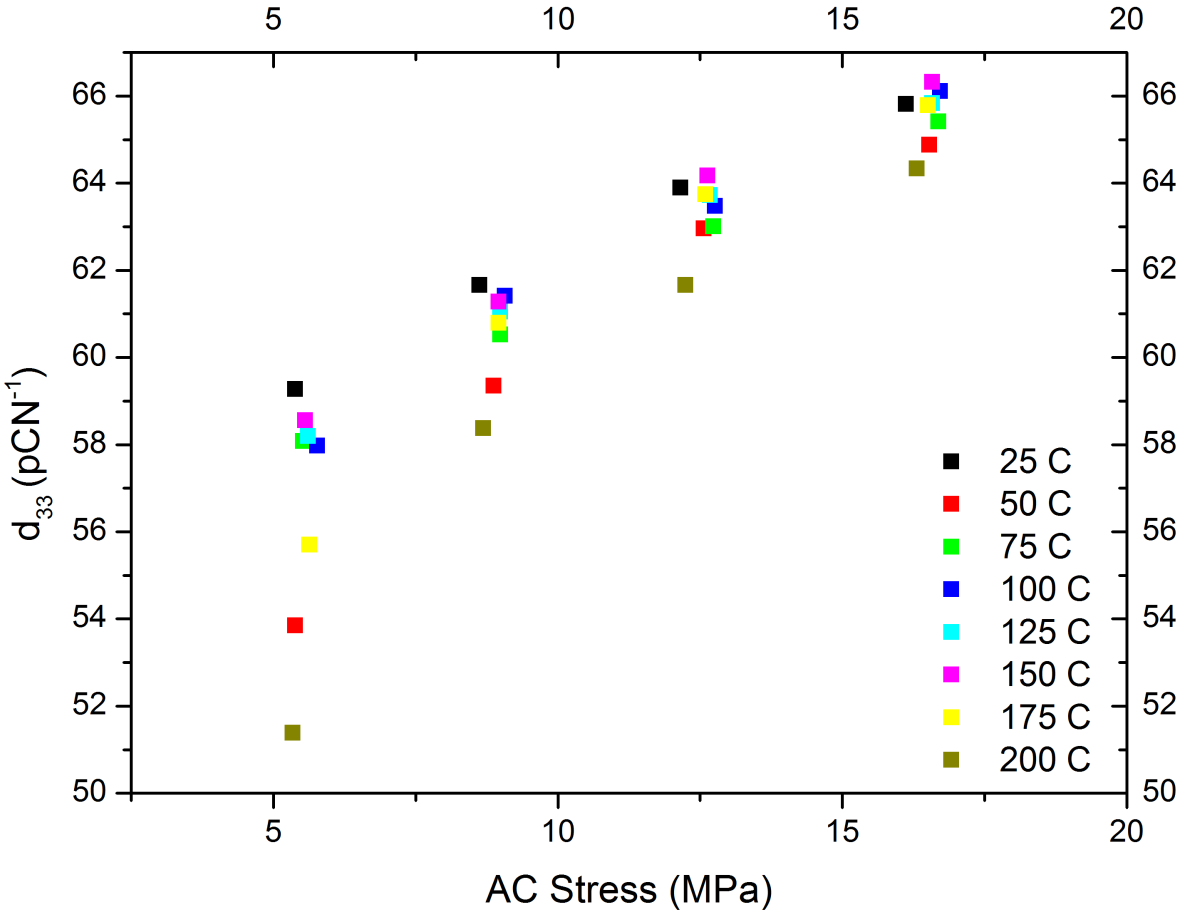

Figure 84: Top: Temperature dependence of irreversible domain wall contributions to the direct-effect response of BFLPT. Bottom: Response of 3 month aged BFLPT to alternating stress.

place. The material is initially heavily negatively temperature dependent with respect to intrinsic contributions (-0.19 pCN^{-1} $\circ C^{-1}$), a dependence which is reduced some 74% after a month of ageing with Rayleigh behaviour also being expressed at more temperatures after 1 month ageing period. The negative temperature dependence of d_{init} is rather unexpected, as one would expect the intrinsic contributions of the material to increase with temperature due to increased dipole and crystallographic mobility and reduced E_C – suggesting a second contributor to the observed piezoelectric response is dominating. Meanwhile extrinsic contributions, observed as the gradient of piezoelectric activity as a function of AC stress (α coefficient) show a heavy temperature dependence (Figure 80) at 48 hours, after 1 month ageing this temperature dependence has relaxed to be fairly insignificant along with a fairly constant contribution of irreversible domain walls.

The observed reduction of both d_{init} and α temperature dependence in PIC255 (Type II) suggests that the reduction of domain wall motion is a very dominant factor in how much intrinsic contributions can be expressed – corroborating conclusions made with respect to BFLPT in Section 8. For intrinsic contributions to be present, there is a requirement for some domain wall motion to allow for the crystallographic mobility needed for intrinsic contributions to be evident (Section 2.1). If the domain wall motion is hindered, this reduces the overall crystallographic mobility – i.e. the intrinsic contribution is constrained within the domain walls.

Table 12: Contribution Temperature Dependence Breakdown

Material	d_{init}	α	d_{33} Intrinsic	d_{33} Reversible Domain Walls
BFLPT (+48 hrs)	16%	31%	12%	4 %
BFLPT (+1 mo)	11%	25%	–	–
Type II (+48 hrs)	9%	31%	5%	4 %
Type II (+1 mo)	2%	6%	–	–

BFLPT on the other hand, stands separate in its behaviour - expressing linear stress response at both ageing points, extremely similar positive temperature dependence of intrinsic contributions and a strong positive temperature dependence of extrinsic contributions, with significantly

aged BFLPT showing negligible intrinsic contribution temperature dependence (Figure 84, bottom), but continuing extrinsic temperature dependence.

An aside to the accuracy of 48 hours ageing being sufficient before experimentation, a critical observation is that of how applicable the Rayleigh law is to ferroelectric ceramics while still clearly ageing. The case of PIC255 highlights this rather well with no linear Rayleigh fit possible when aged for 48 hours, not without a significant degree of inaccuracy, the only definite conclusion the results show is that the material is operating in excess of its Rayleigh region - i.e. at stresses where assumptions made regarding Rayleigh law behaviour cannot be ignored as the stress is likely sufficient to produce domain volumetric changes or even domain switching. The only conceivable means of verifying this theory would be by use of a synchrotron source for crystallographic data of materials at different ageing points under stress and temperature changes. Further, several theories fit the change in behaviour observed in the Type II PZT:

- It is widely known that at approximately 150 °C the mobility of oxygen vacancies increases suggesting the action of these measurements is what has caused the material response to change so drastically – without conclusive compositional information of the Type II PZT, the applicability of this theory is academic at best as too many questions arise without compositional information; how has the material been doped? Are the dopants alio- or isovalent? Basically, has the material been softened (or hardened) to it's Type II state by pure chemistry or by manipulating defect chemistry?

- Assuming the response at 1 month after poling is sound, then what the experiment has induced is rapid ageing in the material - the increased thermal energy has provided the defects in the material a means of "settling" into an energetic minima faster than if the sample were poled and left on a shelf for months before use – a form of *rapid ageing.*

In summary, there is one wide-sweeping conclusion that can be made from this ageing study: The *de facto* ferroelectric ageing time of 48 hours before experimental use is not as widely applicable as believed.

10 Fatigue of Monolithic 3% La-doped Bismuth-Ferrite Lead-Titanate

10.1 Sample Fabrication

As-sintered powders were prepared according to Section 5.1, the resultant cylindrical samples were ground and polished to have an aspect ratio of 1:1 or greater and silver electrodes painted on the correct face for the sample geometry before being polished. Once prepared, the sample was poled to 7 kV mm^{-1} for 1 minute at room temperature, with field applied in accordance with BS EN 60243-1:1998. A minimum of 48 hours were left between initial material poling and all experimental procedures – Rayleigh measurements, fatigue and final Rayleigh measurements.

10.2 Mechanical Cycling

Using data from Section 7.2 as a guide, the BFLPT monolith was cycled at a peak stress of 300 MPa (100 MPa pre-stress) at 10 Hz for 1,000 cycles to elicit a notable fatigue response (Figure 85).

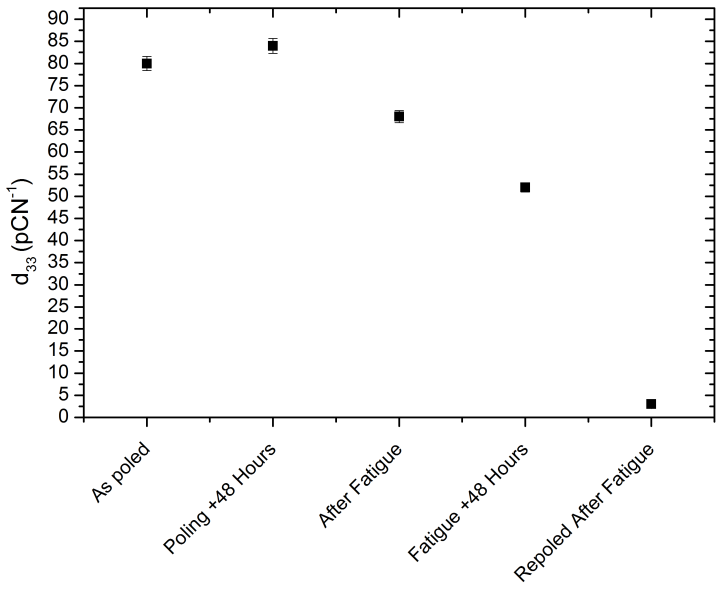

Figure 85: Fatigue response of BFLPT monolith.

Although a dramatic reduction in activity was observed, there was no external visual damage to the monolith.

10.3 Domain Behaviour

48 hours after poling, but before fatigue cycling, the sample was subject to Rayleigh measurements to a temperature of 150 °C – exhibiting a very Rayleigh-like linear response (Figure 88) with a clear temperature dependence of intrinsic contributions to the direct-effect response (Figure 87).

With subsequent fatigue cycling achieving an activity reduction of nearly 40%, the domain behaviour was investigated using the same direct-effect Rayleigh methodology to 200 °C as covered in the previous chapter. The results show a material still possessing a temperature dependence in intrinsic contributions (d_{init}) to its piezoelectric behaviour and a very linear relationship between applied alternating stress and activity (Figure 88), the overall temperature dependence is still linear with a marginally reduced co-efficient of dependence (0.11 pCN^{-1} $°C^{-1}$) for unfatigued and 0.08 pCN^{-1} $°C^{-1}$ for the fatigued material.

Further use of Rayleigh theory can be used to elaborate upon the proportion of total activity as a result of irreversible domain walls by virtue of equation 11.

Application of this to the aforementioned data, yields results shown in figure 89 - mechanical fatigue of the material has led to an increase in irreversible domain wall contributions to its direct effect response, suggesting fatigue has come about as a result of increased domain wall pinning. However, depoling of the fatigued material and attempts at repoling have been futile - the depoled fatigued material capable of withstanding only 0.3 $kVmm^{-1}$ before breakdown at room temperature, suggesting an irreversible change has taken place within the material. Although no cracks have been detected in the material from resonance analysis after fatigue.

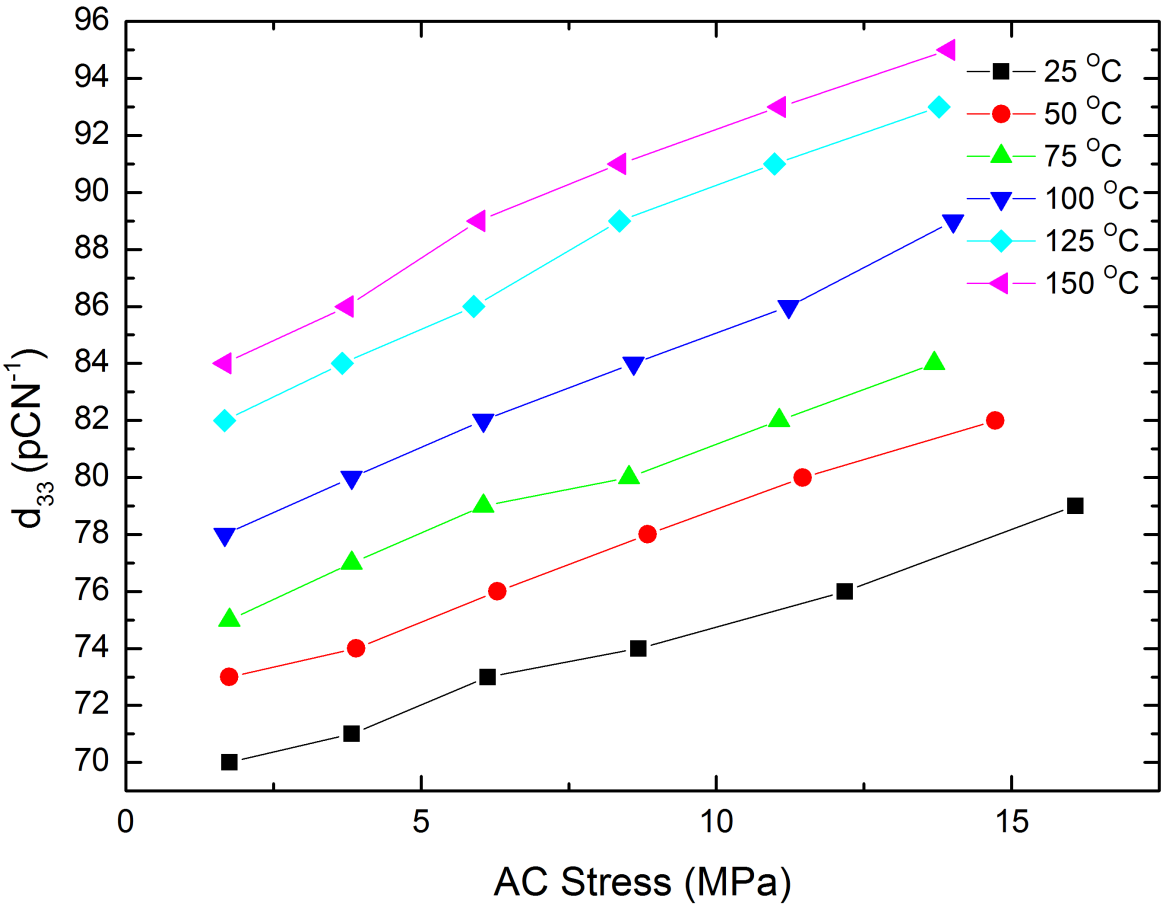

Figure 86: Response of a 48 hours aged La-doped BFLPT cylinder to an applied AC stress (1 Hz).

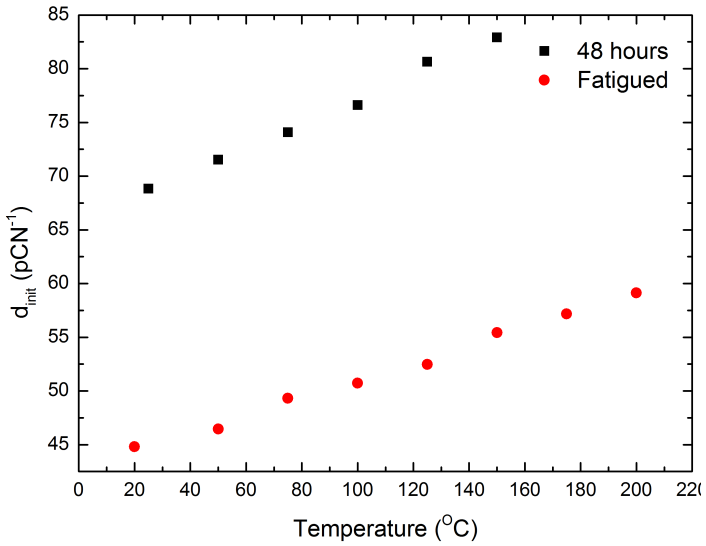

Figure 87: Temperature dependence of d_{init} for a virgin BFLPT sample 48 hours after poling, and a fatigued BFLPT sample 48 hours after poling.

10.4 Conclusions

Although cycling BFLPT at high stresses is possible, without causing any readily observable external damage, it is clear from the inability to re-pole the material after fatigue that there has been some form of defect formation leading to a reduction in dielectric strength and the observed breakdown at 0.3 kV mm^{-1}. Even with this fundamental damage to the material occurring from mechanical fatigue, it is still clearly capable of expressing Rayleigh behaviour when subject to direct-effect experimentation in a fatigued state – showing that there has been little change with respect to both intrinsic and extrinsic contributions. However, the monolith is incapable of being re-poled after thermal depolarisation post-fatigue, because the direct-effect was exploited to cause a fatigue response, the likes of point-defects (Section 3.1.3), oxygen vacancies and electrode chemistry (Section 3.1.2) can largely be ignored as there is no field present to disturb these defects during the fatigue regime. With this in mind the logical conclusion for the damage sustained during mechanical fatigue leading to breakdown at 0.3 kV mm^{-1} is that of microcracks (Section 3.1.4) within the monolith structure – taking the dielectric strength of dry air to be 3 kV mm^{-1}, this yields a fracture size of approximately 100 μm.

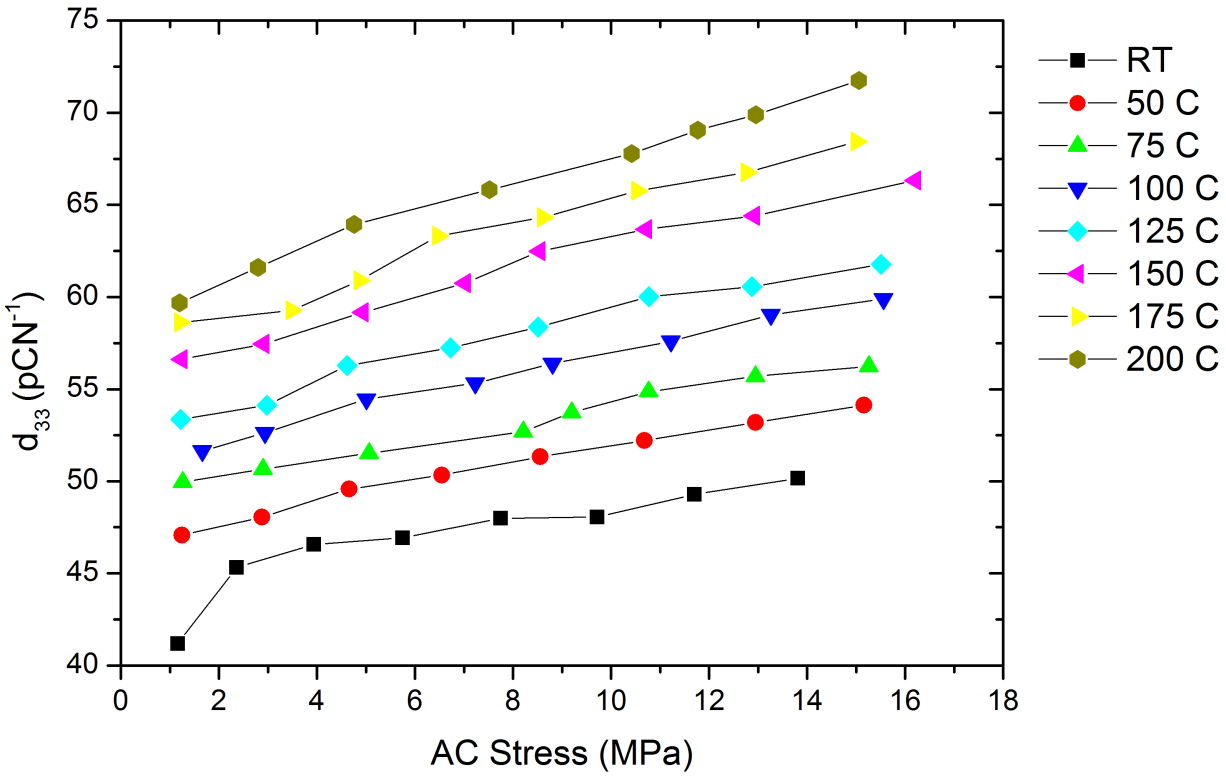

Figure 88: Response of a fatigued La-doped BFPT cylinder to an applied AC stress (1 Hz).

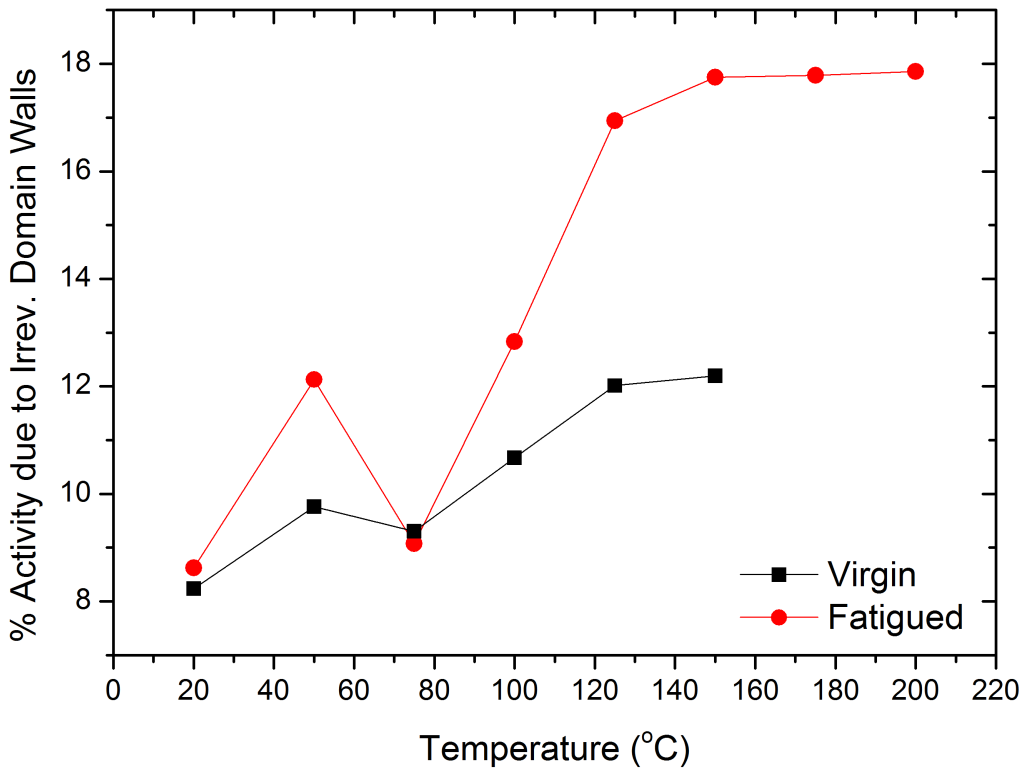

Figure 89: Contributions in the virgin and fatigued BFLPT system.

11 Fatigue of Monolithic Lead Zirconate Titanate

Although investigating BFLPT is interesting, but how it compares to PZT is very important. The same fatigue investigation from the previous chapter was carried out on various PZT compositions.

11.1 Samples

Samples of PIC255 (Type II) and PIC181 (Type I) were prepared by Physik Instrumente with a dimensionality of at least 1:1. The resulting materials were depoled at 500 °C, repoled in a field of 2.25 kV mm^{-1} at approximately 75 °C. A minimum of 48 hours were left between initial material poling, Rayleigh measurements, fatigue and final Rayleigh measurements.

PIC255 samples were cylindrical, with diameter 4.01 mm and length 4.23 mm, while PIC181 took the form of a rectangular prism with dimension 2.00 x 2.00 x 4.00 mm

11.2 Mechanical Cycling

Again, as with BFLPT monoliths, Section 7.2 was reference for the alternating stresses to be applied.

Table 13: Parameters for mechanical cycling of PZT monoliths

Material	Pre-stress (MPa)	Peak Stress (MPa)	Frequency (Hz)
PIC255 (Soft)	25	200	10
PIC181 (Hard)	10	100	10

11.3 Rayleigh Response

11.3.1 Type II PZT - PIC255

Although a strong fatigue response is observed in the PIC255 (Type II) material – an activity reduction of approximately 70%, visually the response (Figure 91) appears very similar to what

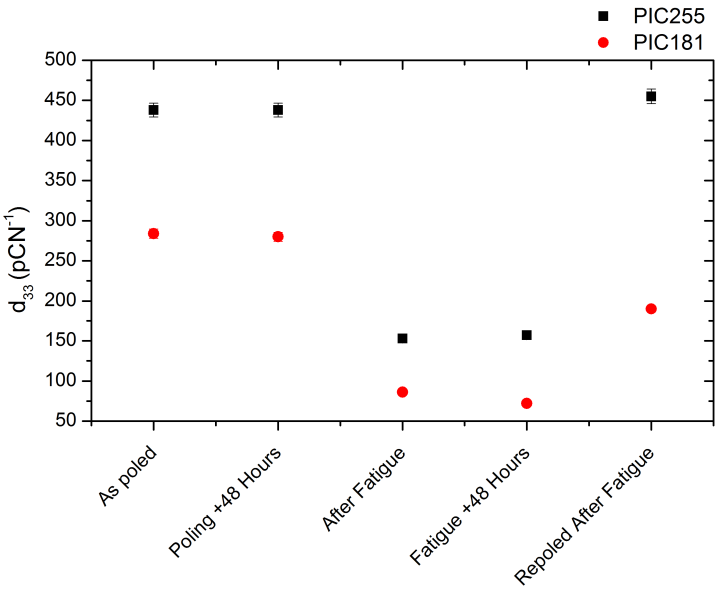

Figure 90: Fatigue response of PIC255 and PIC181 monoliths.

was observed previously (Section 9.2.1). However, proper analysis of the data reveals (Figure 92) the material response to direct-effect stimulus using Rayleigh methodologies previously discussed is unlike that observed previously in virgin material (Figure 80).

The material now shows a strong postitive temperature dependence of intrinsic (d_{init}) and extrinsic (α) contributions - in complete opposition to what was observed when the same material had aged for 48 hours after poling (Figure 80).

11.3.2 Type I PZT - PIC181

With fatigue cycling achieving a substantial activity reduction of approximately 70%, the domain behaviour was investigated using direct-effect Rayleigh methodology up to 150 °C. The most readily observable change in the fatigued PIC181 over the virgin equivalent is the increased mechanical stiffness of the material - where previously a 20 μm displacement from the test apparatus actuator would result in peak compressive stress of approximately 35 MPa, the same effect now produces a peak compressive stress approaching 50 MPa (Figure 93) suggesting the presence of frature toughening in this particular PZT composition (Section 1.4).

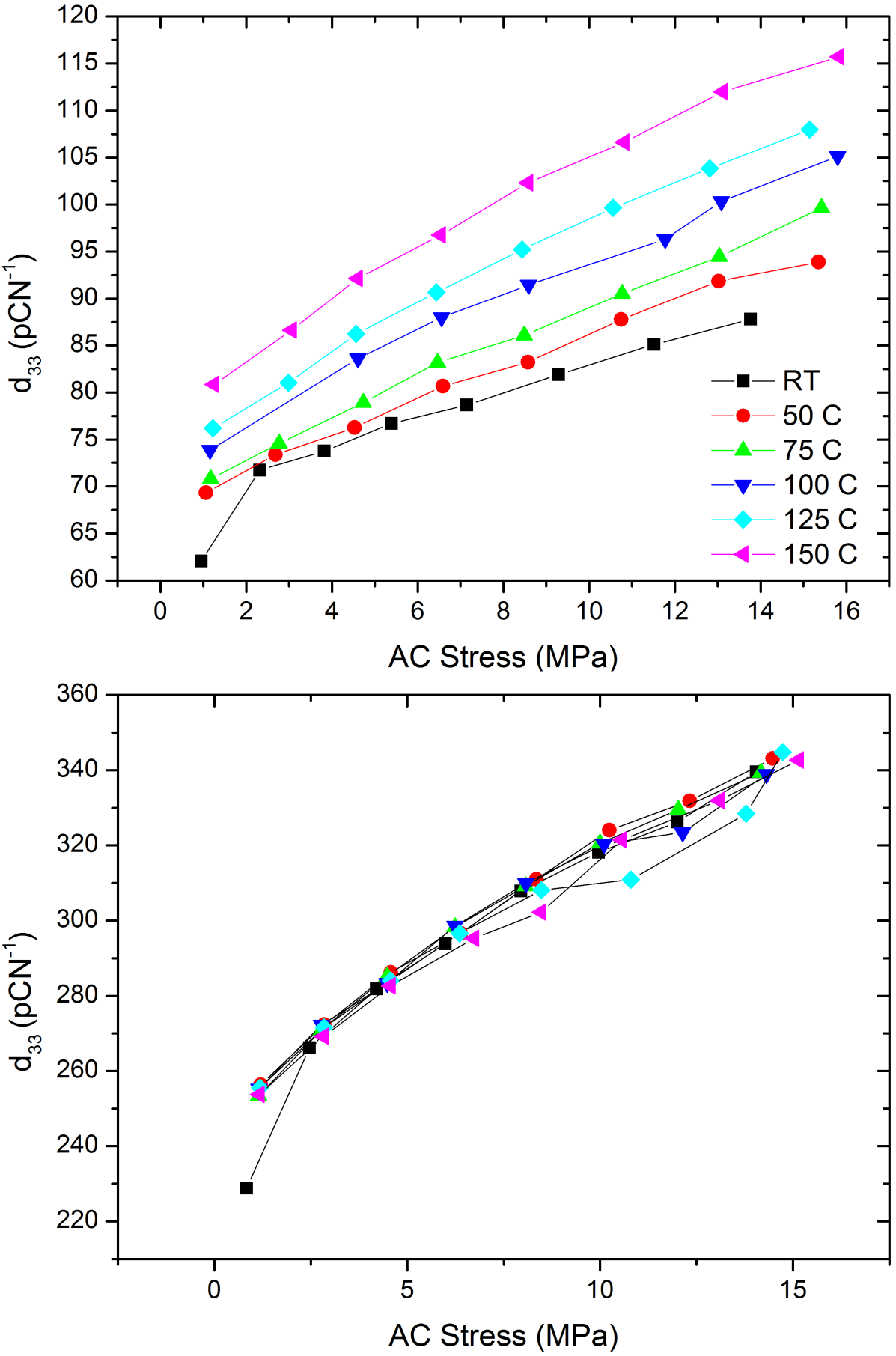

Figure 91: Rayleigh response for PIC255 after fatigue (top) and 48 hours after repoling after fatigue (bottom).

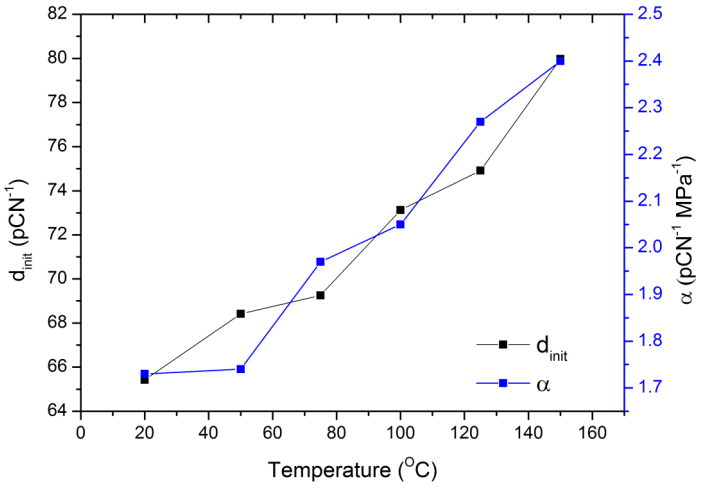

Figure 92: Variation of intrinsic (d_{init} and extrinsic (α) contributions to the direct effect piezoelectric response of fatigued PIC255.

The material still exhibits the previously observed lack of intrinsic contribution (d_{init}) temperature dependence – albeit with slight variation, with extrinsic contributions (α) tending towards zero with increased temperature (Figure 94).

Furthermore, upon repoling the fatigued monolith under the same conditions as when freshly prepared, there is a reduction of activity from 284 pC N^{-1} to 190 pC N^{-1}. Unlike BFLPT, the peak field for poling was achieved with ease without dielectric breakdown. The repoled material, aged for 48 hours, exhibits the same behavioural trend as its virgin counterpart after the equivalent ageing period (Figure 76) albeit with a reduced activity observed.

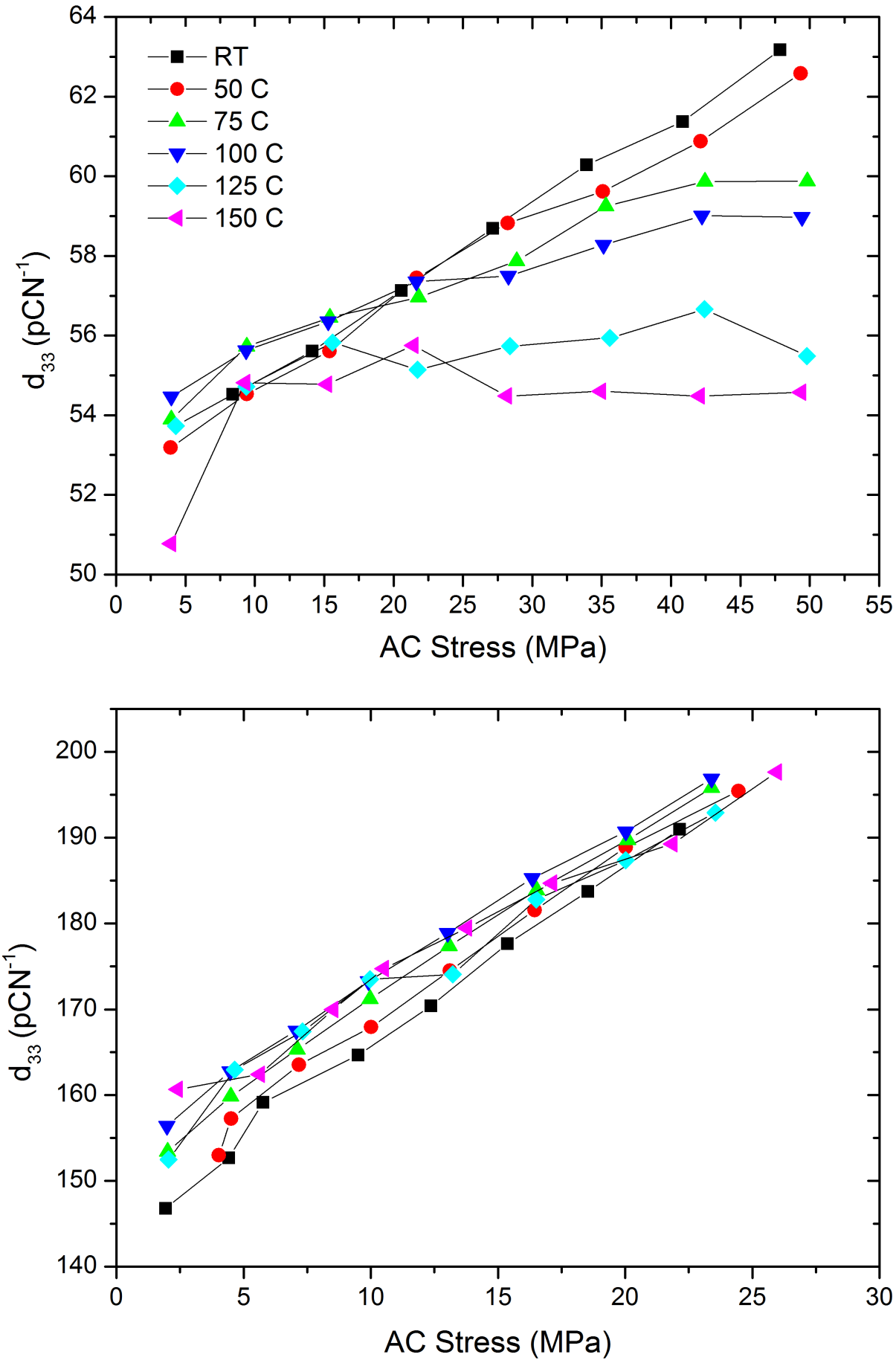

Figure 93: Rayleigh response for PIC181 after fatigue (top) and 48 hours after repoling after fatigue (bottom).

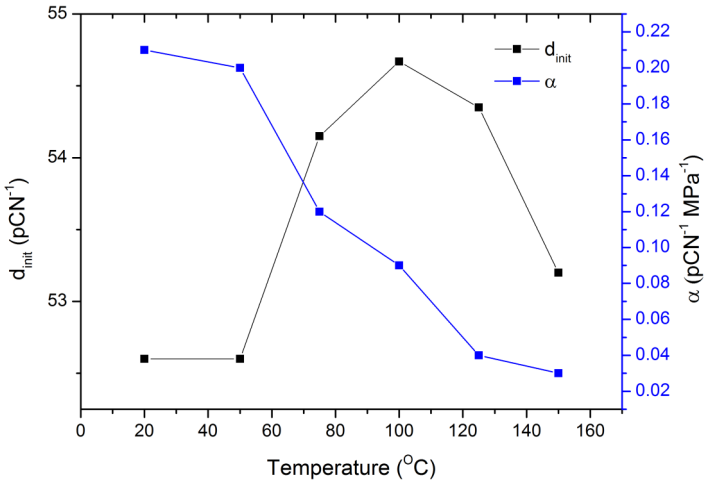

Figure 94: Variation of intrinsic (d_{init} and extrinsic (α) contributions to the direct effect piezoelectric response of fatigued PIC181.

11.4 Conclusions

PIC181s inherent behaviour still remains after a strong fatigue response, further the same inherent character continues to be expressed after repoling of the fatigued material. The softer PIC255 material shows no significant change in Rayleigh response at any stage, aside from the reduced d_{init}, furthermore the ability to repole the material after fatigue to pre-fatigue activity suggests there has been no internal structural damage (as observed in BFLPT) that could lead to dielectric breakdown at weak fields.

12 Overall Summary & Conclusions

Given the several different experimental procedures used during this research, a number of conclusions can be made and are discussed in their respective chapters. With respect to the initial aim of this work – evaluating La-doped BFPT as a competitor to PZT in high temperature applications, several conclusions can be deduced:

- Compared to a well developed, commercial hard PZT material, La-BFPT displays a similar T_C (approx. 400 °C) but has a depolarisation temperature in excess of hard PZT – Section 6.
- La-doped BFPT multilayer elements can be mass produced with a very small manufacturing variation in properties – Section 7.1
- Purely from a mechanical point of view, La-doped BFPT is significantly stronger than PZT in a multilayer configuration – observed in Section 7.2 where BFPT exhibits a yield point of 800 MPa, compared to no greater than 200 MPa for both PZT compositions investigated. This mechanical property advantage extends into mechanical cycling.
- La-doped BFPT has similar lifetime to PZT when used in converse-effect mode, withstanding 2,000 million cycles at 3.3 kV mm^{-1} before an observable decrease in piezoelectric activity (Section 7.3).
- Multilayer devices are capable of withstanding larger alternating stresses than the same composition in a monolithic configuration.

Further conclusions from Rayleigh investigation and ageing effects can be made:

- La-doped BFPT obeys the Rayleigh law for direct-effect measurements throughout a temperature range of 25-200 °C at all ageing time points – Section 8.
- Very soft (NCE55) and very hard (PIC181) PZT obey the Rayleigh law throughout a temperature range 25-150 °C at all ageing time points – Section 8.

- PIC255, a composition softer than PIC181, shows negative temperature dependence of intrinsic contributions shortly after poling, but with sufficient ageing time exhibits behaviour reminiscent of the harder PIC181 – Section 8.
- The *de facto* ageing time for ferroelectric ceramics of 48 hours is not sufficient for the ratio of intrinsic to extrinsic contributions to be stable in some compositions with mixed character, such as PIC255 – Section 8.
- It has been observed from synchrotron X-ray diffraction that in La-doped BFPT a transformation toughening mechanism *may* be in effect – causing a 10% incerase in rhombohedral phase concentration and is theorised to be the cause for the enhanced mechanical properties of the material (Figure 73). This result is being treated with certain degree of scepticism as more information is needed before a transformation toughening effect can be conclusively verified to exist in BFLPT.
- Furthermore this composition has been observed to follow Rayleigh law at weak cycling stresses up to 200 °C, due to the high depolarisation and Curie temperatures exhibited.

PZT has been observed following Rayleigh behaviour for both very hard (PIC181), very soft (NCE55) and *"medium"* hardness (PIC255) ceramics. Although strange temperature dependence in NCE55 and PIC255 compositions with respect to intrinsic and extrinsic contributions has been noted and theorised to be as a result of a constraint of domain motion (extrinsic contributions) reducing polarisation effects (intrinsic contributions). Due to the commercially sensitive nature of the PIC255 composition, the most reasonable explanation for the change in character after ageing pertains to that of defect chemistry (i.e. oxygen vacancies) – the addition of aliovalent species, changing the defect chemistry of the ferroelectric and this influencing domain wall motion. However, it is also possible to soften and harden ferroelectric materials without affecting defect chemistry, by use of isovalent species reducing T_C without any change to the likes of oxygen vacancies, therefore in order to have a conclusive representation of the cause of this character change further experimentation is required.

However, the most interesting conclusion to be made from this research is regarding something which was unintentionally discovered – the ageing of a ferroelectric material is not complete in the assumed 48 hours after poling. Macroscopic measurements of d_{33} and strain-field response are still valid as they are unchanged between 48 hours and 1 month after poling. This means that previously published measurements pertaining to intrinsic and extrinsic contributions, as well as temperature response of ferroelectric materials, may be incorrect as the micro- and nano-scale contributors to the material character have not equilibrated.

Finally, of merit is the development that has taken place of a means to de-convolute an approximation for the ratio of intrinsic to extrinsic contributions in a ferroelectric ceramic using conventional laboratory equipment, without the need for extended synchrotron experimental time.

13 Further Work

Unsurprisingly, given the critical review of fatigue mechanisms in this thesis, there is a significant amount of further research that could be conducted on this subject alone. Beginning with the likes of stereoscopic acoustic emission for mechanical and electrical cycling as a means to gauge crack formation and propagation in bulk ceramics. In addition, electrical fatigue of the bismuth-ferrite lead-titanate system is something missing from this work and would be beneficial in comparing the fatigue response of the system to direct and converse-effect induced fatigue.

Electrode composition changes with respect to fatigue in bulk and multilayer ceramic structures would be beneficial to investigate, as current information regarding electrode species' effects on ferroelectric ceramics resides solely in the domain of thin film materials (Section 3.1.2). The likes of RuO_2 electrodes could easily be deposited within multilayer devices and bulk structures. That is not to say thin film materials are not of interest, thin film experimentation using EBSD for *in situ* imaging of domain orientation and size while undergoing electrical fatigue would be an extremely novel venture and provide insight into the propagation of fatigue within ferroelectric ceramics rather than the stark change observed between virgin and fatigued ceramic when using macroscopic measurements.

Alterations to the piezo testing apparatus developed for this work would also form a key component of any further research arising from this work. A key modification would be the upgrading of thermal capability beyond the T_C of PZT to examine the behaviour of materials using Rayleigh analysis through their depolarisation. Furthermore, as concluded in section 9.3 the applicability of Rayleigh theory becomes more apparent with increased ageing time. The suspected cause for the lack of conformity to this theory is discussed and the logical next step for this work would be the use of a synchrotron source to have a conclusive result on any domain volumetric changes and defect chemistry effects.

The final contentious results are: the presumed transformation toughening occurring in BFLPT - this result is far from conclusive and needs further, more robust validation with

further synchrotron data, and the ageing observed in Type II PZT (PIC255) which would need validation by compositional verification from the manufacturer to explain the doping strategy employed and subsequent repeat Rayleigh measurements on samples at differing ageing time points.

References

[1] Safa O. Kasap. *Principles of Electronic Materials and Devices: Third Edition.* McGraw-Hill Higher Education, third edition, 2005.

[2] A.J Moulson and JM Herbert. *Electroceramics: Materials, Properties, Applications.* John Wiley and Sons Ltd, second edition, 2003.

[3] J. J. O'Dwyer. Current-Voltage Characteristics of Dielectric Films. *Journal of Applied Physics*, 37(2):599, 1966.

[4] Carlos A. Mota Soares, editor. *Mechanics of Composite Materials and Structures: Proceedings of the NATO Advanced Study Institute, Held in Troia, Portugal, 12-24 July, 1998 (NATO Science Series E.* Springer, 1999.

[5] Dragan Damjanovic. Ferroelectric, dielectric and piezoelectric properties of ferroelectric thin films and ceramics. *Reports on Progress in Physics*, 61(9):1267–1324, September 1998.

[6] Cedric Goueffon, Guillaume Rémi Cadiou, and Charles Mangeot. Noliac Piezo Technology Course Manual, 2010.

[7] HANS JAFFE, B JAFFE, and William R Cook. *Piezoelectric Ceramics.* Techbooks, reprint edition, 1989.

[8] J Valasek. Piezoelectric and allied phenomena in Rochelle salt. *Phys. Rev.*, 15:537–538(A), 1920.

[9] L E Cross and R E Newnham. History of Ferroelectrics. 111, 1987.

[10] L. D. Madsen, E. M. Griswold, and L. Weaver. Domain structures in Pb(Zr, Ti)O3 and PbTiO3 thin films. *Journal of Materials Research*, 12(10):2612–2616, January 2011.

[11] A. Gruverman. Domain structure and polarization reversal in ferroelectrics studied by

atomic force microscopy. *Journal of Vacuum Science & Technology B: Microelectronics and Nanometer Structures*, 13(3):1095, May 1995.

[12] Jong Kuk Kim, Sang Su Kim, and Won-Jeong Kim. Solgel synthesis and properties of multiferroic BiFeO3. *Materials Letters*, 59(29-30):4006–4009, 2005.

[13] F Yu, D Yuan, X Duan, L Kong, X Shi, S Guo, L Wang, X Cheng, and X Wang. Citrate sol-gel method to prepare nanoparticles of a piezoelectric crystal material: La3Nb0.5Ga5.5O14 at low temperature. *Journal of Alloys and Compounds*, 459(1-2):L1–L4, July 2008.

[14] I Stolichnov and A Tagantsev. Space-charge influenced-injection model for conduction in Pb(Zr[sub x]Ti[sub 1x])O[sub 3] thin films. *Journal of Applied Physics*, 84(6):3216, 1998.

[15] Bingrong Yuan, Shengwen Yu, Wufeng Yang, Xiaowen Zhou, and Jinrong Cheng. *Composition dependence of xBiFeO¡inf¿3¡/inf¿-(1-x)PbTiO¡inf¿3¡/inf¿ films prepared by sol-gel technique*. Number 149. IEEE, 2009.

[16] T Comyn, D Kanguwe, J He, and a Brown. Synthesis of bismuth ferrite lead titanate nano-powders and ceramics using chemical co-precipitation. *Journal of the European Ceramic Society*, 28(11):2233–2238, 2008.

[17] R. Eitel and C. Randall. Octahedral tilt-suppression of ferroelectric domain wall dynamics and the associated piezoelectric activity in Pb(Zr,Ti)O3. *Physical Review B*, 75(9):1–8, March 2007.

[18] Dragan Damjanovic and Marlyse Demartin. Contribution of the irreversible displacement of domain walls to the piezoelectric effect in barium titanate and lead zirconate titanate ceramics. *Journal of Physics: Condensed Matter*, 9(23):4943–4953, June 1997.

[19] Tadej Rojac, Marija Kosec, Bojan Budic, Nava Setter, and Dragan Damjanovic. Strong ferroelectric domain-wall pinning in BiFeO[sub 3] ceramics. *Journal of Applied Physics*, 108(7):074107, 2010.

[20] D Damjanovic, M Demartin, H S Shulman, M Testorf, and N Setter. AC ? WORS Instabilities in the piezoelectric properties of ferroelectric ceramics. *Sensors And Actuators*, 53:353–360, 1996.

[21] Dragan Damjanovic and Marlyse Demartin. The Rayleigh law in piezoelectric ceramics. *Ferroelectrics*, 29:2057–2060, 1996.

[22] D DAMJANOVIC, S BHARADWAJA, and N SETTER. Toward a unified description of nonlinearity and frequency dispersion of piezoelectric and dielectric responses in Pb(Zr,Ti)O3. *Materials Science and Engineering B*, 120(1-3):170–174, July 2005.

[23] Thomas R. Shrout and Shujun J. Zhang. Lead-free piezoelectric ceramics: Alternatives for PZT? *Journal of Electroceramics*, 19(1):113–126, 2007.

[24] Dragan Damjanovic and Marlyse Demartin. The Rayleigh law in piezoelectric ceramics. *Ferroelectrics*, 2057:10–14, 1996.

[25] Richard H. J. Hannink, Patrick M. Kelly, and Barry C. Muddle. Transformation Toughening in Zirconia-Containing Ceramics. *Journal of the American Ceramic Society*, 83(3):461–487, December 2004.

[26] A.G. Evans and R.M. Cannon. Overview no. 48. *Acta Metallurgica*, 34(5):761–800, May 1986.

[27] C. Leach, N.K. Ali, and D.a. Hall. Direct observation of domain switching and crack nucleation in a piezoelectric material. *Ceramics International*, March 2011.

[28] Gerold a. Schneider. Influence of Electric Field and Mechanical Stresses on the Fracture of Ferroelectrics. *Annual Review of Materials Research*, 37(1):491–538, 2007.

[29] G. Shirane, E. Sawaguchi, and Y. Takagi. Dielectric Properties of Lead Zirconate. *Physical Review*, 84(3):476–481, November 1951.

[30] Z. Gubinyi, C. Batur, A. Sayir, and F. Dynys. Electrical properties of PZT piezoelectric ceramic at high temperatures. *Journal of Electroceramics*, 20(2):95–105, December 2007.

[31] S. a. Mabud. The morphotropic phase boundary in PZT solid solutions. *Journal of Applied Crystallography*, 13(3):211–216, June 1980.

[32] VA Isupov. Direct Polarization of PbTiO3-PbZrO3 Solid Solutions. *Soviet Solid-State Physics*, 12:1084–1088, 1970.

[33] Richard E Eitel, Clive A Randall, Thomas R Shrout, Paul W Rehrig, Wes Hackenberger, and Seung-eek Park. New High Temperature Morphotropic Phase Boundary Piezoelectrics Based on Bi(Me)O3-PbTiO3 Ceramics. *Japanese Journal of Applied Physics*, 40(Part 1, No. 10):5999–6002, 2001.

[34] Alain B. Kounga, Torsten Granzow, Emil Aulbach, Manuel Hinterstein, and Jurgen Rodel. High-temperature poling of ferroelectrics. *Journal of Applied Physics*, 104(2):024116, 2008.

[35] J. E. Garcia, D. a. Ochoa, V. Gomis, J. a. Eiras, and R. Perez. Evidence of temperature dependent domain wall dynamics in hard lead zirconate titanate piezoceramics. *Journal of Applied Physics*, 112(1):014113, 2012.

[36] Richard E. Eitel, Thomas R. Shrout, and Clive A. Randall. Tailoring Properties and Performance of (1- x)BiScO 3 - x PbTiO 3 Based Piezoceramics by Lanthanum Substitution. *Japanese Journal of Applied Physics*, 43(No. 12):8146–8150, 2004.

[37] S. B. Majumder, B. Roy, R. S. Katiyar, and S. B. Krupanidhi. Effect of acceptor and donor dopants on polarization components of lead zirconate titanate thin films. *Applied Physics Letters*, 79(2):239, 2001.

[38] Dragan Damjanovic. Ferroelectric, dielectric and piezoelectric properties of ferroelectric thin films and ceramics. *Reports on Progress in Physics*, 61(9):1267–1324, September 1998.

[39] Jin-rong Cheng, Richard Eitel, and L Eric Cross. Lanthanum-Modified (1 - x)(Bi 0.8 La 0.2)(Ga 0.05 Fe 0.95)O 3 xPbTiO 3 Crystalline Solutions: Novel Morphotropic Phase-Boundary Lead-Reduced Piezoelectrics. *Journal of the American Ceramic Society*, 86(12):2111–2115, December 2003.

[40] Masato Matsubara, Toshiaki Yamaguchi, Koichi Kikuta, and Shin-ichi Hirano. Sinterability and Piezoelectric Properties of (K,Na)NbO 3 Ceramics with Novel Sintering Aid. *Japanese Journal of Applied Physics*, 43(10):7159–7163, October 2004.

[41] Yuji Hiruma, Rintaro Aoyagi, Hajime Nagata, and Tadashi Takenaka. Ferroelectric and Piezoelectric Properties of (Bi 1/2 K 1/2)TiO 3 Ceramics. *Japanese Journal of Applied Physics*, 44(7A):5040–5044, July 2005.

[42] Lin Sun, Chude Feng, Lidong Chen, and Shiming Huang. Dielectric and Piezoelectric Properties of SrBi 2?x Sm x Nb 2 O 9 (x=0, 0.05, 0.1, 0.2, 0.3, and 0.4) Ceramics. *Journal of the American Ceramic Society*, 3881:070922001308003–???, September 2007.

[43] R. E. Eitel, S. J. Zhang, T. R. Shrout, C. a. Randall, and I. Levin. Phase Diagram of the Perovskite System (1x)BiScO[sub 3]-xPbTiO[sub 3]. *Journal of Applied Physics*, 96(5):2828, 2004.

[44] Shujun Zhang, Richard E. Eitel, Clive a. Randall, Thomas R. Shrout, and Edward F. Alberta. Manganese-modified BiScO[sub 3]PbTiO[sub 3] piezoelectric ceramic for high-temperature shear mode sensor. *Applied Physics Letters*, 86(26):262904, 2005.

[45] Ian M. Reaney and Dragan Damjanovic. Crystal structure and domain-wall contributions to the piezoelectric properties of strontium bismuth titanate ceramics. *Journal of Applied Physics*, 80(7):4223, 1996.

[46] Ho Sung Lee and Toshio Kimura. Effects of Microstructure on the Dielectric and Piezoelectric Properties of Lead Metaniobate. *Journal of the American Ceramic Society*, 81(12):3228–3236, December 1998.

[47] T. P. Comyn, T. Stevenson, and A. J. Bell. Piezoelectric properties of BiFeO 3 PbTiO 3 ceramics. *Journal de Physique IV (Proceedings)*, 128:13–17, 2005.

[48] Holly S. Shulman, Martin Testorf, Dragan Damjanovic, and Nava Setter. Microstructure, Electrical Conductivity, and Piezoelectric Properties of Bismuth Titanate. *Journal of the American Ceramic Society*, 79(12):3124–3128, December 1996.

[49] Jiangtao Zeng, Yongxiang Li, Dong Wang, and Qingrui Yin. Electrical properties of neodymium doped CaBi4Ti4O15 ceramics. *Solid State Communications*, 133(9):553–557, March 2005.

[50] Zhen Zhang, Haixue Yan, Xianlin Dong, and Yongling Wang. Preparation and electrical properties of bismuth layer-structured ceramic Bi 3 NbTiO 9 solid solution. 38:241–248, 2003.

[51] P.W. Krempl. Quartz homeotypic gallium-orthophosphate-a new high tech piezoelectric material. In *Proceedings of IEEE Ultrasonics Symposium ULTSYM-94*, pages 949–954 vol.2. IEEE, 1994.

[52] S Zhang, R Xia, L Lebrun, D Anderson, and T Shrout. Piezoelectric materials for high power, high temperature applications. *Materials Letters*, 59(27):3471–3475, 2005.

[53] FRANK KULCSAR. Electromechanical Properties of Lead Titanate Zirconate Ceramics with Lead Partially Replaced by Calcium or Strontium. *Journal of the American Ceramic Society*, 42(1):49–51, January 1959.

[54] FRANK KULCSAR. Electromechanical Properties of Lead Titanate Zirconate Ceramics Modified with Certain Three-or Five-Valent Additions. *Journal of the American Ceramic Society*, 42(7):343–349, July 1959.

[55] Volkan Kalem, brahim Çam, and Muharrem Timuçin. Dielectric and piezoelectric prop-

erties of PZT ceramics doped with strontium and lanthanum. *Ceramics International*, 37(4):1265–1275, May 2011.

[56] Tutu Sebastian, Iasmi Sterianou, Derek C. Sinclair, Andrew J. Bell, David A. Hall, and Ian M. Reaney. High temperature piezoelectric ceramics in the Bi(Mg1/2Ti1/2)O3-BiFeO3-BiScO3-PbTiO3 system. *Journal of Electroceramics*, 25(2-4):130–134, March 2010.

[57] I. Sterianou, I. M. Reaney, D. C. Sinclair, D. I. Woodward, D. a. Hall, a. J. Bell, and T. P. Comyn. High-temperature (1x)BiSc[sub 12]Fe[sub 12]O[sub 3]-xPbTiO[sub 3] piezoelectric ceramics. *Applied Physics Letters*, 87(24):242901, 2005.

[58] T.P. Comyn, S.P. McBride, and A.J. Bell. Processing and electrical properties of BiFeO3PbTiO3 ceramics. *Materials Letters*, 58(30):3844–3846, 2004.

[59] V.V.S.S. Sai Sunder, A. Halliyal, and A.M. Umarji. Investigation of tetragonal distortion in the PbTiO 3 BiFeO 3 system by high-temperature x-ray diffraction. *Journal of Materials Research*, 10(5):1301–1306, May 1995.

[60] Andrew J Bell, Alejandro X Levander, Stuart L Turner, and Tim P. Comyn. *Internal Stress and Phase Coexistence in Bismuth Ferrite-Lead Titanate Ceramics*. IEEE, May 2007.

[61] Thorsten Leist, Wook Jo, Timothy Comyn, Andrew Bell, and Jürgen Rödel. Shift in Morphotropic Phase Boundary in La-Doped BiFeO 3 PbTiO 3 Piezoceramics. *Japanese Journal of Applied Physics*, 48(12):120205, December 2009.

[62] E. C. SUBBARAO. X-Ray Study of Phase Transitions in Ferroelectric PbNb2O6 and Related Materials. *Journal of the American Ceramic Society*, 43(9):439–442, September 1960.

[63] A. A. Nesterov, E. V. Karyukov, and K. S. Masurenkov. Synthesis of phases of composition PbNb2O6 and BaNb2O6 with the use of active precursors. *Russian Journal of Applied Chemistry*, 82(3):370–373, May 2009.

[64] M. G Sahini, T. Grande, and N. Setter. Ferroelectric Lead metaniobate and its solid solutions: Solid state synthesis and characterization. In *Proceedings of ISAF-ECAPD-PFM 2012*, pages 1–3. IEEE, July 2012.

[65] H. Jaffe and William R Cook. *Piezoelectric ceramics: Non-metallic solids: a series of monographs*. 1971.

[66] Malgorzata M. Lencka, Magdalena Oledzka, and Richard E. Riman. Hydrothermal Synthesis of Sodium and Potassium Bismuth Titanates. *Chemistry of Materials*, 12(5):1323–1330, May 2000.

[67] Ying Yuan, Shuren Zhang, Xiaohua Zhou, and Jingsong Liu. Phase Transition and Temperature Dependences of Electrical Properties of [Bi 0.5 (Na 1- x - y K x Li y) 0.5]TiO 3 Ceramics. *Japanese Journal of Applied Physics*, 45(No. 2A):831–834, 2006.

[68] S.A. Fedulov. Complete Phase Diagram of the BiFeO3-PbTiO3 System. *Soviet Solid-State Physics*, 6:375–378, 1964.

[69] S.A. Fedulov. DETERMINATION OF CURIE TEMPERATURE FOR BIFEO3 FERROELECTRIC. *DOKLADY AKADEMII NAUK SSSR*, 139(6):1345, 1961.

[70] David I. Woodward, Ian M. Reaney, Richard E. Eitel, and Clive a. Randall. Crystal and domain structure of the BiFeO[sub 3]PbTiO[sub 3] solid solution. *Journal of Applied Physics*, 94(5):3313, 2003.

[71] Christian Michel, Jean-Michel Moreau, Gary D. Achenbach, Robert Gerson, and W.J. James. The atomic structure of BiFeO3. *Solid State Communications*, 7(9):701–704, May 1969.

[72] W.-M. Zhu, H.-Y. Guo, and Z.-G. Ye. Structural and magnetic characterization of multiferroic (BiFeO3)1x(PbTiO3)x solid solutions. *Physical Review B*, 78(1):1–10, July 2008.

[73] HANS JAFFE. Piezoelectric Ceramics. *Journal of the American Ceramic Society*, 41(11):494–498, March 1958.

[74] M. Overby, A. Chernyshov, L. P. Rokhinson, X. Liu, and J. K. Furdyna. GaMnAs-based hybrid multiferroic memory device. *Applied Physics Letters*, 92(19):192501, 2008.

[75] Tim Stevenson, Tim P. Comyn, Aziz Daoud-Aladine, and Andrew J. Bell. Change in periodicity of the incommensurate magnetic order towards commensurate order in bismuth ferrite lead titanate. *Journal of Magnetism and Magnetic Materials*, 322(22):L64–L67, November 2010.

[76] Manuel Bibes and Agnès Barthélémy. Multiferroics: towards a magnetoelectric memory. *Nature materials*, 7(6):425–6, 2008.

[77] N Hur, S Park, P A Sharma, J S Ahn, S Guha, and S-W Cheong. Electric polarization reversal and memory in a multiferroic material induced by magnetic fields. *Nature*, 429(6990):392–5, 2004.

[78] Tim P. Comyn, Tim Stevenson, Maisoon Al-Jawad, Gilles André, Andrew J. Bell, and Robert Cywinski. Antiferromagnetic order in tetragonal bismuth ferritelead titanate. *Journal of Magnetism and Magnetic Materials*, 323(21):2533–2535, November 2011.

[79] Andrew J Bell, Thorsten Schlegel, Mohamed Alduraibi, Mikael A Khan, Timothy P Comyn, and Jurgen Rodel. Impedance Spectroscopy of Mn-Doped BiFeO¡inf¿3¡/inf¿-PbTiO¡inf¿3¡/inf¿ Ceramics. In *2006 IEEE International Symposium on the Applications of Ferroelectrics*, pages 1–4. IEEE, July 2006.

[80] Gustau Catalan and James F. Scott. Physics and Applications of Bismuth Ferrite. *Advanced Materials*, 21(24):2463–2485, June 2009.

[81] G.A. Smolenskii and I.E. Chupis. Ferroelectromagnets. *Uspekhi Fizicheskih Nauk*, 137(7):415, 1982.

[82] J Seidel, L W Martin, Q He, Q Zhan, Y-H Chu, a Rother, M E Hawkridge, P Maksymovych, P Yu, M Gajek, N Balke, S V Kalinin, S Gemming, F Wang, G Catalan, J F Scott, N a Spaldin, J Orenstein, and R Ramesh. Conduction at domain walls in oxide multiferroics. *Nature materials*, 8(3):229–34, March 2009.

[83] S. R. Das, R. N. P. Choudhary, P. Bhattacharya, R. S. Katiyar, P. Dutta, a. Manivannan, and M. S. Seehra. Structural and multiferroic properties of La-modified BiFeO[sub 3] ceramics. *Journal of Applied Physics*, 101(3):034104, 2007.

[84] V. R. Palkar, Darshan C. Kundaliya, and S. K. Malik. Effect of Mn substitution on magnetoelectric properties of bismuth ferrite system. *Journal of Applied Physics*, 93(7):4337, 2003.

[85] Naigang Wang, J. Cheng, a. Pyatakov, A. Zvezdin, J. Li, L. Cross, and D. Viehland. Multiferroic properties of modified BiFeO3-PbTiO3-based ceramics: Random-field induced release of latent magnetization and polarization. *Physical Review B*, 72(10):1–5, September 2005.

[86] Thorsten Leist, Kyle G. Webber, Wook Jo, Emil Aulbach, Jürgen Rödel, Anderson D. Prewitt, Jacob L. Jones, Josh Schmidlin, and Camden R. Hubbard. Stress-induced structural changes in La-doped BiFeO3PbTiO3 high-temperature piezoceramics. *Acta Materialia*, 58(18):5962–5971, October 2010.

[87] Thorsten Leist, Torsten Granzow, Wook Jo, and Jurgen Rodel. Effect of tetragonal distortion on ferroelectric domain switching: A case study on La-doped BiFeO[sub 3]PbTiO[sub 3] ceramics. *Journal of Applied Physics*, 108(1):014103, 2010.

[88] Jinrong Cheng, Zhongyan Meng, and L. Eric Cross. High-field and high-T[sub c] piezo-

electric ceramics based on Bi(Ga,Fe)O[sub 3]-PbTiO[sub 3] crystalline solutions. *Journal of Applied Physics*, 98(8):084102, 2005.

[89] Jin-Rong Cheng, Nan Li, and L. Eric Cross. Structural and dielectric properties of Ga-modified BiFeO[sub 3]PbTiO[sub 3] crystalline solutions. *Journal of Applied Physics*, 94(8):5153, 2003.

[90] T.P. Comyn, T Stevenson, and A.J. Bell. Piezoelectric properties of BiFeO/sub 3/-PbTiO/sub 3/ ceramics. In *14th IEEE International Symposium on Applications of Ferroelectrics, 2004. ISAF-04. 2004*, volume 00, pages 122–125. IEEE, 2004.

[91] Jin-Rong Cheng and L. Eric Cross. Effects of La substituent on ferroelectric rhombohedral/tetragonal morphotropic phase boundary in (1x)(Bi,La)(Ga[sub 0.05]Fe[sub 0.95])O[sub 3]xPbTiO[sub 3] piezoelectric ceramics. *Journal of Applied Physics*, 94(8):5188, 2003.

[92] K P Rema, a S Divya, and V Kumar. Influence of low lanthanum doping on the electrical characteristics of PZT(53/47). *Journal of Physics D: Applied Physics*, 42(7):075420, April 2009.

[93] S.Q. Zhang, W.L. Li, L.D. Wang, N. Li, and W.D. Fei. Enhanced dielectric and ferroelectric properties of Pb13x/2Lax(Zr0.5Ti0.5)O3 thin films with low lanthanum substitution. *Applied Surface Science*, 257(9):4021–4025, February 2011.

[94] T.P. Comyn and A.J. Bell. *Study of intrinsic / extrinsic piezoelectric contributions in La-doped BiFeO¡inf¿3¡/inf¿ - PbTiO¡inf¿3¡/inf¿ ceramics using the Rayleigh method*, volume 3. IEEE, 2007.

[95] Keisuke Kobayashi, Keiichi Hatano, Youichi Mizuno, and Clive a. Randall. Rayleigh Behavior in the Lead Free Piezoelectric Li$_{x}$(Na$_{0.5}$K$_{0.5}$)$_{1-x}$NbO$_{3}$ Ceramic. *Applied Physics Express*, 5(3):031501, February 2012.

[96] Fei Li, Shujun Zhang, Zhuo Xu, Xiaoyong Wei, Jun Luo, and Thomas R Shrout. Composition and phase dependence of the intrinsic and extrinsic piezoelectric activity of domain engineered (1-x)Pb(Mg(13)Nb(23))O(3)-xPbTiO(3) crystals. *Journal of applied physics*, 108(3), August 2010.

[97] Matthew Davis. Direct piezoelectric effect in relaxor-ferroelectric single crystals. *Journal of Applied Physics*, 95(10):5679, 2004.

[98] SW Gotmare and SO Leontsev. Thermal Degradation and Aging of HighTemperature Piezoelectric Ceramics. *Journal of the American Ceramic Society*, 1969(26278):1965–1969, 2010.

[99] Abhijit Pramanick, Dragan Damjanovic, John E. Daniels, Juan C. Nino, and Jacob L. Jones. Origins of Electro-Mechanical Coupling in Polycrystalline Ferroelectrics During Subcoercive Electrical Loading. *Journal of the American Ceramic Society*, 94(2):293–309, February 2011.

[100] Dragan Damjanovic. Stress and frequency dependence of the direct piezoelectric effect in ferroelectric ceramics. *Journal of Applied Physics*, 82(4):1788, 1997.

[101] A K Tagantsev, I Stolichnov, E L Colla, and N Setter. Polarization fatigue in ferroelectric films: Basic experimental findings, phenomenological scenarios, and microscopic features. *Journal of Applied Physics*, 90(3):1387, 2001.

[102] Atsushi Furuta and Kenji Uchino. Dynamic Observation of Crack Propagation in Piezoelectric Multilayer Actuators. *Journal of the American Ceramic Society*, 76(6):1615–1617, June 1993.

[103] Hideaki Aburatani, Shuichi Harada, Kenji Uchino, Atsushi Furuta, and Yoshiaki Fuda. Destruction Mechanisms in Ceramic Multilayer Actuators. *Japanese Journal of Applied Physics*, 33(Part 1, No. 5B):3091–3094, May 1994.

[104] A. Chynoweth. Surface Space-Charge Layers in Barium Titanate. *Physical Review*, 102(3):705–714, May 1956.

[105] U Robels and G Arlt. Domain wall clamping in ferroelectrics by orientation of defects. *Journal of Applied Physics*, 73(7):3454, 1993.

[106] S. B. Desu. Minimization of fatigue in ferroelectric films. *Physica Status Solidi (a)*, 151(2):467–480, October 1995.

[107] J Nuffer. Damage evolution in ferroelectric PZT induced by bipolar electric cycling. *Acta Materialia*, 48(14):3783–3794, September 2000.

[108] I. Dutta and R.N. Singh. Effect of electrical fatigue on the electromechanical behavior and microstructure of strontium modified lead zirconate titanate ceramics. *Materials Science and Engineering: B*, 166(1):50–60, 2010.

[109] N Zhang. Frequency dependence of ferroelectric fatigue in PLZT ceramics. *Journal of the European Ceramic Society*, 21(5):677–681, May 2001.

[110] Yi-Hsien Lee, Jenn-Ming Wu, and Chih-Huang Lai. Influence of La doping in multiferroic properties of BiFeO[sub 3] thin films. *Applied Physics Letters*, 88(4):042903, 2006.

[111] Hong Wang, Andrew a. Wereszczak, and Hua-Tay Lin. Fatigue response of a PZT multilayer actuator under high-field electric cycling with mechanical preload. *Journal of Applied Physics*, 105(1):014112, 2009.

[112] Ming Liu and K. Jimmy Hsia. Locking of electric-field-induced non-180 domain switching and phase transition in ferroelectric materials upon cyclic electric fatigue. *Applied Physics Letters*, 83(19):3978, 2003.

[113] C Verdier. Unipolar fatigue of ferroelectric leadzirconatetitanate. *Journal of the European Ceramic Society*, 23(9):1409–1415, August 2003.

[114] Cz. Pawlaczyk, A. K. Tagantsev, K. Brooks, I. M. Reaney, R. Klissurska, and N. Setter. Fatigue, rejuvenation and self-restoring in ferroelectric thin films. *Integrated Ferroelectrics*, 9(4):293–316, August 1995.

[115] D Smyth. Defect structure in perovskite titanates. *Current Opinion in Solid State and Materials Science*, 1(5):692–697, October 1996.

[116] a. K. Tagantsev and I. A. Stolichnov. Injection-controlled size effect on switching of ferroelectric thin films. *Applied Physics Letters*, 74(9):1326, 1999.

[117] D P Vijay. Electrodes for PbZr[sub x]Ti[sub 1x]O[sub 3] Ferroelectric Thin Films. *Journal of The Electrochemical Society*, 140(9):2640, 1993.

[118] X J Lou and J Wang. Unipolar and bipolar fatigue in antiferroelectric lead zirconate thin films and evidences for switching-induced charge injection inducing fatigue. page 10, January 2010.

[119] Zhuo Li and Huiqing Fan. Oxygen vacancy-induced aging of Mn-doped Ba0.8Sr0.2TiO3 ceramics in paraelectric and ferroelectric state. *Solid State Ionics*, 180(20-22):1139–1142, August 2009.

[120] M Brazier, S Mansour, and M. McElfresh. Ferroelectric fatigue of Pb(Zr,Ti)O[sub 3] thin films measured in atmospheres of varying oxygen concentration. *Applied Physics Letters*, 74(26):4032, 1999.

[121] Jurgen Nuffer, Doru C. Lupascu, Jurgen Rodel, and Michael Schroeder. Negligible oxygen liberation during bipolar electric cycling of ferroelectric lead zirconate titanate ceramics. *Applied Physics Letters*, 79(22):3675, 2001.

[122] Atushi Ochi, Sadayuki Takahashi, and Satoru Tagami. Temperature Characteristics for Multilayer Piezoelectric Ceramic Actuator. *Japanese Journal of Applied Physics*, 24:209–212, 1985.

[123] Takenobu Sakai and Hiroshi Kawamoto. Durability Properties of Piezoelectric Stack Actuator. *Japanese Journal of Applied Physics*, 37(Part 1, No. 9B):5338–5341, September 1998.

[124] M S Senousy, R K N D Rajapakse, D Mumford, and M S Gadala. Self-heat generation in piezoelectric stack actuators used in fuel injectors. *Smart Materials and Structures*, 18(4):045008, April 2009.

[125] Jiehui Zheng, Sadayuki Takahashi, Shoko Yoshikawa, Kenji Uchino, and J. W. C. Vries. Heat Generation in Multilayer Piezoelectric Actuators. *Journal of the American Ceramic Society*, 79(12):3193–3198, December 1996.

[126] I YOO and S DESU. Fatigue modeling of lead zirconate titanate thin films. *Materials Science and Engineering: B*, 13(4):319–322, April 1992.

[127] M OKAYASU, S AOKI, and M MIZUNO. Effects of silver-based metal electroplate on fatigue properties of PZT ceramics. *International Journal of Fatigue*, 30(6):1115–1124, 2008.

[128] A Gruverman, O Auciello, and H Tokumoto. Nanoscale investigation of fatigue effects in Pb(Zr,Ti)O3 films. *Applied Physics Letters*, 69(21):3191, 1996.

[129] S.D. Bernstein, T.Y. Wong, Yanina Kisler, and R.W. Tustison. Fatigue of ferroelectric PbZr x Ti y O 3 capacitors with Ru and RuO x electrodes. *Journal of Materials Research*, 8(1):12–13, January 1993.

[130] H. N. Al-Shareef, O. Auciello, and A I Kingon. Electrical properties of ferroelectric thin-film capacitors with hybrid (Pt,RuO2) electrodes for nonvolatile memory applications. *Journal of Applied Physics*, 77(5):2146, 1995.

[131] K. Maki, B. T. Liu, H. Vu, V. Nagarajan, R. Ramesh, Y. Fujimori, T. Nakamura, and H. Takasu. Controlling crystallization of Pb(Zr,Ti)O[sub 3] thin films on IrO[sub 2]

electrodes at low temperature through interface engineering. *Applied Physics Letters*, 82(8):1263, 2003.

[132] Yong Kwan Kim, Hitoshi Morioka, and Hiroshi Funakubo. Fatigue Properties of Epitaxial Pb(Zr 0.35 Ti 0.65)O 3 Films with Various Volume Fractions of 90 Domains Grown on (100) c SrRuO 3 /(100)SrTiO 3 Substrates. *Japanese Journal of Applied Physics*, 45(No. 8A):6382–6384, August 2006.

[133] S Aggarwal, I G Jenkins, B Nagaraj, C J Kerr, C Canedy, R Ramesh, G. Velasquez, L. Boyer, and J. T. Evans. Switching properties of Pb(Nb, Zr, Ti)O[sub 3] capacitors using SrRuO[sub 3] electrodes. *Applied Physics Letters*, 75(12):1787, 1999.

[134] Ming-Sen Chen, Tai-Bor Wu, and Jenn-Ming Wu. Effect of textured LaNiO3 electrode on the fatigue improvement of Pb(Zr0.53Ti0.47)O3 thin films. *Applied Physics Letters*, 68(10):1430, 1996.

[135] Wan In Lee, J. K. Lee, J. S. Lee, and I. K. Yoo. Preparation and electrical properties of high quality PZT thin films on RuOx electrode. *Integrated Ferroelectrics*, 10(1):145–154, October 1995.

[136] Doru C. Lupascu. *Fatigue in Ferroelectric Ceramics and Related Issues*. Springer, 2004.

[137] W. L. Warren, D. Dimos, B. A. Tuttle, R. D. Nasby, and G. E. Pike. Electronic domain pinning in Pb(Zr,Ti)O3 thin films and its role in fatigue. *Applied Physics Letters*, 65(8):1018, 1994.

[138] M Raymond. Defects and charge transport in perovskite ferroelectrics. *Journal of Physics and Chemistry of Solids*, 57(10):1507–1511, October 1996.

[139] Lawrence F. Schloss, Paul C. McIntyre, Bryan C. Hendrix, Steven M. Bilodeau, Jeffrey F. Roeder, and Stephen R. Gilbert. Oxygen tracer studies of ferroelectric fatigue in Pb(Zr,Ti)O[sub 3] thin films. *Applied Physics Letters*, 81(17):3218, 2002.

[140] Ming-Jen Pan, Seung-Eek Park, Colin W. Park, Kelley A. Markowski, Shoko Yoshikawa, and Clive A. Randall. Superoxidation and Electrochemical Reactions during Switching in Pb(Zr2Ti)O3 Ceramics. *Journal of the American Ceramic Society*, 79(11):2971–2974, November 1996.

[141] J. F. Scott, C. A. Araujo, B. M. Melnick, L. D. McMillan, and R. Zuleeg. Quantitative measurement of space-charge effects in lead zirconate-titanate memories. *Journal of Applied Physics*, 70(1):382, 1991.

[142] Dage Liu, Chen Wang, Hongxi Zhang, Junwei Li, Liancheng Zhao, and Chunli Bai. Domain configuration and interface structure analysis of sol-gel-derived PZT ferroelectric thin films. *Surface and Interface Analysis*, 32(1):27–31, August 2001.

[143] Doru Lupascu and Ute Rabe. Cyclic Cluster Growth in Ferroelectric Perovskites. *Physical Review Letters*, 89(18):187601, October 2002.

[144] Sun Haishan and Chen Shoutian. Charge-discharge breakdown of dielectric ceramic. In *Proceedings of the 6th International Conference on Properties and Applications of Dielectric Materials (Cat. No.00CH36347)*, volume 2, pages 1029–1032. IEEE.

[145] W. P. Mason. Aging of the Properties of Barium Titanate and Related Ferroelectric Ceramics. *The Journal of the Acoustical Society of America*, 27(1):73, 1955.

[146] D BERLINCOURT, H KRUEGER, and B JAFFE. Stability of phases in modified lead zirconate with variation in pressure, electric field, temperature and composition. *Journal of Physics and Chemistry of Solids*, 25(7):659–674, July 1964.

[147] Helmut H. a. Krueger. Stress Sensitivity of Piezoelectric Ceramics: Part 3. Sensitivity to Compressive Stress Perpendicular to the Polar Axis. *The Journal of the Acoustical Society of America*, 43(3):583, 1968.

[148] H. H. A. Krueger. Effects of High Static Stress on the Piezoelectric Properties of Transducer Materials. *The Journal of the Acoustical Society of America*, 33(10):1339, 1961.

[149] Dragan Damjanovic and David. Taylor. Contributions to the nonlinear dielectric and piezoelectric response of ferroelectric thin films and ceramics. *Ferroelectrics*, 221(772815469):137–146, January 1999.

[150] F. Xu, S. Trolier-McKinstry, W. Ren, Baomin Xu, Z.-L. Xie, and K. J. Hemker. Domain wall motion and its contribution to the dielectric and piezoelectric properties of lead zirconate titanate films. *Journal of Applied Physics*, 89(2):1336, 2001.

[151] G. Yang. *Uniaxial stress dependence of the piezoelectric properties of lead zirconate titanate ceramics*. SPIE, 2000.

[152] Rattikorn Yimnirun, Yongyut Laosiritaworn, and Supattra Wongsaenmai. Effect of uniaxial compressive pre-stress on ferroelectric properties of soft PZT ceramics. *Journal of Physics D: Applied Physics*, 39(4):759–764, February 2006.

[153] Rattikorn Yimnirun, Supon Ananta, Ekarat Meechoowas, and Supattra Wongsaenmai. Effects of uniaxial stress on dielectric properties lead magnesium niobatelead zirconate titanate ceramics. *Journal of Physics D: Applied Physics*, 36(13):1615–1619, July 2003.

[154] Q.M. Zhang, J. Zhao, K. Uchino, and J. Zheng. Change of the weak field properties of Pb(ZrTi)O 3 piezoceramics with compressive uniaxial stresses and its links to the effect of dopants on the stability of the polarizations in the materials. *Journal of Materials Research*, 12(1):226–234, January 1997.

[155] S. W. Meeks and R. W. Timme. Effects of one-dimensional stress on piezoelectric ceramics. *Journal of Applied Physics*, 46(10):4334, 1975.

[156] M Alguero. Degradation of the d33 piezoelectric coefficient for PZT ceramics under static

and cyclic compressive loading. *Journal of the European Ceramic Society*, 21(10-11):1437–1440, 2001.

[157] Walter A. Schulze and Kiyoshi Ogino. Review of literature on aging of dielectrics. *Ferroelectrics*, 87(1):361–377, November 1988.

[158] G. H. JONKER. Nature of Aging in Ferroelectric Ceramics. *Journal of the American Ceramic Society*, 55(1):57–58, January 1972.

[159] Jürgen Nuffer, Doru Lupascu, and Jürgen Rödel. Acoustic emission in PZT under bipolar electric driving and uniaxial mechanical stress. *Ferroelectrics*, 240(909770856):1293–1302, January 2000.

[160] Mitsuhiro Okayasu, Eriko Sugiyama, and Mamoru Mizuno. In situ measurement of material properties of lead zirconate titanate piezoelectric ceramics during cyclic mechanical loading. *Journal of the European Ceramic Society*, 30(6):1445–1452, 2010.

[161] Abdolghaffar Barzegar, Dragan Damjanovic, and Nava Setter. The effect of boundary conditions and sample aspect ratio on apparent d33 piezoelectric coefficient determined by direct quasistatic method. *IEEE transactions on ultrasonics, ferroelectrics, and frequency control*, 51(3):262–70, March 2004.

[162] Mark Stewart, Will Battrick, and Markys Cain. Measurement Good Practice Guide No . 44: Measuring Piezoelectric d 33 coefficients using the Direct Method. *Measurement Good Practice Guide*, (44), 2001.

[163] Section 6 [IEEE Std 176-1978]. *IEEE Transactions on Sonics and Ultrasonics*, 31(2):54–54, March 1984.

[164] 176-1987 - IEEE Standard on Piezoelectricity. *Institute of Electrical and Electronics Engineers Ultrasonics, Ferroelectrics, and Frequency Control Society*, 1988.

[165] British Standard. *BS EN 12291:2003 Advanced technical ceramics Mechanical properties of ceramic composites at high temperature in air at atmospheric pressure Determination of compression properties*, volume 3. 2003.

[166] British Standard and B S En. *BS EN 12290:2005 Advanced technical ceramics Mechanical properties of ceramic composites at high temperature under inert atmosphere Determination of compression properties*, volume 3. BSI, 2005.

[167] Robert Bosch Corp. Linear Bushings and Shafts.

[168] Philtec Inc. Model D63 Specifications, 2010.

[169] Piezotest Ltd. Piezotest PM300 d33 Meter Specifications, 2003.

[170] V. Sundar and R. E. Newnham. Electrostriction and polarization. *Ferroelectrics*, 135(1):431–446, October 1992.

[171] Hans Kungl and Michael J. Hoffmann. Temperature dependence of poling strain and strain under high electric fields in LaSr-doped morphotropic PZT and its relation to changes in structural characteristics. *Acta Materialia*, 55(17):5780–5791, October 2007.

List of Figures

14 Appendix

The materials used in section 7 are now known by different names due to revised nomenclature of the manufacturer. CMAP 07 is NCE57 material, while CMAP11 is NAC2025 material.

Rayleigh Data

NCE55

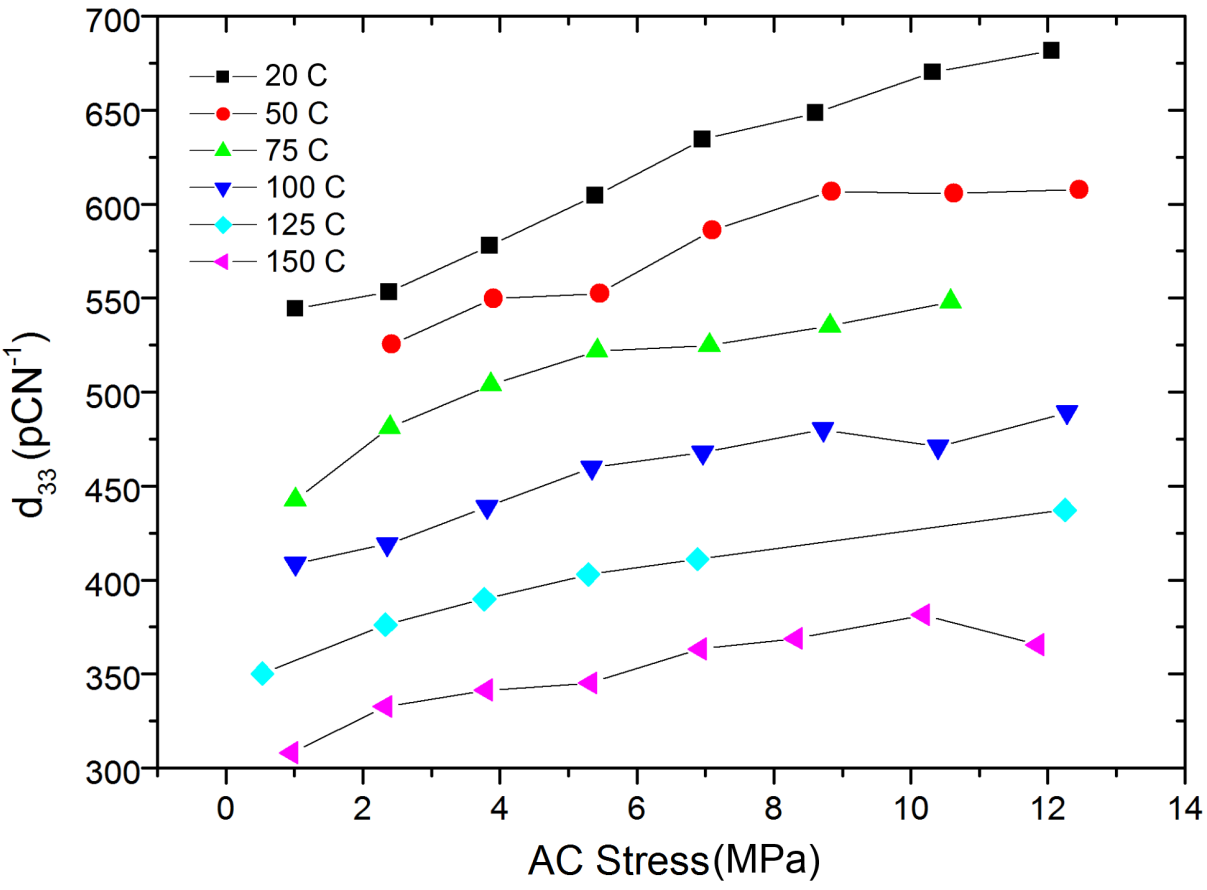

Figure 95: Direct-effect response of NCE55 48 hours after poling.

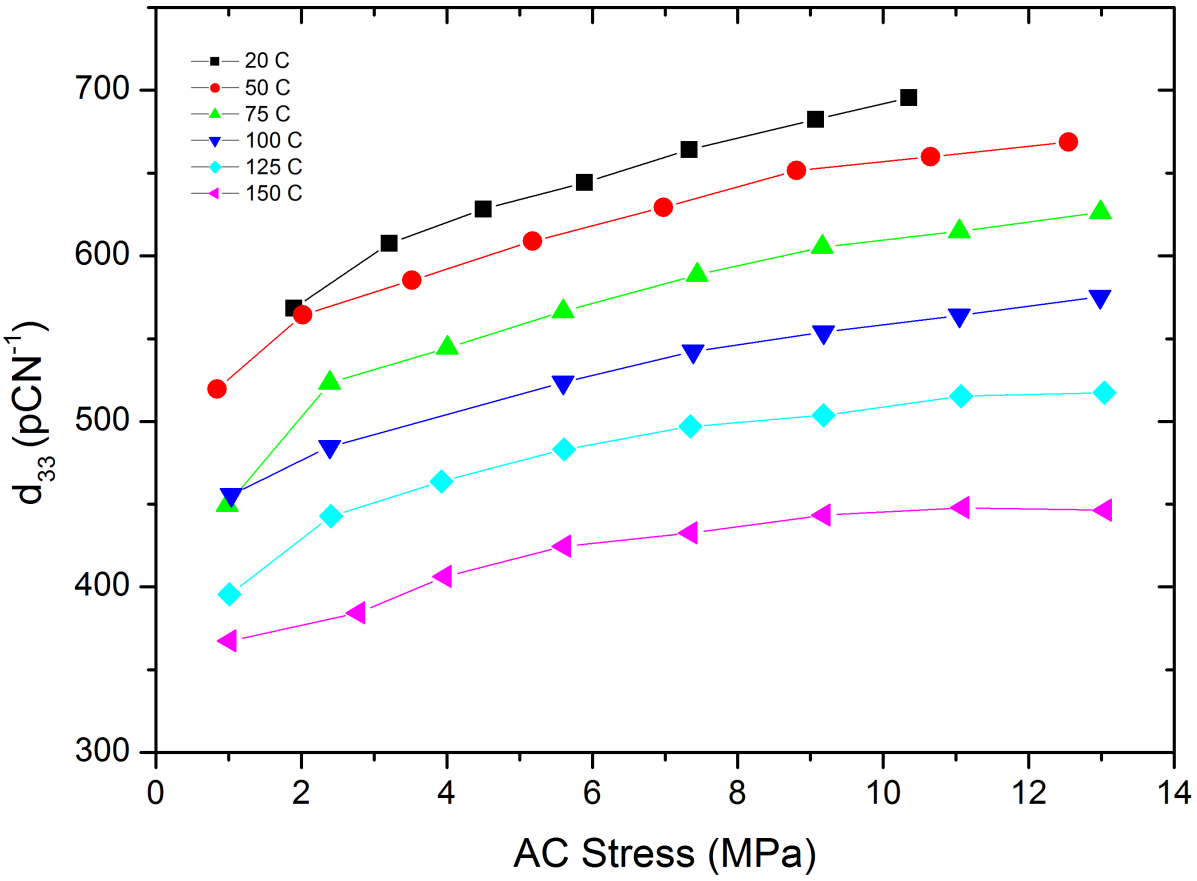

Figure 96: Direct-effect response of NCE55 1 month after poling.

PIC181

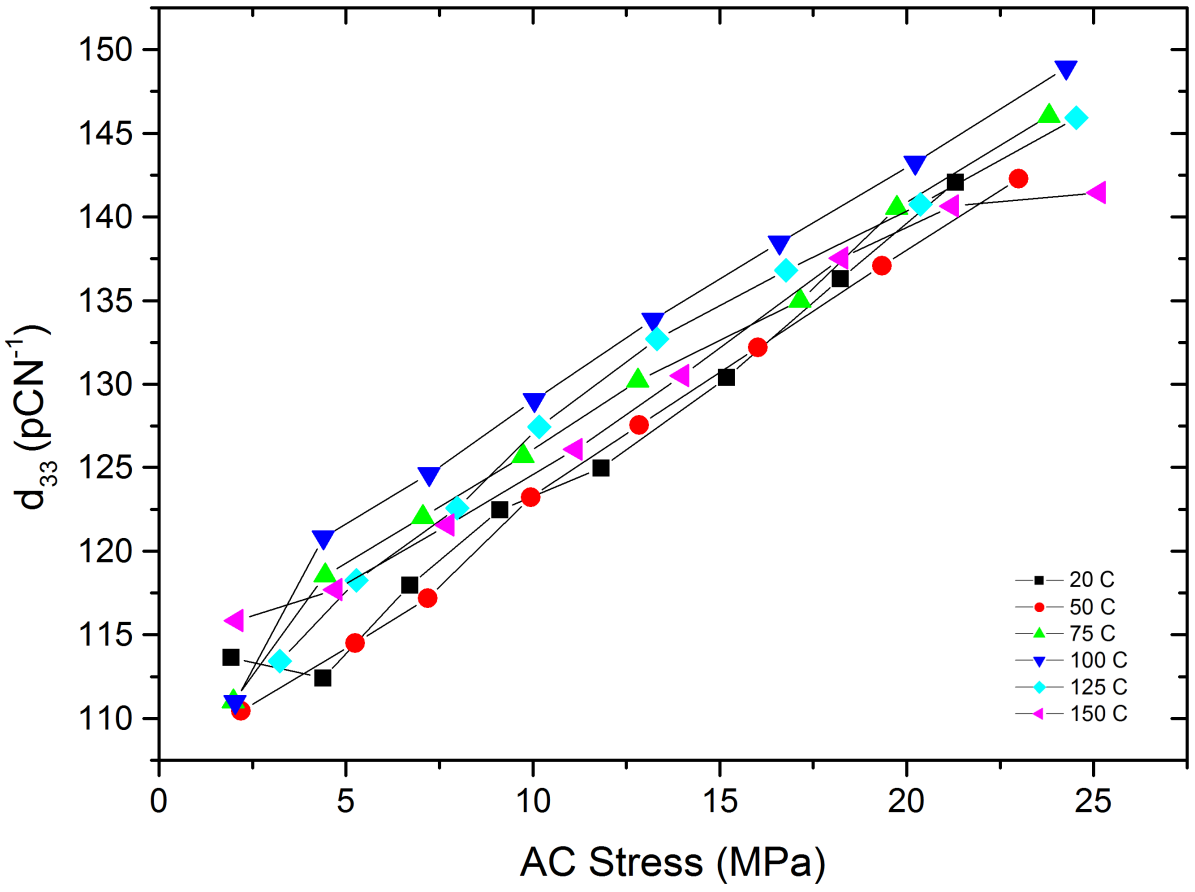

Figure 97: Direct-effect response of PIC181 48 hours after poling.

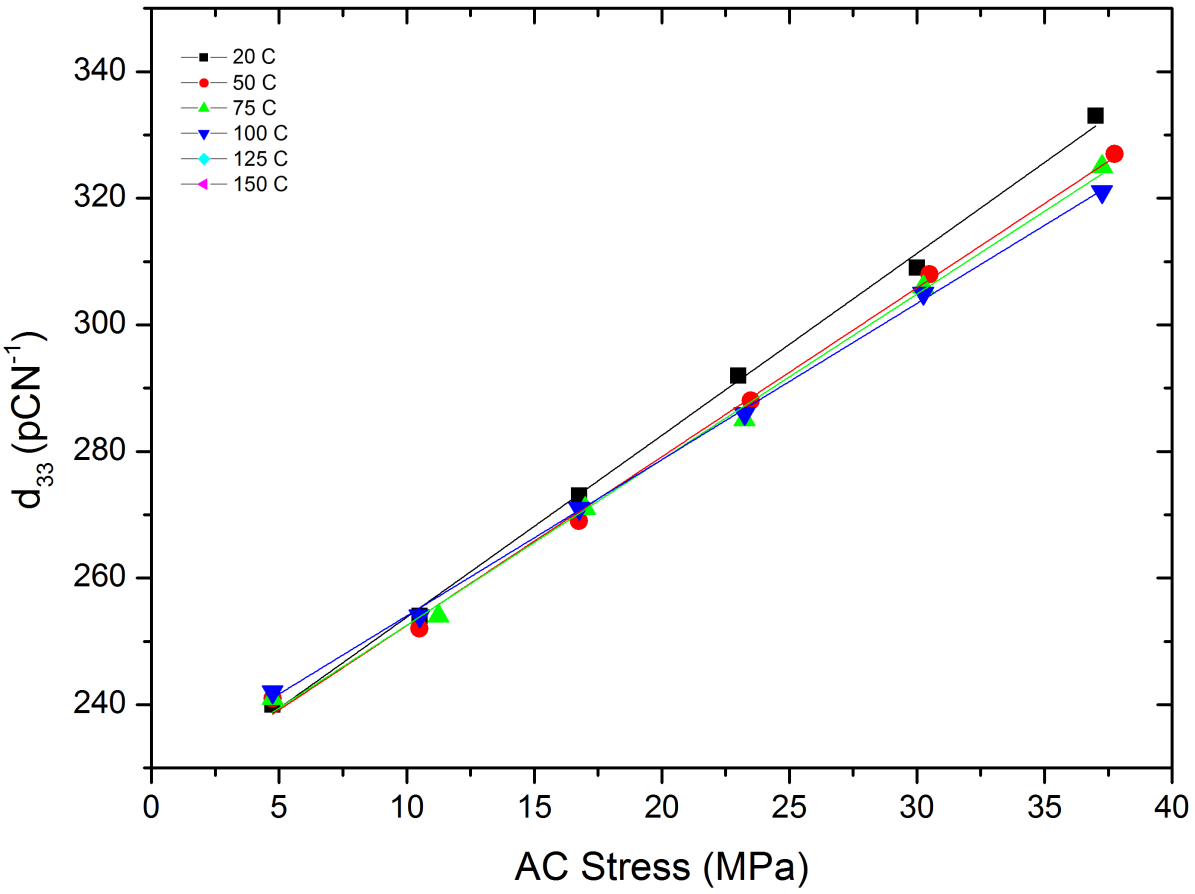

Figure 98: Response of 1 month aged PIC181 to alternating stress.

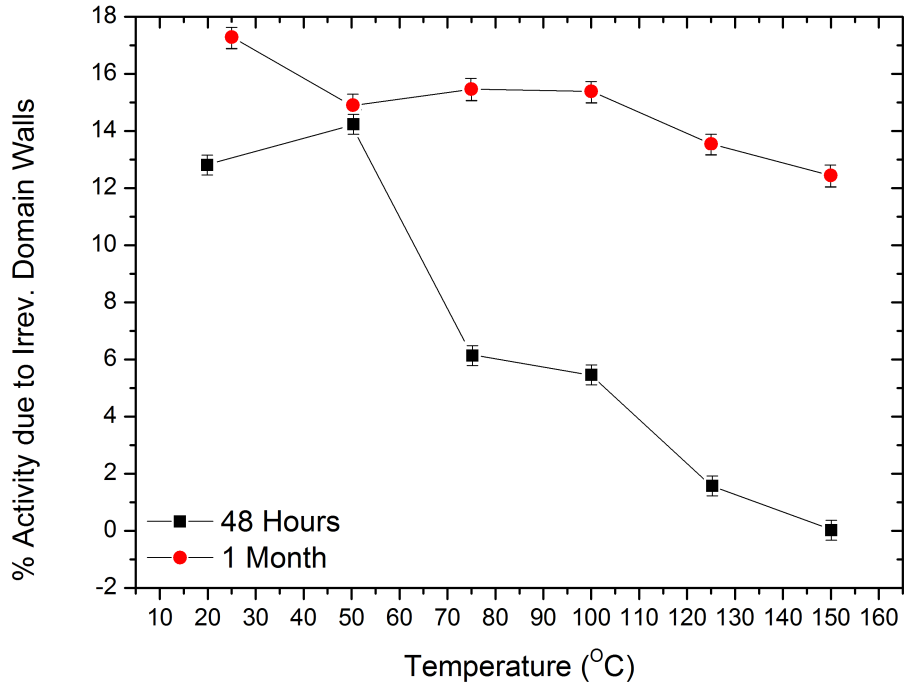

Figure 99: Calculated activity in PIC181 arising from irreversible domain wall contributions 48 hours and 1 month after poling.

Rayleigh DIAdem Data Analysis Script

```
Call ChnLinScale("[1]/Kistler","/Kistler Scaled",130,0) '... Y,E,ChnScaleFactor,ChnScaleOffset
Call ChnLinScale("[1]/Charge","/Charge Scaled",9990,0) '... Y,E,ChnScaleFactor,ChnScaleOffset
Call DataBlDel("'[2]/Kistler Scaled', '[2]/Charge Scaled'",1,79999,1) '...
                                                    ChnNoStr,ChnRow,ValNo,ValDelOnly
Call DataBlDel("'[2]/Kistler Scaled', '[2]/Charge Scaled'",480000,999999,1) '...
                                                    ChnNoStr,ChnRow,ValNo,ValDelOnly
Call ChnRegrXYCalc("[2]/Kistler Scaled","[2]/Charge Scaled","/RegressionX1",
                      "/RegressionY1","linear","Partition complete area",100,1) '...
                                                     XW,Y,E,E,RegrType,XChnStyle,XNo,XDiv
Call PicLoad("Template")
Call GraphObjNew("2D-Axis","2DAxis1" )
Call GraphObjOpen("2DAxis1")
  Call  GraphObjNew("2D-Curve","New_Curve") 'Creates a new curve
  Call GraphObjOpen("New_Curve")            'Opens the curve object
    D2CChnXName      = "Kistler Scaled"
    D2CChnYName      = "Charge Scaled"
  Call GraphObjClose("New_Curve")
Call GraphObjClose("2DAxis1")
  Call PicUpdate
MsgBox(Str(RegrCoeffB))
MsgBox(Str(CCh("[2]/Kistler Scaled", 2)))
MsgBox(Str(CCh("[2]/Kistler Scaled", 1)))
```

15 Publications

Shukla, R., Adam Qaisar, S., & Bell, A. J. (2010). Towards the development of efficient low frequency piezoelectric energy harvesters. 2010 IEEE International Symposium on the Applications of Ferroelectrics (ISAF) (pp. 1-4). IEEE. doi:10.1109/ISAF.2010.5712228

T.P. Comyn, T. Stevenson, S. A. Qaisar, A.J. Bell (2012). High performance piezoelectric materials. Actuator 2012

16 Attended Conferences, Meetings & Awards

19th IEEE International Symposium on the Applications of Ferroelectrics (ISAF)

Edinburgh, United Kingdom (Poster)

Piezo 2011

Sestriere, Italy

20th IEEE International Symposium on Applications of Ferroelectrics & International Symposium on Piezoresponse Force Microscopy & Nanoscale Phenomena in Polar Materials (ISAF-PFM)

Vancouver, Canada (Poster)

8th Beihang Autumn Academic Forum (BAAF), Beihang University

Beijing, China (Lecture: A Device for *in situ* Measurements and Fatigue of Piezoelectric Elements)

Award: Best abstract in measurement forum

21st IEEE International Symposium on the Applications of Ferroelectrics (ISAF)

Aveiro, Portugal (Presentation)

Ferroelectrics UK 2013

Sheffield, United Kingdom (Presentation)

2013 Joint UFFC, EFTF and PFM Symposium - IUS-ISAF-PFM-IFCS-EFTF

Prague, Czech Republic (Poster)

Award: ISAF student paper competition winner